



CENPD-392-A  
Revision 00

# **10x10 SVEA Fuel Critical Power Experiments and CPR Correlations: SVEA-96**

C E N u c l e a r P o w e r L L C



## **LEGAL NOTICE**

This report was prepared as an account of work sponsored by CE Nuclear Power LLC. Neither CENP LLC nor any person acting on its behalf:

- A. Makes any warranty or representation, express or implied including the warranties of fitness for a particular purpose or merchantability, with respect to the accuracy, completeness, or usefulness of the information contained in this report, or that the use of any information, apparatus, method, or process disclosed in this report may not infringe privately owned rights; or
- B. Assumes any liabilities with respect to the use of, or for damages resulting from the use of, any information, apparatus, method, or process disclosed in this report.

CENPD-392-A

Revision 00

# 10x10 SVEA Fuel Critical Power Experiments and CPR Correlations: SVEA-96

September 2000

Author: WR Harris  
William R. Harris  
Nuclear Fuel

Author: YY Yung  
Yat-Yan Yung  
Nuclear Fuel

Approved: Derek Ebeling-Koning  
Derek Ebeling-Koning  
Nuclear Fuel

---

CE Nuclear Power LLC  
2000 Day Hill Road  
Windsor, CT 06095

©2000 CE Nuclear Power LLC  
All Rights Reserved

## **COPYRIGHT NOTICE**

This report has been prepared by CE Nuclear Power LLC (CENP), a subsidiary of Westinghouse Electric Company LLC, and bears a CE Nuclear Power LLC copyright notice. The information in this report is the property of and contains copyright information owned by CENP and/or its subcontractors and suppliers. It is transmitted to you in confidence and trust, and you agree to treat this document and the information contained therein in strict accordance with the terms and conditions of the agreement under which it was provided to you.

You are permitted to make the number of copies of the information contained in this report which are necessary for your internal use in connection with your implementation of the report results for your plant(s) in your normal conduct of business. Should implementation of this report involve a third party, you are permitted to make the number of copies of the information contained in this report that are necessary for the third party's use in supporting your implementation at your plant(s) in your normal conduct of business if you have received the prior, written consent of CENP to transmit this information to a third party or parties. All copies made by you must include the copyright notice in all instances and the proprietary notice if the original was identified as proprietary.

The NRC is permitted to make the number of copies beyond those necessary for its internal use that are necessary in order to have one copy available for public viewing in the appropriate docket files in the NRC public document room in Washington, DC if the number of copies submitted is insufficient for this purpose, subject to the applicable federal regulations regarding restrictions on public disclosure to the extent such information has been identified as proprietary. Copies made by the NRC must include the copyright notice in all instances and the proprietary notice if the original was identified as proprietary.



**UNITED STATES  
NUCLEAR REGULATORY COMMISSION**

WASHINGTON, D.C. 20555-0001

June 30, 2000

Mr. Ian C. Rickard, Director  
Nuclear Licensing  
Combustion Engineering Nuclear Power  
2000 Day Hill Road  
P.O. Box 500  
Windsor, Connecticut 06095-0500

**SUBJECT: ACCEPTANCE FOR REFERENCING OF CENPD-392-P, "10X10 SVEA FUEL  
CRITICAL POWER EXPERIMENTS AND CPR CORRELATIONS: SVEA-96"  
(TAC NO. MA5999)**

Dear Mr. Rickard:

We have concluded our review of the subject topical report submitted by Combustion Engineering Nuclear Power, Inc (ABB-CE) by letter dated May 28, 1999. The report is acceptable for referencing in licensing applications subject to the limitations specified in the report and in the associated NRC safety evaluation (SE), which is enclosed. The SE defines the basis of acceptance of the report.

This report describes the analyses conducted by ABB-CE pertaining to the application of the critical power correlation to the SVEA-96 fuel design. The critical power ratio (CPR) correlation for the ABB SVEA-96 fuel is referred to as ABBD1.0. The ABBD1.0 correlation was developed by ABB-CE for application to design and licensing calculations for the SVEA-96 water cross fuel assemblies over the range of steady state, and operational transient conditions for boiling water reactor (BWR) plants.

Pursuant to 10 CFR 2.790, we have determined that the enclosed SE does not contain proprietary information. However, we will delay placing the SE in the public document room for a period of ten (10) working days from the date of this letter to provide you with the opportunity to comment on the proprietary aspects only. If you believe that any information in the enclosure is proprietary, please identify such information line by line and define the basis pursuant to the criteria of 10 CFR 2.790.

We do not intend to repeat our review of the matters described in the report, and found acceptable, when the report appears as a reference in license applications, except to assure that the material presented is applicable to the specific plant involved. Our acceptance applies only to matters described in the report.

In accordance with procedures established in NUREG-0390, "Topical Report Review Status," we request that ABB Combustion Engineering publish accepted versions of this topical report, proprietary and non-proprietary, within 3 months of receipt of this letter. The accepted versions shall incorporate this letter and the enclosed SE between the title page and the abstract. It must be well indexed such that information is readily located. Also, it must contain in appendices historical review information, such as questions and accepted responses, and

Mr. Ian C. Rickard

- 2 -

June 30, 2000

original report pages that were replaced. The accepted versions shall include an "-A" (designating accepted) following the report identification symbol.

Should our criteria or regulations change so that our conclusions as to the acceptability of the report are invalidated, Combustion Engineering Nuclear Power and/or the applicants referencing the topical report will be expected to revise and resubmit their respective documentation, or submit justification for the continued applicability of the topical report without revision of their respective documentation.

Sincerely,

A handwritten signature in black ink, appearing to read 'Stuart A. Richards', with a stylized, sweeping flourish at the end.

Stuart A. Richards, Director  
Project Directorate IV & Decommissioning  
Division of Licensing Project Management  
Office of Nuclear Reactor Regulation

Project No. 692

Enclosure: Safety Evaluation

cc w/encl: See next page



UNITED STATES  
NUCLEAR REGULATORY COMMISSION  
WASHINGTON, D.C. 20555-0001

SAFETY EVALUATION BY THE OFFICE OF NUCLEAR REACTOR REGULATION  
RELATING TO TOPICAL REPORT CENPD-392-P,  
"10x10 SVEA FUEL CRITICAL POWER EXPERIMENTS AND  
CPR CORRELATIONS: SVEA-96"  
ABB COMBUSTION ENGINEERING, INC.

1.0 INTRODUCTION AND BACKGROUND

CENPD-392-P describes the analyses conducted by (ABB-CE) pertaining to the application of the critical power correlation to the SVEA-96 fuel design (Reference 1). The critical power ratio (CPR) correlation for the ABB SVEA-96 fuel is referred to as ABBD1.0. The SVEA-96 fuel assembly design is very similar to the NRC approved SVEA-96+ fuel assembly design, and each consist of four sub-bundles in a 5x5 lattice configuration with one fuel rod missing. The only difference between the SVEA-96 and the SVEA-96+ assemblies is in the design, number, and location of the spacers (Reference 2).

The ABBD1.0 correlation was developed by ABB-CE for application to design and licensing calculations for the SVEA-96 water cross fuel assemblies over the range of steady state and operational transient conditions for boiling water reactor (BWR) plants. The ABBD1.0 correlation for the SVEA-96 fuel is very similar to the NRC-approved ABBD2.0 correlation for the SVEA-96+ fuel, and is intended to replace the existing the XL-S96 correlation (Reference 3) currently in use with the SVEA-96 fuel. The XL-S96 correlation was developed with cosine axial power shape, while the ABBD1.0 correlation was developed with substantial additional data, including top-peaked and bottom-peaked axial power shape data that was not available at the time of the development of the XL-S96 correlation. As expected, the additional data resulted in a much enhanced correlation now referred to as the ABBD1.0 correlation.

CENPD-392-P provides a description of the methodology behind the application of the ABBD1.0 correlation to the ABB-CE SVEA-96 fuel design. CENPD-392-P also contains test data taken specifically at the FRIGG loop test facility at Vasteras, Sweden, in support of the application of the ABBD1.0 correlation to the SVEA-96 fuel design, and to the determination of the associated correlation "Additive Constants."

The additive constants are determined in accordance with the NRC-approved procedure described in reference 3. The uncertainties associated with these additive constants are then used in the approved ABB-CE safety limit methodology for BWR fuel designs. The approved methodology is used to ensure that less than 0.1 percent of the fuel rods are in boiling transition during steady-state operation and during anticipated operational occurrences.

The ABBD1.0 correlation is similar to the XL-S96 correlation described in reference 3. However, the definitions of the associated parameters (dependent and independent) as described in Reference 1, are specific to the application of the ABBD1.0 correlation to the SVEA-96 fuel design. The technical analysis of the ABBD1.0 correlation and its exclusive application to the SVEA-96 fuel type is presented below.

## 2.0 EVALUATION

### 2.1 The ABBD1.0 Correlation

The ABBD1.0 correlation is a new correlation designed and developed to address the critical power behavior of the ABB-CE SVEA-96 fuel design. The ABBD1.0 correlation is an empirically derived correlation from the SVEA-96 fuel test data using the critical quality-boiling length form directly derived from the base GEXL correlation developed by General Electric (Reference 4). The critical quality-boiling length correlation represents a proven form capable of adequately predicting the onset of dryout during a transient.

The ABBD1.0 correlation is an empirically derived expression that is a complex function of the input parameters: boiling-length, mass flow, and system pressure. These input parameters cover the ranges of pressure, mass velocity, and inlet cooling, consistent with expected operating and accident conditions. The correlation is based on local coolant conditions predicted from uniform and non-uniform axial power distribution test data. The correlation includes correction factors to account for geometry and non-uniform axial power distributions that deviate from the test data conditions.

Low-flow and high-flow behavior of the correlation are captured by refining the parameters in the correlation equations. These parameters address the impact of the variations in the local enthalpy from the planar average enthalpy. One of these parameters is the R-effective, which characterizes the fuel rod local behavior, such as enthalpy rise, and which also factors in additive constants into the calculations. The additive constants are a measure of the dryout sensitivity of each rod in the sub-bundle.

Although the ABBD1.0 correlation is derived from sub-bundle data, ABBD1.0 is applied to full bundles. Overprediction of the critical power is prevented by assuring that the R-factor is modified to accommodate the sub-bundle mismatch among the four sub-bundles comprising the SVEA-96 fuel assembly.

### 2.2 SVEA-96 Data Base and Test Strategy

The ABBD1.0 correlation data base consisted of 1612 steady-state 24-rod sub-bundle data points. Eighty percent of this data was used to develop the ABBD1.0 correlation and 20 percent of this data set was used to validate the ABBD1.0 correlation. All data was taken at the FRIGG loop at the ABB-Atom laboratories at Vasteras, Sweden. The test setup consists of electrically heated rods that are physically the same as the SVEA 96 fuel assembly. The tests are designed to reproduce the local conditions typically present in a BWR fuel assembly and support the full range of applicability of the ABBD1.0 correlation.



The sub-bundle assemblies were tested subject to the intended full range applicability of the SVEA-96 fuel. The test programs were developed to accumulate a data base representative of the appropriate statistical requirements for the SVEA-96 fuel design. This approach ensures that an adequate number of tests are performed and that sufficient data are gathered to perform appropriate simulation of the behavior of the SVEA-96 fuel design.

Both steady-state and transient tests were performed as part of the validation of the ABBD1.0 correlation. In each case, the tests were designed to include test runs with peaked rods at selected locations. The data base consists of more than 1600 data points taken in a large number of tests performed at the FRIGG test facility. The data base consists of top peaked, bottom peaked, and cosine axial power shapes accounting for adjacent rod positions, rods on the interior of an assembly, and rods adjacent to the water cross, a feature unique to the SVEA-96 fuel design.

The local power peaking patterns were selected to determine the effects of the top peaked axial power profiles as compared to the cosine power profiles in several regions of the test bundle. Local power peaking data were also collected at the corners, and peripheral rows, as well as around the internal water cross to ensure complete understanding of the fuel bundle power performance in these regions.

The range of local power distributions were selected to cover local power distributions expected during reactor operations and to allow an accurate determination of the dryout sensitivity of each fuel rod in the sub-bundle. A broad range of sub-bundle power mismatch factors are also obtained to account for sub-bundle power differences among the four sub-bundles (References 1 and 2). In addition, the full range of R-factors anticipated during normal BWR operations, as well as anticipated operational occurrences (AOOs) and accidents, were covered by the large number of local power distributions performed in the sub-bundle and full bundle tests.

All the data collected was validated by performing periodic instrumentation reliability checks, as well as conducting periodic calibration checks to ensure the accuracy of the data. Instrumentation were checked before and after each test period. Heat balances were performed to ensure that power, flow, and temperature measurements were correct. Pressure drop across the bundle and at different flow rates were measured. Power generated by the heater rods were compared to that of the power supply output for all test points subject to the criteria that the two bundle powers had to agree within +/-1 percent.

### 2.3 Description of the ABBD1.0 Additive Constants

Correlation parameters such as R-factors account for the local peaking factor effect on the bundle critical power. One part of the R-factor accounts for the local power distribution of the rod of interest and its immediate neighbors, the other part accounts for other local effects, such as bundle cross section geometry and spacer grid designs. These spacer and bundle geometry effects influence the critical power behavior of the bundle. Therefore, an offset term is applied to each rod in the bundle, subject to the rod's position in the bundle. This offset term is called the "additive constant." The additive constant can be considered as a flow/enthalpy redistribution characteristic of a particular lattice/spacer design, so the additive constants are unique to a particular fuel design.

ABB-CE's testing program consisted of a number of tests conducted at different local rod power distributions, selected in a systematic way, to ensure that each unique rod location has a sufficient database to determine an associated unique additive constant. The additive constants are explicitly determined for each lattice/spacer design configuration and are utilized in design calculations for the corresponding fuel bundle.

To assert the ability of the correlation to predict steady-state as well as transient upskew and downskew axial power shape, only the cosine test data were used in the determination of the additive constants, thus validating the use of the additive constants in steady-state and transient calculations. The additive constants are experimentally determined from a large data bank representative of the power profile expected during the operational range of the SVEA-96 fuel design.

### 3.0 STATISTICAL ASPECTS OF THE SVEA-96 CORRELATION

The ABBD1.0 correlation is designed to predict heat flux from several physical input parameters, including mass flux, outlet pressure, subcooling temperature, and power shape ("profile"). The data base used in the evaluation ("correlation development") stage consists of 1289 steady-state critical power points. These points reflect 234 sub-bundle local power distributions, randomly selected to represent the complete applicable range of the input parameters. The selection of the associated points was made by using well established Monte Carlo procedures.

Perhaps the most telling performance index derived in this study, regarding the correlation ability to "predict" is the CPR. A good correlation would predict a CPR value near 1.00 (unity), with a very small associated uncertainty. ABB-CE's calculation fluctuates near 1.00 for all subsets of the data (different pressure, mass flux, and subcooling range). The calculation of the CPR also involves the calculation of an individual additive constant that accounts for the geometric position of a rod within a bundle. A detailed description of the process used in identifying and generating those constants is given in Chapter 4 of the topical report; since the calculated additive constant are estimates, there is a measure of variability associated with their calculation. Both additive constants and their variability are considered in the total variability of the correlation development. No attempt is made (nor is one needed) to isolate or calculate the contribution of individual components from the total variability of the correlation.

To ensure that the overall uncertainty of the correlation is within the accepted limit, ABB-CE performed a 95/95 upper tolerance limits for the CPR calculations (Reference 1, Tables D 5.3 and D 5.5). The staff confirmed ABB-CE's limits by running parallel calculations using parametric (less conservative, assuming a normal distribution) statistics. Both ABB-CE's and the NRC staff's calculation of the 95/95 upper tolerance limit were found to be well within reasonable and acceptable statistical bounds.

The applicability and behavior of the correlation over a wide range of parameters was demonstrated and documented by charting (plotting) the correlation against a full range of each parameter of interest. The charts demonstrate convincingly that the correlation is more than adequate in its ability to predict the CPR. Furthermore, the quality (error) associated with the

CPR calculation does not deteriorate as one moves from one range of the parameter to another.

The validation of the correlation is achieved by applying the prediction method to assemblies that are not part of the evaluation (correlation construction) data. To that end ABB-CE uses 323 sub-bundle critical power points. The mean error of the sub-bundle validation data is smaller, in both magnitude of error and in the associated standard deviation, than the statistics obtained for the evaluation data, thus validating the appropriateness of the correlation for sub-bundle operations.

#### 4.0 SVEA-96 CORRELATION BEHAVIOR

The SVEA-96 correlation (ABBD1.0) was tested to ensure smooth functions and that no significant discontinuities exist in its behavior over the entire range of operability of the fuel. ABBD1.0 is a critical boiling-length plane correlation. Its main objective is to correlate the SVEA-96 critical power test data. The boiling-length correlation has proven in the past (GE has used it and continues to use this type of correlation), to be a very good correlation for representing the onset of dryout during steady-state and transient conditions. The credibility of ABBD1.0 (which was formulated under steady-state conditions), is established by adequately predicting the change in critical power during a transient condition.

A number of tests were conducted to determine the sensitivity of the major functions within the ABBD1.0 to flow, inlet -subcooling, pressure variation, R-factors, and axial power shape. The R-factors account for the local power distributions, cross section geometry, and the spacer grid configuration. Review of the data, figures, and tables, indicate that the SVEA-96 correlation behaves well over the applicable range of the fuel.

#### 5.0 SVEA-96 CORRELATION VALIDATION

ABB-CE performed several tests to validate the behavior of the SVEA-96 correlation in steady-state and transient events. The validation data base consisted of steady-state data points that were not included in the correlation data base. The data were collected from tests conducted on 24-rod sub-bundles. The validation data set (20 percent of the total data set) was used to: (1) validate the analytical method of the ABBD1.0 critical power ratio (CPR) correlation, and (2) to further validate the overall predictive capability of the ABBD1.0 CPR correlation. The predicted results of the ABBD1.0 correlation critical power versus the measured critical power for these tests showed very good agreement and that no biases exist as a function of critical power, mass flux, inlet subcooling or outlet pressure. In addition, no bias was detected with respect to the ABBD1.0 correlation as a function of the R-factor and as a function of boiling length. After reviewing submitted figures and tables indicative of the ABBD1.0 correlation behavior, the staff agrees with the conclusion that the ABBD1.0 correlation provides a good fit to the test data, and that no apparent systematic biases exist that would limit the validation of the correlation to predict the bundle critical power performance in design and licensing applications.

## 6.0 ABBD1.0 TRANSIENT APPLICATION

Transient CPR predictions involve evaluation of the flow, enthalpy, and pressure in the fuel assembly at each axial node as a function of time during the transient. ABB-CE uses the BISON-SLAVE channel code to conduct the transient system analysis. ABB-CE's objective of this analysis is to confirm the proper implementation of the steady-state CPR correlation in the transient code and also to confirm the capability of the steady-state CPR correlation to calculate dryout during transients with adequate accuracy to provide conservative predictions.

The NRC-approved ABBD2.0 correlation (Reference 2) also used the BISON-SLAVE code to demonstrate the ability of the ABBD2.0 correlation to conservatively predict transient behavior. Since the ABBD1.0 correlation is very similar in construction (different coefficients), ABB-CE assumed that the ABBD1.0 correlation, in conjunction with the BISON-SLAVE code, will also predict conservative results. The staff agrees with this conclusion.

The same transient data used to validate the approved XL-S96 correlation (Reference 3) for the same SVEA-96 fuel, was used to validate the transient behavior of the ABBD1.0 correlation.

The BISON-SLAVE channel version of the time domain reactor dynamics code BISON (References 5 and 6) is used in conjunction with the ABBD1.0 CPR correlation to predict transient CPR behavior for reload fuel licensing analysis applications and other operational transient simulations.

BISON is a time domain BWR dynamics code used for analyzing operational and safety related transients. The core simulates the entire primary core coolant loop including the recirculating pumps. A two-group diffusion theory model describes the axial distributions of neutron flux and power generation in the reactor core. Heat conduction in the fuel is solved in the radial direction at each axial segment. The influence from external systems such as the turbine, control systems, scram signals and relief valves can also be simulated in BISON. The ABBD1.0 CPR correlation is incorporated in the BISON-SLAVE code. The various instantaneous fluid properties such as mass flow, pressure, and inlet subcooling, are used in evaluating the CPR correlation under transient condition.

Five transient tests were conducted at the FRIGG loop. All five tests were simulated by the BISON-SLAVE code. The BISON-SLAVE code was used in conjunction with the ABBD1.0 correlation to predict transient critical power ratio (CPR) behavior for reload fuel licensing analysis applications and other operational transient simulations. Review of the BISON-SLAVE simulation results indicates that the BISON-SLAVE code predicted dryout to occur in two of the five tests, thus demonstrating that the dryout threshold in the BISON-SLAVE code provides a conservative indication of dryout. Predicted times to dryout were also compared with measured times to dryout, with the BISON-SLAVE code predicting shorter times to dryout than measured times for all five tests. Thus, the predicted BISON-SLAVE times are conservative. The staff agrees with the submitted analysis and results.

## 7.0 TECHNOLOGY TRANSFER

ABB-CE described the technology transfer program (Reference 7) which the licensees must successfully complete in order to perform their own thermal-hydraulic calculations using any ABB-CE BWR CPR correlation and associated transient code in support of reload analyses, and which has satisfied the appropriate NRC acceptance criteria. The overall process consists of training, benchmarking, and change control. In addition, ABB-CE described the process for a licensee to implement the NRC approved correlation. This process includes performance of an independent benchmarking calculation by ABB-CE for comparison to the licensee-generated results to verify that the new CPR correlation is properly applied. The staff has reviewed the process and finds it acceptable because training benchmarking and change control have been adequately addressed.

## 8.0 CONCLUSION

The staff has reviewed the analyses in Topical Report CENPD-392-P, "10X10 SVEA Fuel Critical Power Experiments and CPR Correlations: SVEA-96." Topical Report CENPD-392-P is acceptable for licensing applications, subject to the range of parameters which encompass the test data used to develop the ABBD1.0 CPR correlation. If ABB-CE wishes to extend the range of applicability of the ABBD1.0 CPR correlation beyond the data range documented in Table 5.7 in Section 5 of CENPD-392-P, it will either revalidate or develop a new correlation and submit one or the other for NRC staff review and approval. ABB-CE concurs with this conclusion (Reference 7).

## 9.0 REFERENCES

1. Letter from Ian C. Rickard to the U.S. Nuclear Regulatory Commission, submitting Topical Report CENPD-392-P, May 28, 1999.
2. Letter from Ian C. Rickard to the U.S. Nuclear Regulatory Commission, submitting Topical Report CENPD-389-P, June 9, 1998.
3. "SVEA-96 Critical Power Experiments on Full Scale 24-Rod Sub-Bundle," ABB Report UR-89-210-P-A, October 1993.
4. "General Electric BWR Thermal Analysis Basis (GETAB): Data, Correlation and Design Application," NEDO-10958, November 1973.
5. "BISON - A One Dimensional Dynamic Analysis Code for Boiling Water Reactors," ABB Report RPA 90-90-P-A, December 1991.
6. "BISON - A One Dimensional Dynamic Analysis Code for Boiling Water Reactors: Supplement 1 to Code Description and Qualification," ABB Report CENPD-292-P-A, July 1996.

7. Letter from Ian C. Rickard to the U.S. Nuclear Regulatory Commission, "Methodology Constraint Affirmation and Minimum Criteria for Licensee Performing Licensing Basis Analyses Using the ABB1.0 CPR Correlation," May 8, 2000.

Principal Contributor: A. Attard

Date: June 30, 2000

TABLE OF CONTENTS

ABSTRACT.....	iii
1 INTRODUCTION .....	1
2 TEST FACILITY.....	4
2.1 Description.....	4
2.2 TEST SECTION.....	4
2.3 HEATER RODS.....	6
2.4 POWER SUPPLY AND CONTROL.....	7
2.5 INSTRUMENTATION .....	7
2.6 DATA ACQUISITION SYSTEM.....	8
2.7 CRITICAL POWER TESTING PROCEDURE.....	9
3 TEST PROGRAM.....	21
3.1 RANGE OF TEST PARAMETERS.....	21
3.2 JUSTIFICATION FOR RANGE OF TEST PARAMETERS.....	22
3.2.1 Mass Flux.....	22
3.2.2 System Pressure .....	22
3.2.3 Inlet Subcooling.....	23
3.2.4 Axial Power Distribution.....	23
3.2.5 Local Power Distribution.....	23
3.2.6 Combinations of Parameters.....	24
3.2.7 Summary .....	24
3.3 DATA VALIDATION CRITERIA AND PROCEDURES.....	25
3.4 DATA TRENDS.....	27
3.4.1 SVEA-96 Sub-bundle Cosine Axial Power Shape Tests (SF24A).....	27
3.4.2 SVEA-96 Sub-bundle Bottom-and Top-peaked Axial Power Shape Tests .....	27
4 CRITICAL POWER CORRELATION.....	64
4.1 FORM OF THE CORRELATION .....	64
4.2 ABBD1.0 CPR CORRELATION.....	65
4.3 CALCULATION OF THE SUB-BUNDLE R-FACTOR FOR SVEA-96.....	68
4.4 DETERMINATION OF ABBD1.0 ADDITIVE CONSTANTS AND CORRELATION COEFFICIENTS.....	69
4.5 ASSEMBLY R-FACTOR - TREATMENT OF SUB-BUNDLE POWER MISMATCH.....	71

5	CORRELATION EVALUATION .....	77
5.1	ABBD1.0 PERFORMANCE RELATIVE TO THE SVEA-96 DATA BASE .....	77
5.2	CORRELATION UNCERTAINTY AND RANGE OF THE CORRELATION .....	81
6	CONFIRMATION FOR TRANSIENT APPLICATION.....	114
6.1	INTRODUCTION .....	114
6.2	TRANSIENT IMPLEMENTATION VALIDATION METHODOLOGY .....	115
6.3	TRANSIENT DRYOUT EXPERIMENTS .....	116
6.3.1	FRIGG Loop .....	116
6.3.2	Test Section.....	116
6.3.3	Transient Tests Description .....	116
6.3.4	Dryout Threshold Temperature.....	117
6.3.5	Transient Data .....	117
6.4	IMPLEMENTATION VALIDATION FOR BISON CODE .....	117
6.4.1	BISON Code .....	118
6.4.2	BISON Model .....	118
6.4.3	BISON Test Simulation Results .....	119
6.5	SUMMARY .....	119
7	CONCLUSIONS.....	129
8	REFERENCES .....	131
APPENDIX A	SVEA-96 ASSEMBLY DESCRIPTION .....	A-1
APPENDIX B	SVEA 96 STEADY STATE CRITICAL POWER TEST DATA (BOTTOM-PEAKED AXIAL POWER SHAPE) .....	B-1
APPENDIX C	SVEA 96 STEADY STATE CRITICAL POWER TEST DATA (TOP- PEAKED AXIAL POWER SHAPE).....	C-1
APPENDIX D	RESPONSE TO THE NRC REQUEST FOR ADDITIONAL INFORMATION .....	D-1



## ABSTRACT

ABB is currently completing a program expanding the critical power data bases and developing improved Critical Power Ratio (CPR) correlations for ABB 10x10 SVEA fuel. Critical power data have been obtained for the SVEA-96, SVEA-96+ and SVEA-96 Optima designs. The SVEA-96 Optima design is an advanced product that has not yet been introduced in reload quantities. Based on measurements for these fuel designs, advanced CPR correlations utilizing the same general form have been established for the SVEA-96, SVEA-96+ and SVEA-96 Optima designs.

This report describes the development of the advanced critical power correlation for ABB SVEA-96 BWR fuel assemblies. The advanced CPR correlation for SVEA-96 fuel is referred to as ABBD1.0. A report (CENPD-389-P-A) that describes the corresponding advanced CPR correlation for SVEA-96+ fuel has been reviewed and accepted by NRC. It is anticipated that a subsequent report will be submitted for the SVEA-96 Optima design.

The current CPR correlation for the SVEA-96 assembly is referred to as the XL-S96 CPR correlation. The XL-S96 CPR correlation has been reviewed and approved by the NRC and is described in UR 89-210-P-A.

Three different test series have been performed for the ABBD1.0 CPR correlation development. These test series were performed with 24-rod sub-bundles with three different axial power shapes. The tests include measurements of critical power at pressures between [ ] and an inlet subcooling temperature range from [ ]. The mass flux range in the tests is [ ]. The critical power measurements were performed at [ ] different local power distributions to capture the influence on critical power of various local peaking factors and various peak power rod locations.

The SVEA-96 data from the measurements were correlated by adapting a critical power correlation with a critical quality/boiling length form [ ]. This CPR correlation is referred to as the ABBD1.0 correlation.

The ABBD1.0 correlation predicts the measured critical powers over the entire data base with a mean error of [ ].

## 1 INTRODUCTION

This report describes the development of an advanced critical power ratio (CPR) correlation for the ABB SVEA-96 water cross BWR fuel assembly. The SVEA-96 fuel assembly is described in detail in UR-89-210-P-A (Reference 1). The SVEA-96 assembly is composed of four sub-bundles in a 5x5 lattice configuration with one fuel rod missing and [ ] For convenience, a brief overview of the SVEA-96 assembly is provided in Appendix A.

The current CPR correlation for the SVEA-96 assembly is referred to as the XL-S96 CPR correlation. The XL-S96 CPR correlation has been reviewed and accepted by the NRC and is described in Reference 1. The XL-S96 CPR correlation was developed based on cosine axial power shape tests. The CPR correlation for SVEA-96 fuel described in this report is based on an expanded data base including top-peaked and bottom-peaked axial power shape data and is referred to as ABBD1.0. The SVEA-96+ testing and correlation development program discussed in References 5 through 7 indicated a SVEA-96 assembly CPR correlation based on an expanded data base including top-peaked and bottom-peaked axial power shape data in conjunction with the form used for ABBD2.0 could represent an improvement relative to the XL-S96 correlation described in Reference 1.

The SVEA-96 Critical Power data obtained for a cosine axial power shape is described in Section 3 and Appendix A of Reference 1. These data have also been used in the development of the ABBD1.0 CPR correlation described in this report. The ABBD1.0 CPR correlation data base also contains Critical Power measurements based on top-peaked and bottom-peaked axial power shapes. The Critical Power measurement data based on top-peaked and bottom-peaked axial power shapes are contained in this report. The sub-bundle R-factor model in the XL-S96 CPR correlation has been retained for the ABBD1.0 correlation. As shown in this report, the additive constants developed for the XL-S96 CPR correlation in Reference 1, in conjunction with the optimized ABBD1.0 correlation parameters, provide a good fit to the expanded SVEA-96 data base containing cosine, top-peaked, and bottom-peaked axial power shapes. Therefore, the additive constants developed in Reference 1 were retained for the ABBD1.0 CPR correlation, and the description of their derivation is not repeated in this report. The practice of basing the derivation of additive constants on the cosine axial power shape data base was also successfully applied to the ABBD2.0 CPR correlation described in References 5 through 7.

The critical power test section consisted of a 24-rod bundle simulating a sub-bundle of the SVEA-96 fuel assembly. Indirectly heated rods connected to several individual rectifier units made it possible to control the local power (i.e. relative rod power) distribution in a simple way and test a wide range of local power

distributions. The objectives of these tests and the CPR evaluation program were as follows:

1. To expand the SVEA-96 data base to include top-peaked and bottom-peaked axial power shapes and to support the same type of CPR correlation formulation which has been adopted for SVEA-96+ fuel (Reference 5).
2. To confirm that the CPR correlation for the SVEA-96 assembly (ABBD1.0) developed from the steady state critical power data base adequately describes the data base and to establish appropriate biases and uncertainties for licensing applications. Since the correlation was developed from steady state data, it will provide best estimate CPR values for steady state applications. For licensing applications, the correlation will be applied in computer codes accepted by the NRC.
3. To confirm that the CPR correlation for the SVEA-96 assembly (ABBD1.0) established under steady state conditions provides an adequate description of the change in critical power ( $\Delta\text{CPR}$ ) during transient applications. This confirmation is performed by comparing the predictions of the ABBD1.0 CPR correlation for transient conditions with available transient CPR test data. The ABBD1.0 CPR correlation is compared with the same SVEA-96 transient data base described in Reference 1. The ABB methodology for performing this confirmation is illustrated for the BISON-SLAVE code documented in Reference 2.

The test matrix described in Reference 1 and in this document was selected to cover the entire steady state and transient operating range expected for U.S. BWR's and to sufficiently cover off nominal conditions to allow its application to transient and accident conditions. Particular emphasis has been placed on capturing the dependence of local power distributions within the bundle since this is expected to be a very important bundle-specific effect.

The ABBD1.0 critical power correlation developed for the SVEA-96 assembly is a critical quality-boiling length form [ .] It is referred to as the ABBD1.0 correlation. [

.]

[

.]

The degree to which the correlation fits the experimental data is reflected by the average percent deviation of the correlation prediction relative to the measured critical power over the entire data range. [

.]

The ABBD1.0 CPR correlation has been implemented in the BISON-SLAVE dynamic system transient analysis code. Conservative predictions of CPR behavior during postulated transients has been demonstrated by comparisons of BISON-SLAVE code/ABBD1.0 correlation predictions with FRIGG Loop dynamic flow reduction test data. These results using ABBD1.0 provide further confirmation of the conclusion reached in Reference 5 that a CPR correlation with the ABBD1.0/ABBD2.0 correlation form derived from steady-state data in conjunction with the BISON-SLAVE code provides a conservative treatment of CPR changes during postulated transients. The evaluation in Section 6 provides an illustration using the BISON-SLAVE dynamic code of the ABB methodology for confirming that a CPR correlation based on steady-state data conservatively predicts CPR behavior under transient conditions. This methodology can also be used to confirm that other CPR changes during transient events are conservatively treated in other dynamic codes.

## 2 TEST FACILITY

The cosine axial power shape tests supporting the ABBD1.0 CPR correlation were described in detail in Reference 1. The additional test results with bottom-peaked and top-peaked axial power shapes supporting the ABBD1.0 CPR correlation are described in this document.

All of the cosine, top-peaked, and bottom-peaked axial power shape data supporting the ABBD1.0 CPR correlation were performed in the FRIGG Loop test facility. This facility, as well as the measurement of the cosine shaped axial power shape data, were described in Reference 1. Therefore, the description of the test facility and measurements in this document is focused on the measurement of the top- and bottom-peaked axial power shaped data

### 2.1 Description

The SVEA-96 critical power tests were performed in the FRIGG loop at the ABB Atom laboratories at Vasteras, Sweden. The FRIGG loop has been utilized for many years to perform thermal hydraulic tests in support of the ABB BWR nuclear program.

A diagram of the FRIGG loop is shown in Figure 2.1. The loop contains a main circulation loop with the test section, a cooling circuit, and a purification system. The head of the main circulation pump can be continuously controlled by means of a variable speed motor. When steam is produced in the test section, the loop pressure is controlled by regulating the cold water flow to spray nozzles in the condenser. Heat is removed by a heat exchanger in the cooling circuit from which water is pumped to the spray nozzles. During start-up and heat balance tests, the loop is filled with water, and the pressure is regulated by balancing the amount of water by means of the feed water pump and a drainage valve. The inlet subcooling is controlled by feeding water from the cooling circuit into the main circulation loop upstream of the pump.

The loop is designed for a maximum pressure of 100 bar and a maximum temperature of 311 °C. Carbon steel is used throughout as a construction material, and water quality is carefully controlled. Demineralized and deaerated water is used for filling the loop. Purification is continued during the tests to keep water quality within specified limits. Normally water conductivity is in the range of 0.15 - 0.30  $\mu\text{S}/\text{cm}$ .

### 2.2 Test Section

The test section consists of a pressure vessel, a Zircaloy flow channel and a SVEA 5x5-1 sub-bundle with 24 heater rods. [ ]  
To avoid deformation at extreme test conditions and the subsequent flow redistribution, the flow channel is reinforced by an outer support structure. Pressure taps are connected to the flow channel at different elevations as shown in Figure 2.2. The

pressure transmission lines are brought out of the test section through an instrumentation ring.

An orifice plate is installed at the inlet of the flow channel to provide an even distribution of flow into the channel. [

.]

The heated rods are constrained by six Inconel spacers of the same type used in the standard reload SVEA-96 assembly. Additional Inconel spacers which are not used in the standard SVEA-96 are positioned at the inlet and exit of the test section. These additional spacers do not impact the dryout results. The axial locations of the spacers and the pressure taps (DP) are shown in Figure 2.2.

The pressure vessel top flange contains pressure seals similar in design to valve stem packing seals, which retain the heater rods in fixed position. The difference in thermal expansion between the heater rods and the pressure vessel is taken care via O-ring pressure seals in the bottom flange.

Dimensions of the test section are compared with actual SVEA-96 design parameters in Figure 2.3. The design dimensions of the SVEA-96 test section, which might affect dryout, are not identical to those of the standard SVEA-96 reload fuel assembly. [

.] Therefore, the effects on critical power of the small differences between the SVEA-96 sub-bundle test section geometry and the reload fuel assembly are either negligible or are accounted for in the correlation. It should be noted that minor differences in the flow area of the test sections used for the three axial power shape test series due to the slight variations in the diameter of the rods were specifically accounted for in the correlation derivation and evaluation.

The numbers assigned to the heater rods in Figure 2.3 are used to identify the heater rods in Appendices B and C. As shown in Figure 2.3, the heater rod numbering scheme identifies the rod location in the sub-bundle.

Tables 2.1 through 2.3 and Figure 2.4 show the axial power shapes used in the three 24-rod sub-bundle test series.

### 2.3 Heater Rods

The heater rods used in the tests are indirectly heated rods rated at 200 kW at 380 V DC. A heater rod schematic is shown in Figure 2.5. Each heater rod contains a heater element, electrical insulation, Inconel-600 cladding, and [

] The heater element is made from a Monel K-500 tube. The heater element terminals consisted of a solid nickel transition piece welded to the Monel tube at one end, and a copper electrode brazed to the Monel tube at the other end. The heater-rod non-uniform axial power profile was generated by laser cutting a spiral on the Monel tube with a variable pitch.

The electrical insulation was machined from solid boron nitride (BN) pieces. After the BN sleeves were assembled over the heater element, grooves were cut axially to hold the thermocouples in position. Then the heater element assembly was inserted into the oversized Inconel tube used as cladding. The final heater rod dimensions were obtained by swaging the heater assembly to its final dimensions. The swaging operation also provided good contact between the heater element, the insulation material, and the cladding inner surface assuring good heat transfer with low variability from the heating element to the cladding surface.

The thermocouples (dryout detectors) are embedded between the cladding and the insulation sleeves. The thermocouples used were 0.5 mm ungrounded Inconel sheathed type K with MgO insulation. The thermocouple wire used was of premium grade. The thermocouple tips were backfilled with BN powder and compacted by swaging to provide a faster response to temperature changes.

[  
.] Figure 2.6 shows the rod types and the axial positions of the thermocouples used in the bottom-peaked axial power shape tests. Figure 2.7 shows the rod types and the axial positions of the thermocouples used in the top-peaked axial power shape tests.

It should be noted that in Figures 2.6 and 2.7, rod types “A” and “B” are identical with the exception of the thermocouple locations. As shown in Figure 2.6, fifteen B-type and nine A-type rods were used in the bottom-peaked axial sub-bundle tests. The thermocouples in the B-type rods in this test series are located in positions to assure that dryout with a bottom-peaked axial power shape will be detected. The thermocouples in the A-type rods are not positioned in a manner to indicate dryout. Therefore, A-type rods are placed only in symmetrical positions to the B-type rods in the bottom-peaked test section. The relative powers for the A-type rods were maintained sufficiently lower than the B-type rods in the bottom-peaked sub-bundle tests to assure that dryout would not occur on the A-type rods. As shown in Figure 2.7, fifteen A-type and nine B-type rods were used in the top-peaked axial sub-bundle tests. The thermocouples in the A-type rods in this test series are located in positions to assure that dryout with a top-peaked

axial power shape will be detected. The thermocouples in the B-type rods are not positioned in a manner to indicate dryout. Therefore, B-type rods are placed only in symmetrical positions to the A-type rods in the top-peaked test section. The relative powers for the B-type rods were maintained sufficiently lower than the A-type rods in the top-peaked sub-bundle tests to assure that dryout would not occur on the B-type rods.

## 2.4 Power Supply and Control

For the top-peaked and bottom-peaked axial power shape tests, electrical power to the heater rods was supplied by a 4.5 MW DC electrical power system operating at 380 V. The system consisted of seven units, all rated at 640 kW each.

The upgraded FRIGG loop has a very flexible system for connecting the individual heater rods to selected units. This configuration provides the capability to conveniently obtain numerous combinations of relative rod powers by adjusting the computer signals that control the voltage across each unit. It is this capability which allows a thorough determination of sub-channel factors (e.g. R-factors) providing the relative dryout sensitivity of each fuel rod.

## 2.5 Instrumentation

The parameters defining the operating conditions during the tests consist of temperature, pressure, flow, differential pressure and bundle power. These variables and the method by which they are monitored are defined as follows:

- |                                       |  |
|---------------------------------------|--|
| p (bar)                               | is the pressure at the test section outlet. The pressure is measured with a precision pressure transducer in the test section inlet. Estimated accuracy in the measured pressure is $\pm 0.5$ bar.   |
| $\Delta T$ sub ( $^{\circ}\text{C}$ ) | is the inlet subcooling. This parameter is defined as the difference between the saturation temperature at the test section outlet and the test section inlet temperature. The temperatures were measured with type-K premium grade thermocouples for the SVEA-96 sub-bundle tests. Estimated accuracy in the measured inlet subcooling is $\pm 1$ $^{\circ}\text{C}$ .  |
| Q (kW)                                | is the power provided to the coolant by the rod bundle. The power is obtained by the summation of the power generated by each heater rod. Heater rod power is calculated as the product of measured current through each rod multiplied by the measured voltage drop across the rod group in which the heater rods are connected. Heater rod current is measured by a calibrated precision shunt connected to the ground electrical leads. |

The bundle power is obtained by reducing the measured power by 0.4% to account for the heat generated in heater rod



extensions at the inlet and outlet. This power is dissipated in the flanges and is not delivered to the coolant. The estimated accuracy in measured bundle power is  $\pm 1\%$  of the reading at power levels typical at dryout.

$$G = \dot{m} / A \quad (\text{kg/m}^2\text{s})$$

is the mass flux.  $A$  is the flow area in the test bundle at room temperature. The flow rate,  $\dot{m}$ , is measured with an orifice plate in the recirculation line. The estimated accuracy in  $G$  is 20 kg/m<sup>2</sup>s.

The above accuracies in the major variables represent an accuracy (tolerance) in critical power of about  $\pm 2\%$ .

Rosemount differential pressure (D/P) cells, calibrated to an accuracy of  $\pm 0.5\%$  of full scale, were used to measure pressure drops across various part of the bundle and across the main line flow meter. The main line flow meter was equipped with two D/P cells having different ranges in order to minimize the flow measurement error due to errors in differential pressure measurements.

Thermocouples were located at five elevations along the test vessel in order to measure the fluid temperature in the annulus between the pressure vessel and the flow channel (i.e. the temperature in the bundle differential pressure transmission lines).

## 2.6 Data Acquisition System

A typical data acquisition system is shown in Figure 2.8. Signals reflecting important parameters (e.g. temperature, voltage, current differential pressure and mass flow) are connected to HP3852A data loggers. A sampling frequency of 1.0 Hz was used.

In addition to the data collecting function, the computer was also used as a dryout monitor by utilizing software which allows it to recognize a temperature rise over the initial local temperature in up to 112 heater rod thermocouples. In this case the computer identified the channel(s) indicating dryout. Steady state dryout is assumed to occur for a minimum measured temperature rise of [      ].

In addition to the dryout indication, two additional limits were used to protect the bundle. A temperature rise of 50 °C and a temperature above 450 °C automatically cause a decrease in bundle power of 25%. A temperature rise of 75 °C causes the bundle power to be shut off completely.

The dryout monitoring function must be in operation before power is provided to the test section. When dryout was detected, the loop conditions were kept constant

for about 20 seconds to clearly define average loop conditions at dryout for that test point.

## **2.7 Critical Power Testing Procedure**

The measuring instruments used and the data acquisition system are discussed in Sections 2.5 and 2.6. The tests were recorded in blocks of a maximum size of 2400 samples of each parameter, which corresponds to 2400 seconds at a sampling frequency of 1 Hz. Each block generally included several critical power measurements at different mass flows.

The procedure for establishing critical power was as follows:

- The test identification number was entered into the computer.
- The target local power distribution was entered into the computer, which established the corresponding rectifier settings.
- The target bundle inlet subcooling temperature, system pressure, and mass flux were established.
- The bundle power was slowly increased in small steps. The power was increased until a temperature excursion exceeding [       ] occurred and triggered an alarm. All the thermocouples were connected to the data loggers, and their outputs recorded during the test. In addition, selected thermocouple outputs were displayed on a monitor in the control room.

[illegible]**CE Nuclear Power LLC**

**TABLE 2.2 BOTTOM-PEAKED AXIAL POWER PROFILE**

[illegible]

**BHL = Bottom of Heated Length (See Figure 2.2)**

[illegible]

BHL = Bottom of Heated Length (See Figure 2.2)

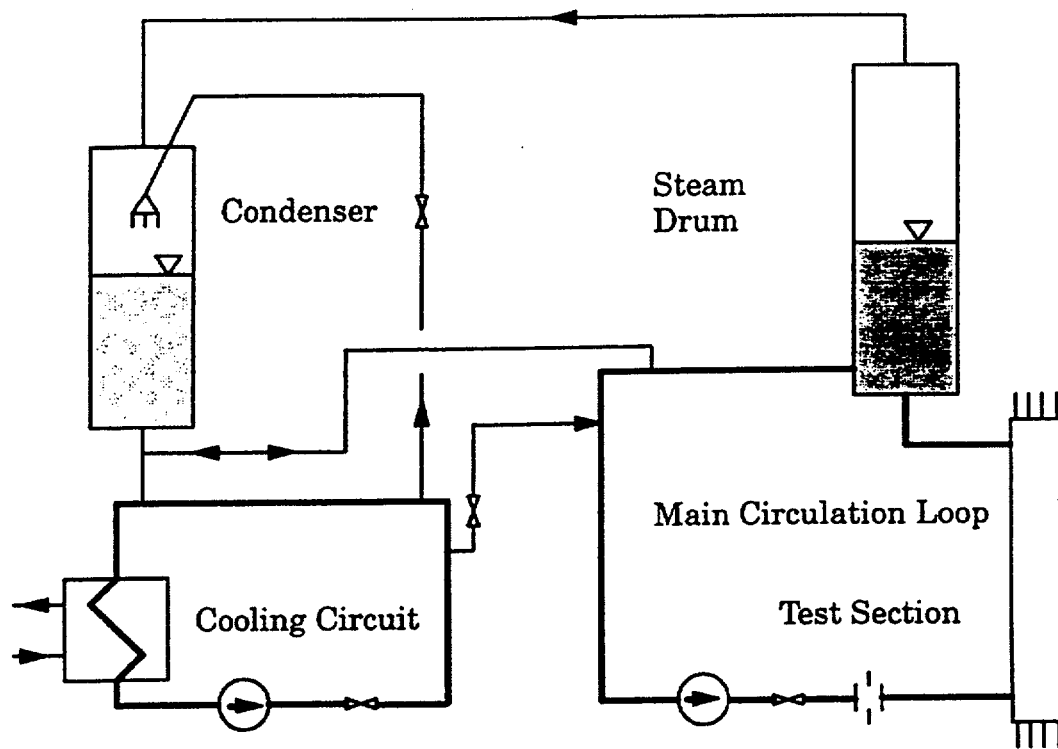
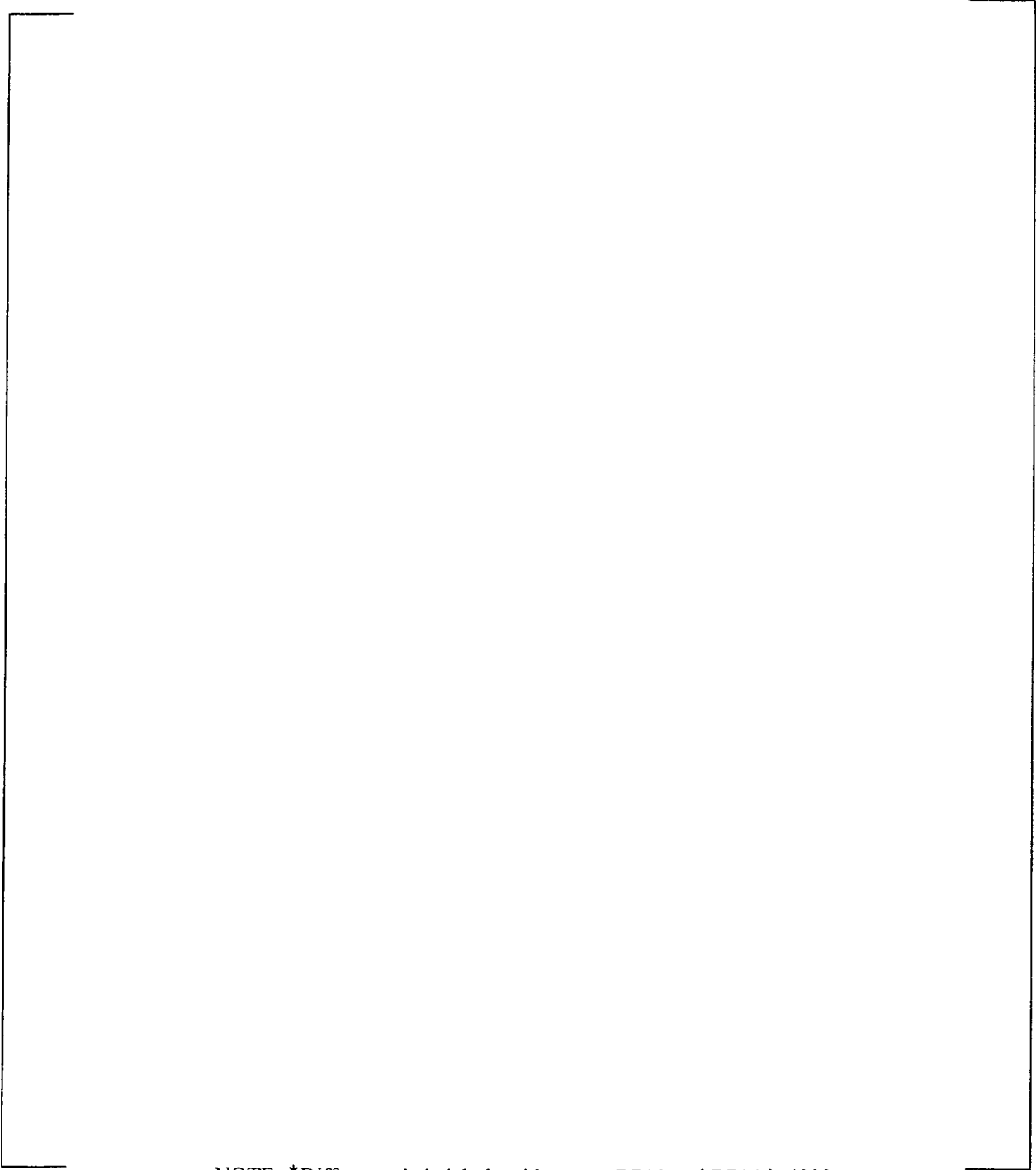


Figure 2.1 FRIGG loop diagram



NOTE: \*Difference in height level between DP10 and DP14 is 4000 mm.  
EHL - End of Heated Length, BHL - Beginning of Heated Length

Figure 2.2 Axial positions of spacers and pressure taps

Test section data

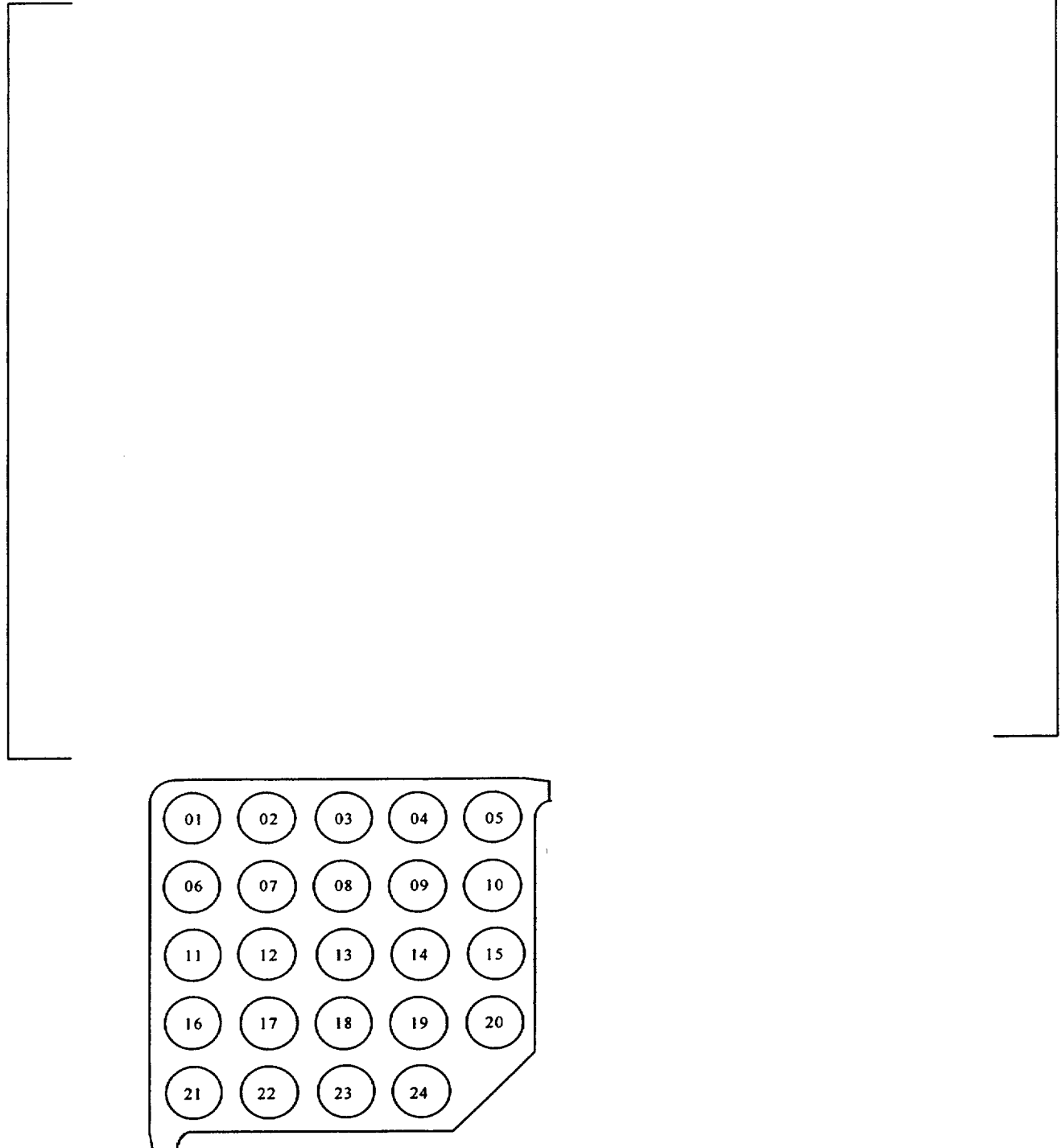


Figure 2.3 Numbering of rods in the FRIGG loop





*Figure 2.4 Axial power shape used in the FRIGG tests  
(C-cosine, B-Bottom, T-top)*

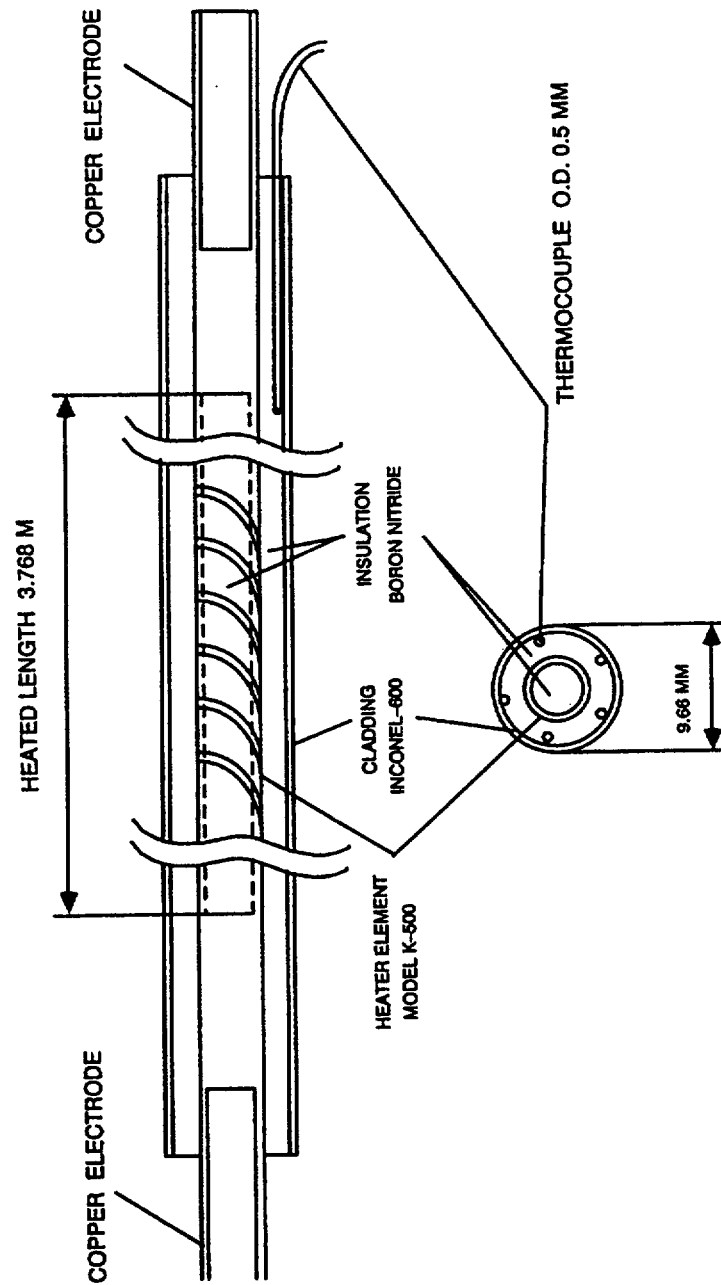


Figure 2.5 Heater rod design

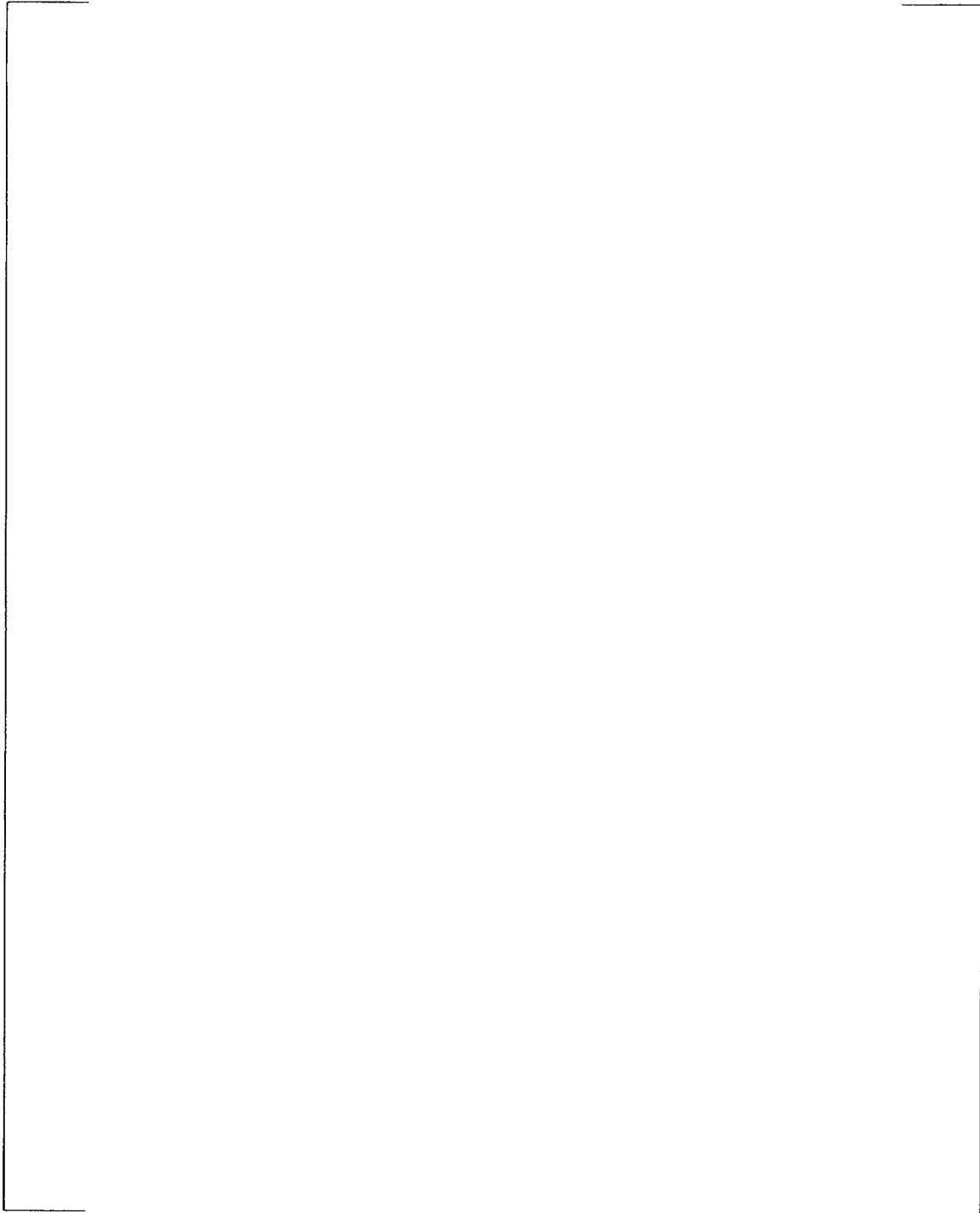


Figure 2.6 Rod types and axial positions of thermocouple  
(Bottom-peaked axial power shape tests)

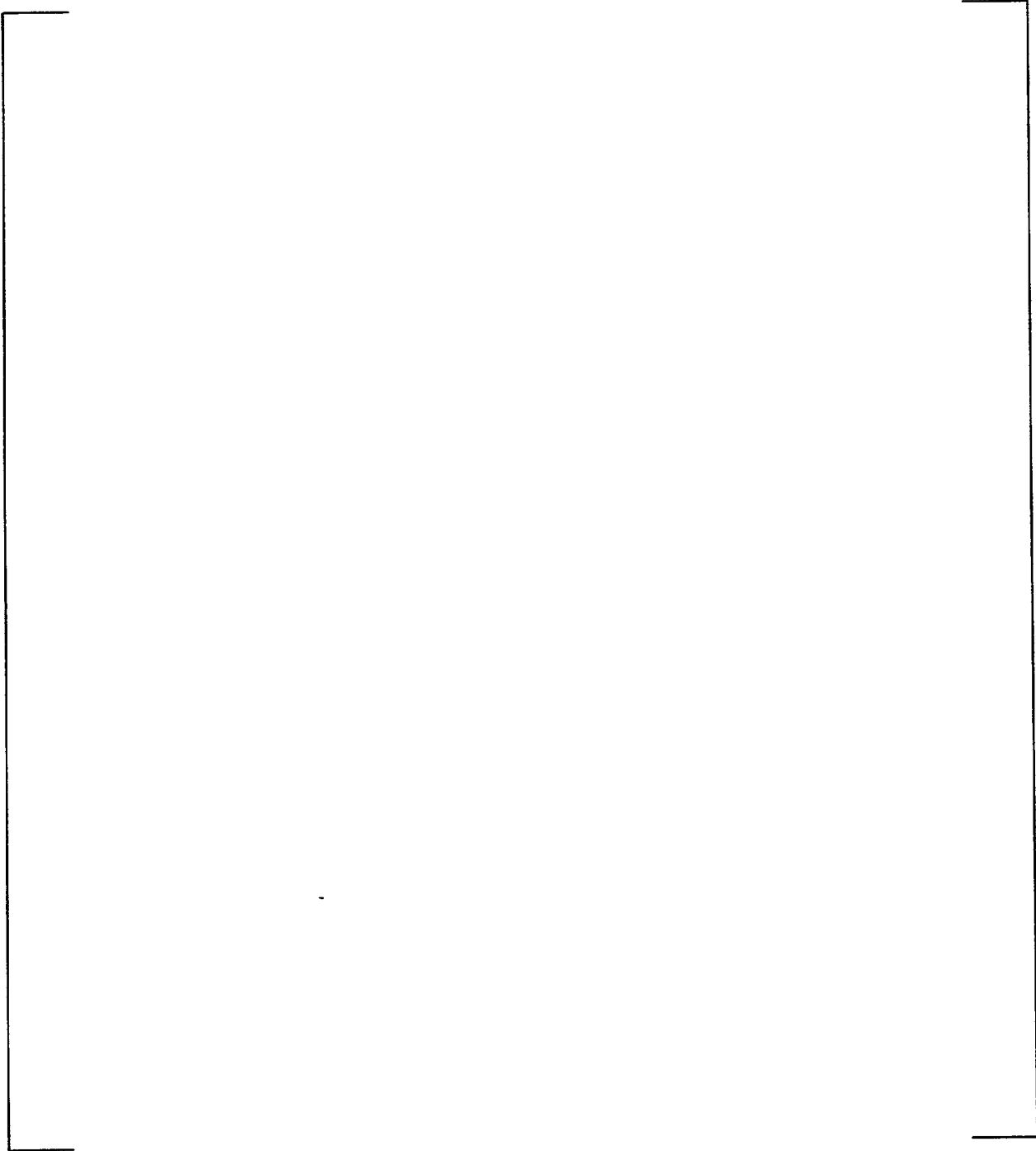


Figure 2.7 Rod types and axial positions of thermocouples  
(Top-peaked axial power shape tests)

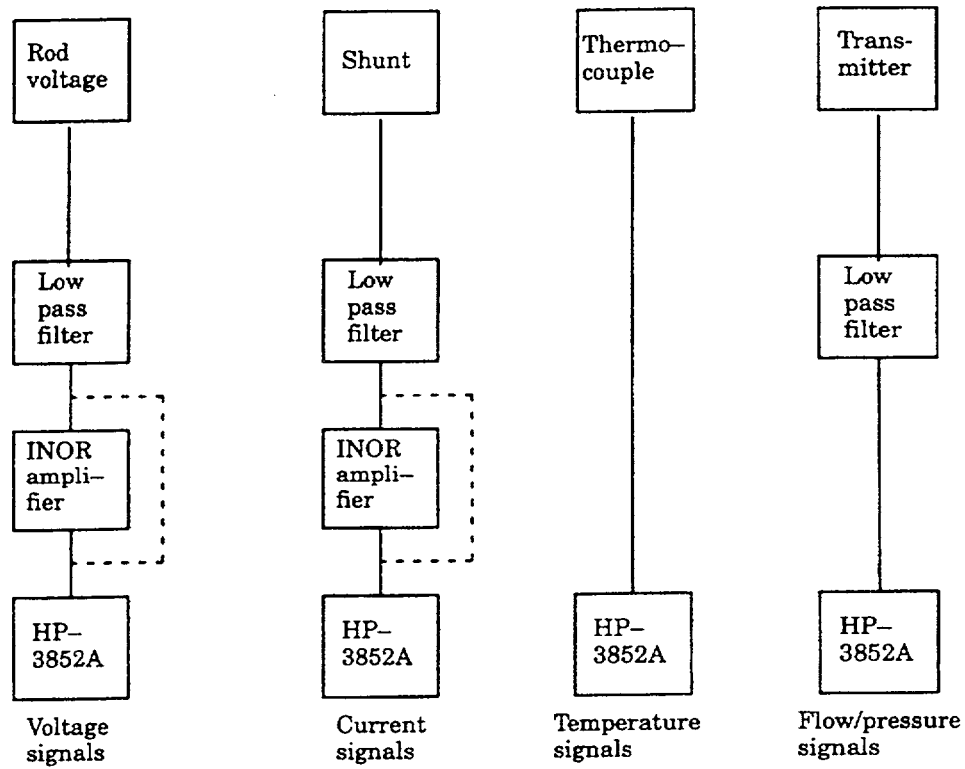


Figure 2.8 Data acquisition system

### 3 TEST PROGRAM

As discussed in Section 2, the test program included three separate test series. These series were performed with full-length SVEA-96 24-rod sub-bundle test sections. The three sub-bundle test series differ with respect to the axial power shape provided by the heater rods. Sub-bundle data were obtained for cosine, bottom-peaked, and top-peaked axial power shapes. The test results for the three sub-bundle test series are given in Appendix A of Reference 1 (cosine axial power shape), Appendix B of this document (bottom-peaked axial power shape), and Appendix C of this document (top-peaked axial power shape). The test series are identified by the following test identification ranges:

<b>Axial Power Shape</b>	<b>Initial Test Point</b>	<b>Final Test Point</b>	<b>Data Point Table</b>
Cosine	1104-1-AA	2118-10-KLL	Ref. 1, Appendix A
Bottom-Peaked	1033-1-AA4	1091-48-AA16	Appendix B
Top-Peaked	1025-1-AA4	1090-16-AA13	Appendix C

The number of data points and local power distributions in the cosine, bottom-peaked, and top-peaked test series are summarized in Table 3.1. As noted in Reference 1 and Appendices B and C of this document, the actual local power distribution at which the data point was measured may differ slightly from the nominal distribution. The local power distributions actually measured for each data point, and the R-factor corresponding to that distribution, were used in the correlation derivation and evaluation.

#### 3.1 Range of Test Parameters

The ranges of test parameters over which the sub-bundle critical power tests were conducted are shown in Table 3.2.

Histograms defining the ranges of mass flux, pressure, inlet subcooling, and local power distribution as reflected by the CPR correlation R-factor values are shown in Figures 3.1a through 3.1d, 3.2a through 3.2d, 3.3a through 3.3d, and 3.4a through 3.4d, respectively. In each case, the figure denoted "a" is a histogram showing the entire range of data for all three axial power shapes. The figures denoted "b", "c", and "d" indicate histograms showing the range of data for the cosine, bottom-peaked, and top-peaked axial power shapes, respectively. The number of data points obtained in each parameter range (mass flux, pressure, inlet subcooling) are also shown in Tables 3-3 through 3-6 for the cosine axial power shape tests, bottom-peaked axial power shape tests, and top-peaked axial power shape tests, respectively.

[

. ]

### 3.2 Justification for Range of Test Parameters

The critical power performance of a test bundle is a function of mass flux, system pressure, inlet subcooling, axial power distribution, and local power distribution. The range of the test parameters for which the critical power tests were conducted is presented in Section 3.1. Justification for the ranges is summarized in the following subsections.

#### 3.2.1 Mass Flux

The critical power is a strong function of mass flux. Therefore, data were obtained at numerous points [ ] over the range of mass flux considered to establish the correlation at various values of pressure, inlet subcooling, and bundle local powers.

[ ] The range of mass flux representing normal operations and AOOs is very broad [ ] The mass flux points used for the tests cover this expected operating range.

#### 3.2.2 System Pressure

Data were obtained at 6 different system pressures: [ ]

[ ] This range provided sufficient data to determine the system pressure dependence of critical power over the expected range of application of

the correlation. [

]

### 3.2.3 Inlet Subcooling

It is well known (e.g. References 1, 3 and 5) that critical power is a linear function of the inlet subcooling at constant mass flux and system pressure.

[

.] A 10 °C inlet subcooling corresponds to the reactor normal operating condition, and 45 °C inlet subcooling covers the loss of feedwater heating Anticipated Operational Occurrence.

### 3.2.4 Axial Power Distribution

Sub-bundle critical power data were obtained for a chopped cosine axial power distribution as well as for bottom-peaked and top-peaked axial power shapes. The cosine axial power shape is reasonably representative of typical operation. The bottom-peaked and top-peaked axial power shapes were selected to capture the effect of axial power shape over the range expected in reactor operation.

### 3.2.5 Local Power Distribution

The critical power performance of a test bundle is dependent on the test bundle local power distribution. One advantage of the FRIGG test loop is that the test bundle local power distribution can be easily varied. Systematic series of tests were conducted to investigate the critical power performance at various local peaking factors and various peak power rod locations. SVEA-96 critical power measurements were obtained at [ ] to establish the effect of local power distribution on critical power. Figure 3.1 in Reference 1 and Appendices B and C of this document show the nominal local power distributions tested. The local power distribution may differ slightly from point-to-point in tests with the same nominal radial power distribution. The local power distribution actually measured for each data point was used in the correlation development and evaluation.

The local power distributions used in the tests were designed to establish the local power distribution dependence of the bundle critical power performance. The local power distributions involve rods with peaking factors between [

.]



To summarize the discussion of the range of individual parameters in Sections 3.2.1 through 3.2.5: the ranges of parameters shown in Figures 3.1 through 3.4 were selected to cover values of parameters impacting Critical Power expected during normal BWR operations as well as Anticipated Operational Occurrences (AOOs) and accidents. In selecting the test matrices, greatest emphasis is placed on those regions in which the reactor will usually operate. Therefore, while pressure and inlet subcooling ranges of [

] The mass flux points shown in Figures 3.1a through 3.1d cover this range. The range of local power distributions were selected to cover local power distributions expected during reactor operations and to allow an accurate determination of the dryout sensitivity of each rod in the sub-bundle. [

]

### 3.2.6 Combinations of Parameters

In order to confirm that the parameter ranges considered in the Critical Power tests cover the combinations of conditions expected during typical reactor application, the parameter ranges expected during reactor application (See Table 3.7) are superimposed on the ranges of test points for various combinations of test parameters in Figures 3.5 through 3.10. The expected boundaries of typical reactor application are shown by rectangles in these figures. As shown in Figures 3.5 through 3.10, the ranges of parameters including combinations of parameters at their extremities (i.e. "corner to corner" ranges) expected during typical reactor operation are adequately covered by the ranges of test points. Figures 3.5 through 3.7 confirm that the ranges of mass flux, inlet subcooling, and pressure expected during reactor operation are within the corresponding ranges considered in the tests. Figures 3.8 through 3.10 indicates that the expected sub-bundle R-factor range for potentially limiting assemblies during reactor operation is sufficiently well represented by the sub-bundle data base.

### 3.2.7 Summary

A side by side comparison of the range of the parameters in the tests with that of a typical reactor application is shown in Table 3.7. The combined range is based on the composite range of all the tests and is considered to be the range of validity of ABBD1.0. As discussed in Section 3.2.6 and seen in Table 3.7, the range for a typical application is adequately bounded by the range of validity of ABBD1.0.

[

.]

### **3.3 Data Validation Criteria and Procedures**

Data validation is supported with instrumentation performance reliability checks. All data collection instrumentation is periodically calibrated to assure the accuracy of the data.

The data validation process is further reinforced by assuring that all instrumentation is checked for proper operation prior to the performance of each test. Before and after each shift, a reading from every transmitter is recorded and compared with the expected value for that transmitter. In the event of an abnormal reading, corrective actions are taken before the actual test is run. In addition, the following checks are performed at the beginning of each test period:

1. A heat balance is calculated to insure that power, flow, and temperature measurements are correct.
2. The overall pressure drops across the bundle at different flow rates are measured.
3. The sum of the power generated by each heater rod is compared with the sum of the power outputs from each power supply unit for all test points. These two bundle power measurements are accepted if they agree to within  $\pm 1\%$ .

Critical power reference test points are periodically repeated to assure that the measurements are stable. The reference points for the SVEA-96 test series are defined by the following nominal conditions:

Bundle Outlet Pressure [ ]

Inlet Subcooling [ ]

and with mass flux covers the range [ ]

These reference test measurements were performed, at a minimum, for a uniform local power distribution.

The reproducibility of the critical power was found to be very good for the SVEA-96 test series. Examples of the reproducibility are shown in Table 3.8.

Conversion of the data to engineering units by the computer allowed preliminary test validation to be done upon completion of a run and before the data analysis took place. This preliminary validation provided immediate feedback on facility operation and data collecting equipment performance.

After the instrumentation had been functionally checked, and the test parameters and performance had been compared with the test matrix, the final data validation was performed during the data reduction and analysis stage.

### 3.4 Data Trends

This section shows trends in the measured Critical Power data. These trends are addressed to confirm that the SVEA-96 Critical Power database is physically realistic and consistent with similar measurements obtained for other assembly designs. The figures in this section show the measured data points and the corresponding ABBD1.0 Correlation predictions (See Section 4) of the data measurements. The correlation predicted critical power data is denoted with suffix "Pred". Furthermore, it should be noted that some spurious spread is introduced into the data when it is plotted in this manner since all of the points were not obtained at precisely the target condition.

A test bundle is referred to with a designation such as SF24A. The designation SF24A (S=SVEA, F=FRIGG, 24 = number of rods, A = a serial number) stands for dryout power measurements on a SVEA-96 sub-bundle test section with the cosine axial power shape. The designation SF24AB refers to dryout power measurements on a SVEA-96 sub-bundle test section with the bottom-peaked axial power shape. The designation SF24AT refers to dryout power measurements on a SVEA-96 sub-bundle test section with the top-peaked axial power shape.

#### 3.4.1 SVEA-96 Sub-bundle Cosine Axial Power Shape Tests (SF24A)

The SVEA-96 data trends for the cosine axial power shape obtained with the SF24A test section were presented in Section 4 of Reference 1 and are not repeated in this document. The evaluation of the SVEA-96 Critical Power data based on a cosine axial power shape in Section 4 of Reference 1 showed that the dependence of the SVEA-96 test data on hydraulic parameters agrees with the critical power data taken for other designs and at other facilities.

#### 3.4.2 SVEA-96 Sub-bundle Bottom-and Top-peaked Axial Power Shape Tests

The results from the bottom-peaked (SF24AB) and top-peaked (SF24AT) tests at approximately [

] are compared with the results from the SF24A tests for these local power distributions (uniform, optimized, and realistic) in Figures 3.11, 3.12 and 3.13. "Uniform" local power distributions are intended to provide the same power to each of the 24 heater rods. The term "optimized" refers to a rod power distribution that gives the highest dryout power for a given set of mass flux, system pressure, inlet subcooling and axial power shape conditions. The optimized rod power distribution is achieved by [

.] A “realistic” local power distribution typical power distribution expected during assembly operation.

The critical power decreases as the axial power shapes become more top-peaked in Figures 3.11 through 3.13. This tendency is in agreement with measurements obtained for other assembly designs such as the SVEA-96+ design discussed in Reference 5. The monotonic increase in Critical Power as a function of mass flux is also consistent with other designs and the data obtained in other facilities. Therefore, the trends in these data reflect the expected dependence on assembly flow and axial power shape based on previous testing of earlier designs and the physical nature of the dryout process for various local power distributions.

Trends in exit pressure and inlet subcooling for various local power distributions are shown for the bottom-peaked axial power distribution (test bundle SF24AB) and the top-peaked axial power distribution (test bundle SF24AB) in Figures 3.14 through 3.19 and Figures 3.20 through 3.24, respectively.

The influence of inlet subcooling at an [

]

Critical power as a function of pressure for various constant mass flows and inlet subcoolings are shown in Figures 3.16 to 3.19 for the bottom-peaked axial power shape and Figures 3.22 to 3.24 for the top-peaked axial power shape. As shown in these figures, [

.] The same type of behavior as a function of system pressure was observed for the SVEA-96+ design reported in Reference 5 and is also consistent with other earlier designs.

The purpose in providing data trend plots in Figures 3.14 through 3.24 is to show that the trends in the data are physically reasonable and consistent with expectations. ABBD1.0 predictions are included in these figures to help the correlation review as previously requested in the review of the ABBD2.0 Correlation (Reference 5).

**TABLE 3.1**  
**NUMBER OF POINTS IN SVEA-96 TEST SERIES**


**TABLE 3.2**  
**RANGE OF TEST PARAMETERS**


[illegible]**CE Nuclear Power LLC**

### NUMBER OF DATA POINTS AT VARIOUS PARAMETER RANGES (COSINE AXIAL POWER SHAPE)

[illegible]**CE Nuclear Power LLC**



[illegible]**CE Nuclear Power LLC**

**TABLE 3.6**[illegible]

Range is defined as Lower Bound < parameter value ≤ Upper Bound

**TABLE 3.7**  
**RANGE OF PARAMETERS**


Note:

1. With control rod inserted, non-limiting assembly
2. With control rod out, potential limiting assembly
3. The SVEA-96 test data were obtained for a 24-rod sub-bundle. The R-factor range corresponding to the measured sub-bundle data is expanded for a full assembly due to sub-bundles operating at different relative powers. Justification for this range for a full assembly is discussed in Section 3.2.7.
4. Sub-bundles with relative rod powers of 0.0 and 0.489 were tested to confirm the adequacy of the R-factor model for water rods and very low power (e.g. burnable absorber) rods.

**TABLE 3.8**  
**EXAMPLES OF TEST REPRODUCIBILITY**




*Figure 3.1a Histogram for SVEA-96 tests, Frequency versus Mass Flux*



*Figure 3.2a Histogram for SVEA-96 tests, Frequency versus Pressure*



*Figure 3.3a Histogram for SVEA-96 tests, Frequency versus Subcooling*



*Figure 3.4a Histogram for SVEA-96 tests, Frequency versus R-factor*



*Figure 3.1b Histogram for SVEA-96 tests, Frequency versus Mass Flux*

*(Cosine Axial Power Shape)*



*Figure 3.2b Histogram for SVEA-96 tests, Frequency versus Pressure*

*(Cosine Axial Power Shape)*



*Figure 3.3b Histogram for SVEA-96 tests, Frequency versus Subcooling (Cosine Axial Power Shape)*



*Figure 3.4b Histogram for SVEA-96 tests, Frequency versus R-factor (Cosine Axial Power Shape)*





*Figure 3.1c Histogram for SVEA-96 tests, Frequency versus Mass Flux  
(Bottom-Peaked Axial Power Shape)*



*Figure 3.2c Histogram for SVEA-96 tests, Frequency versus Pressure (Bottom-Peaked Axial Power Shape)*



*Figure 3.3c Histogram for SVEA-96 tests, Frequency versus Subcooling (Bottom-Peaked Axial Power Shape)*



*Figure 3.4c Histogram for SVEA-96 tests, Frequency versus R-factor (Bottom-Peaked Axial Power Shape)*



*Figure 3.1d Histogram for SVEA-96 tests, Frequency versus Mass Flux  
(Top-Peaked Axial Power Shape)*



*Figure 3.2d Histogram for SVEA-96 tests, Frequency versus Pressure  
(Top-Peaked Axial Power Shape)*



*Figure 3.3d Histogram for SVEA-96 tests, Frequency versus Subcooling*

*(Top-Peaked Axial Power Shape)*



*Figure 3.4d Histogram for SVEA-96 tests, Frequency versus R-factor*

*(Top-Peaked Axial Power Shape)*



*Figure 3.5 Range of test parameters (pressure vs. mass flux) in comparison to typical application*

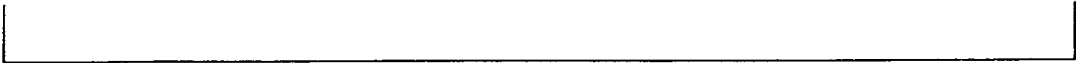




*Figure 3.6 Range of test parameters (pressure vs. subcooling) in comparison to typical application*



*Figure 3.7 Range of test parameters (subcooling vs. mass flux) in comparison to typical application*



*Figure 3.8 Range of test parameters (R-factor vs. mass flux) in comparison to typical application*

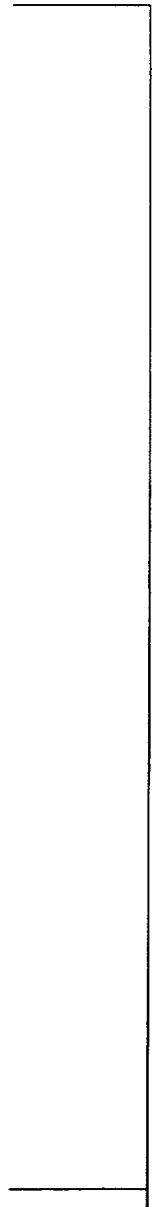
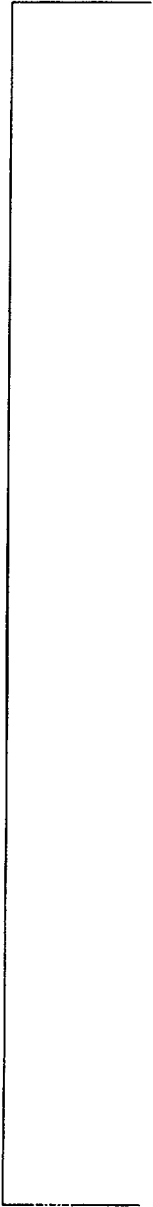




*Figure 3.9 Range of test parameters (R-factor vs. pressure) in comparison to typical application*



*Figure 3.10 Range of test parameters (R-factor vs. subcooling) in comparison to typical application*



*/*

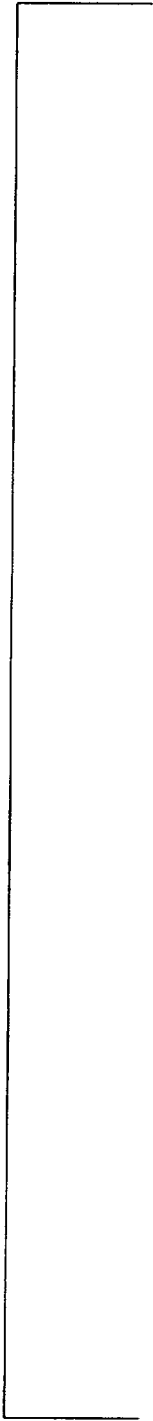
*/*



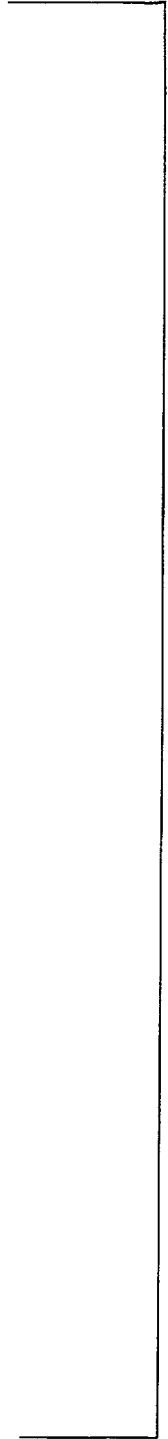
*/*



*/*



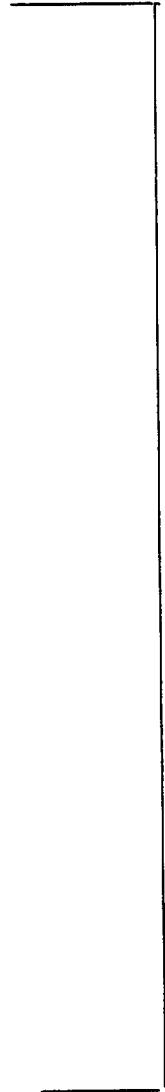
*/*



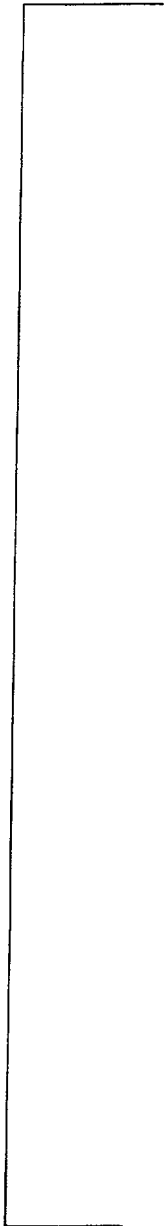
*/*



*I*



*I*



*I*



*I*



*I*



*I*



[REDACTED]

/

[REDACTED]

/



*/*



*/*

[

]

/

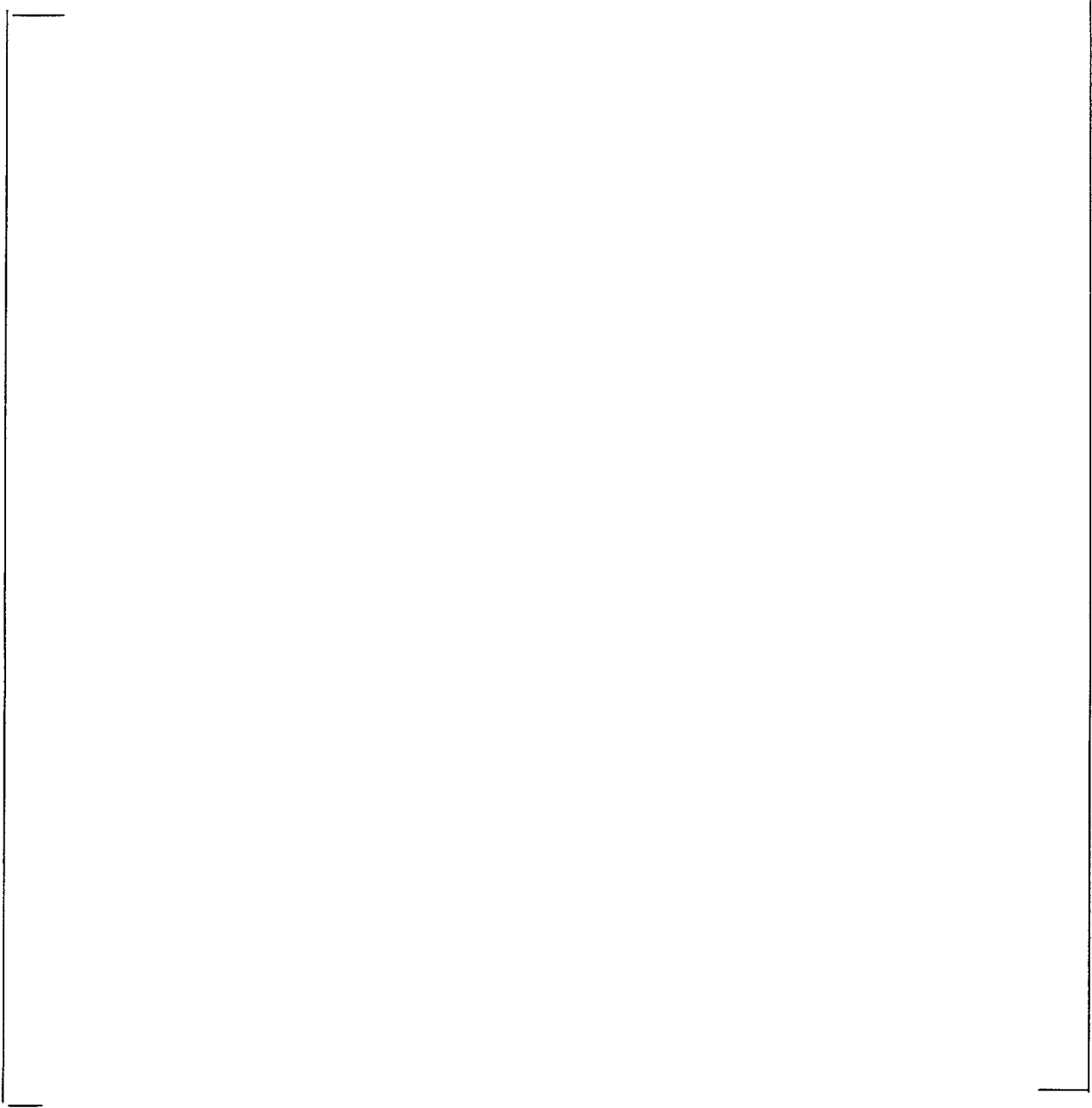
/

[

]

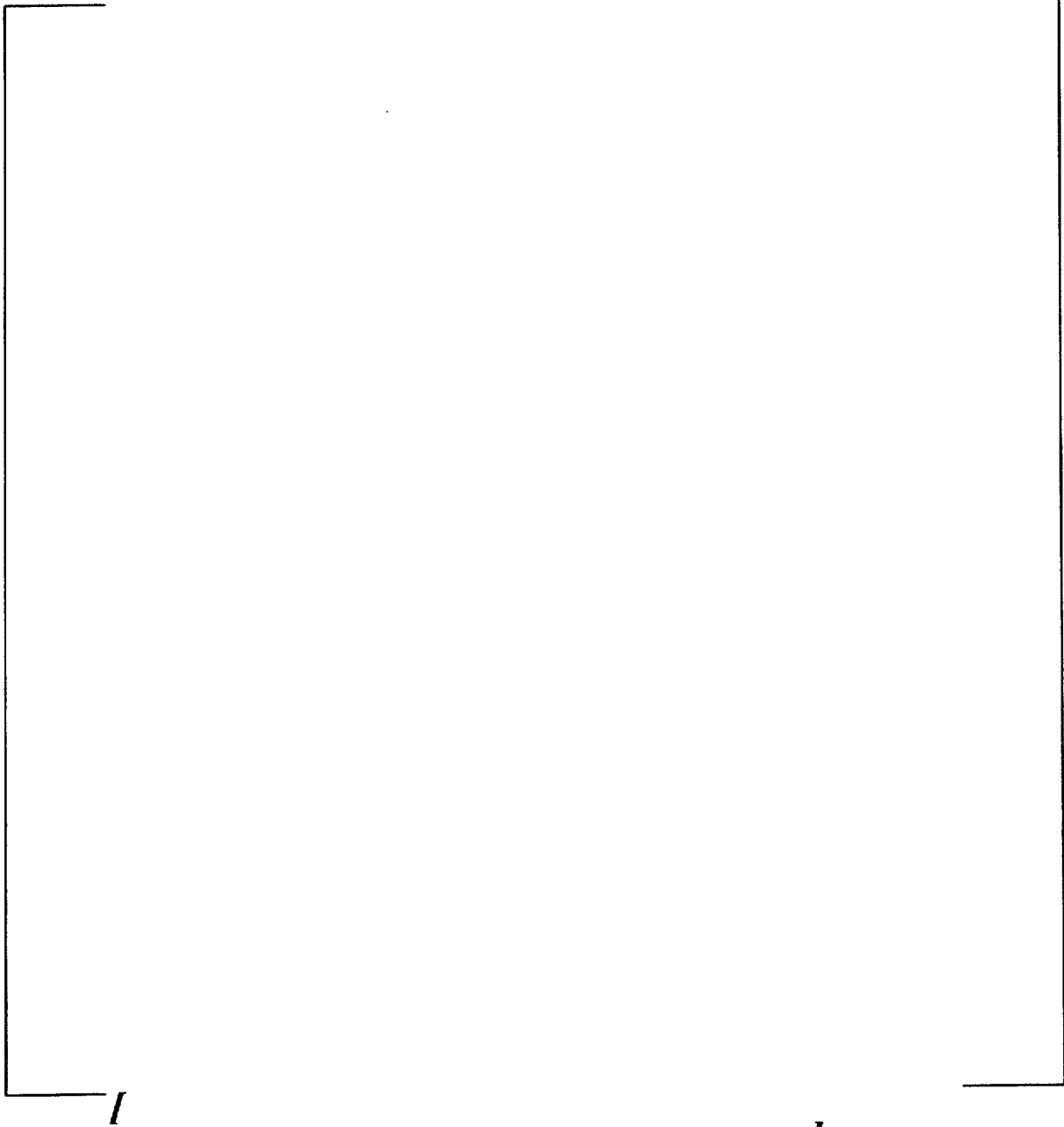
/

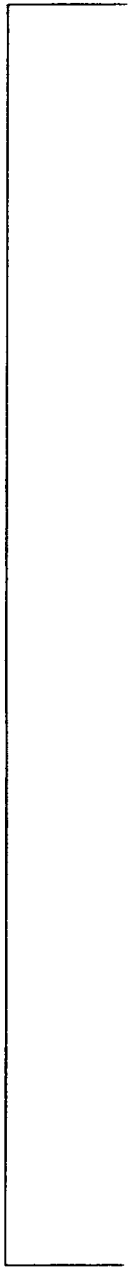
/



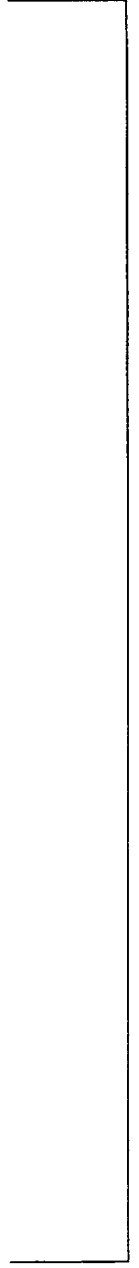
*/*

*/*





*I*



*I*



*I*



*I*



## 4 CRITICAL POWER CORRELATION

### 4.1 Form of the Correlation

There are two common methods used to correlate critical power test data. One is to correlate the critical power test data in the critical quality-boiling length plane, and the other method is to correlate the critical power data in the critical heat flux-quality plane.

The critical quality-boiling length form has been selected to correlate the SVEA-96 critical power test data.

Since the trends in the SVEA-96 data are similar to trends for other BWR fuel, a critical quality-boiling length correlation would be expected to accurately correlate the SVEA-96 data.

This decision is confirmed by the results in Section 5 which demonstrate that a critical quality - boiling length correlation [

] sufficiently capture the dependence of all important parameters to which CPR is sensitive for the SVEA-96 design. This SVEA-96 critical power ratio correlation is described in this section and is referred to as ABBD1.0.

Experience has also shown that a critical quality-boiling length correlation represents a proven form capable of adequately predicting the onset of dryout during a transient. The process to confirm that ABBD1.0 provides an adequate prediction of the change in critical power during a transient code application is described in Section 6.

[

.]

Finally, application of the ABBD1.0 correlation based on sub-bundle data to a full SVEA-96 assembly in a manner that assures critical powers will not be overpredicted requires a further modification to the R-factor. This modification accommodates sub-bundle power mismatch.

These adaptations to the critical quality-boiling length correlation form [ ] resulted in the ABBD1.0 CPR correlation. The ABBD1.0 CPR correlation is described in this section.

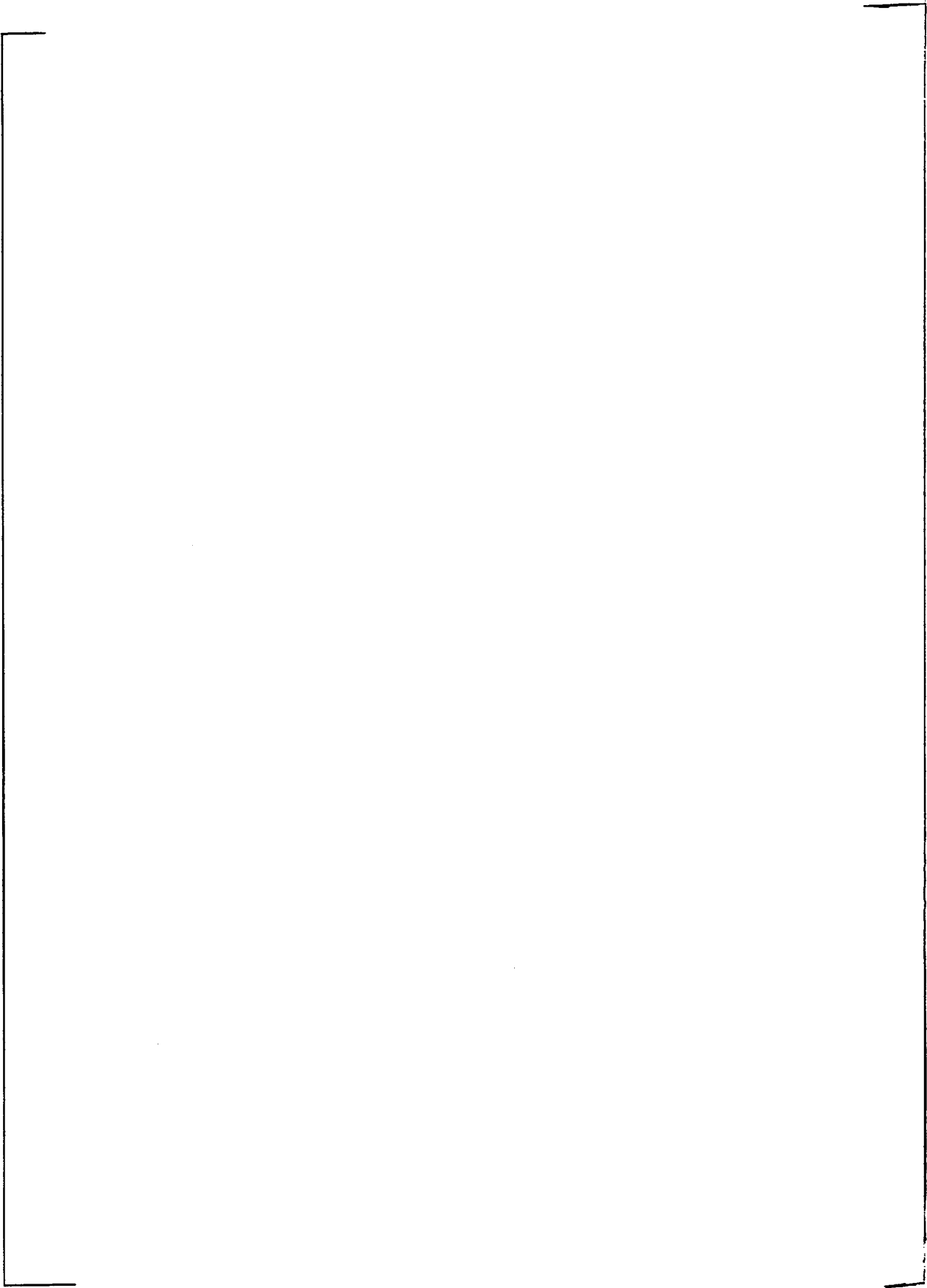
## 4.2 ABBD1.0 CPR Correlation

Like the GEXL Correlation described in Reference 3, the ABBD1.0 and XL-S96 CPR correlations are both based on a critical quality-boiling length relationship. The form of the ABBD1.0 CPR Correlation is identical to that of the ABBD2.0 Correlation described in References 5 through 7 and, therefore, is not the same form as the XL-S96 Correlation described in Reference 1. The XL-S96 CPR correlation uses the critical quality given by the GEXL correlation and appropriate correction factors. ABBD1.0 and ABBD2.0 correlate critical quality to second order polynomials in mass flux, pressure, boiling length, R-factor and annular flow length and include all cross terms. A detailed description of the differences in form between the ABBD2.0 Correlation and XL-S96 is provided in the ABB response to NRC Request Number 2 in Reference 6. The description in the response to Request Number 2 in Reference 6 also applies to the ABBD1.0 correlation.

All parameters discussed below are in SI units unless otherwise noted.







#### 4.3 Calculation of the Sub-bundle R-factor for SVEA-96

The R-factor accounts for the local power distribution, cross section geometry, and the spacer grid configuration.

#### 4.4 Determination of ABBD1.0 Additive Constants and Correlation Coefficients

As shown in Table 3.1, the SVEA-96 data base is extensive. Therefore, a systematic approach was required to establish the additive constants and correlation coefficients:

1. The SVEA-96 additive constants in Figure 4.5 were established from the cosine sub-bundle test series summarized in Table 3.1. They were developed for the XL-S96 correlation as described in Reference 1. The

additive constants developed for the XL-S96 correlation were retained for ABBD1.0. This approach is justified by the correlation evaluation in Section 5 which demonstrates that the additive constants developed for XL-S96, in conjunction with the optimized ABBD1.0 correlation parameters, provide a good fit to the expanded SVEA-96 data base containing cosine, top-peaked and bottom-peaked axial power shapes.

It should be noted that the principles used to develop the additive constants for XL-S96 are same as those used to establish the additive constants for ABBD2.0. Detailed descriptions of the development of the ABBD2.0 additive constants and the associated uncertainties were presented in the responses to Request Numbers 13 and 34 in Reference 6.

2.

3.

#### 4.5 Assembly R-Factor - Treatment of Sub-bundle Power Mismatch

1. The methodology used to establish the mismatch factor for ABBD1.0 is the same as that used for ABBD2.0 in Reference 5. The actual mismatch factor established by this methodology is specific to the ABBD1.0 correlation and reflects the actual SVEA-96 characteristics.
2. The radial configuration of the sub-bundles and integral water cross channel are identical for the SVEA-96 and SVEA-96+ assemblies. The minor differences between the SVEA-96 and SVEA-96+ designs are only an additional spacer in the SVEA-96+ design and a minor modification in the spacer design. Expansion of the sub-bundle R-factor to the full assembly involves calculations of the radial flow redistribution between the sub-bundles. The relatively minor impact of the differences in spacer arrangement and design on the radial flow redistribution is captured by applying the methodology separately for both assembly designs.



The quantity, R, is the R-factor which is input to the ABBD1.0 correlation for full assembly applications.



*Figure 4.1 The  $X_G$ ,  $X_P$ ,  $X_{Bl}$ ,  $X_{Al}$ , and  $X_{G,Al}$  functions*



*Figure 4.2 The  $X_{G,P}$ ,  $X_{G,Bl}$ ,  $X_{P,Al}$ ,  $X_{P,Bl}$ , and  $X_{Al,Bl}$  functions*



*Figure 4.3 The  $X_R$ ,  $X_{P,R}$ ,  $X_{G,R}$ ,  $X_{Bl,R}$ , and  $X_{Al,R}$  functions*

*Figure 4.4 Rod Index*


*Figure 4.5 SVEA-96 additive constants*

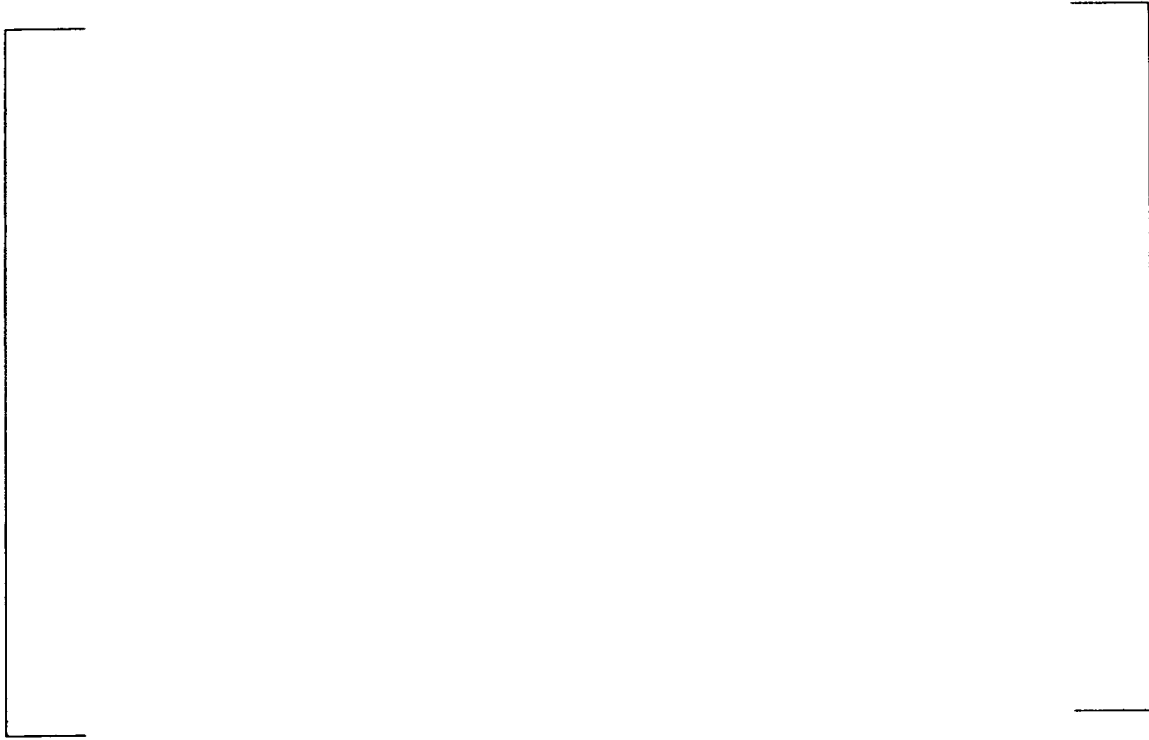


*Figure 4.6  $MF_S$  as a function of relative sub-bundle power*

## 5 CORRELATION EVALUATION

The functional form of the ABBD1.0 dryout correlation has been developed to correlate the critical power test data in the critical quality-boiling length plane.

The ABBD1.0 CPR correlation data base is composed of a total of [ ] steady state critical power measurements. Evaluation of the ABBD1.0 CPR correlation relative to the steady state data base is contained in this section. In addition, Section 6 contains the evaluation of the ABBD1.0 CPR correlation relative to transient critical power measurements.

The steady state CPR data base is composed of [ ] points measured with a full scale 24-rod sub-bundle. This critical power data base was divided into two data sets. The [ ] evaluation data set represented 80% of the data base and was used in the correlation derivation. The [ ] validation data set represents 20% of the data base and was used for validation of the ABBD1.0 CPR correlation. The number of data points and local power distributions for the evaluation and validation data sets are summarized in Table 5.1 and 5.2, respectively.

The 24-rod SVEA-96 data base obtained with a cosine axial power distribution is discussed in Reference 1. The results of the measurements obtained with the cosine axial power shape are shown in Appendix A of Reference 1, and the test bundle local power distributions used to generate that data base are shown in Figure 3.1 of Reference 1. The 24-rod SVEA-96 data base obtained with the bottom-peaked axial power distribution and test bundle local power distributions used to generate that data base are shown in Appendix B. The 24-rod SVEA-96 data base with the top-peaked axial power distribution and the test bundle local power distributions used to generate that data base are shown in Appendix C.

### 5.1 ABBD1.0 Performance Relative to the SVEA-96 Data Base

Table 5.3 shows mean prediction errors, standard deviations, numbers of data points, and 95/95 tolerance limits for the ABBD1.0 CPR correlation relative to the entire 24-rod SVEA-96 data base as well as relative to subsets of that data base. The prediction error,  $\varepsilon$ , is given by:

$$\varepsilon = \left[ \frac{\text{predicted power}}{\text{measured power}} - 1 \right] \times 100 \quad \text{Equation 5-1}$$

As shown in Table 5.3, the mean prediction error and standard deviation over the entire SVEA-96 data base is [ ]. The mean prediction error and standard deviation over the validation data set is [ ].

.] Since the validation data set was selected in a systematic, unbiased manner over the entire data base, the fact that the statistics in Table 5.3 [

.]

A useful graphical validation technique for a calculated function is to plot the function versus the measured values. Figure 5.1 is a comparison of the critical powers predicted with the ABBD1.0 correlation as a function of the measured critical powers for all [ ] data points used to develop and validate the correlation. The solid lines in Figure 5.1 represent variations from the correlation prediction of  $\pm 5\%$ . The designations "C", "B", and "T" refer to data obtained with chopped cosine, bottom-peaked, and top-peaked axial power distributions, respectively. As shown in Figure 5.1, the ABBD1.0 correlation shows good agreement with the measured data and does not show a bias as a function of critical power. Table 5.4 provides the number and percentage of predictions exceeding the 5% boundary.

Another standard graphical validation technique is to plot the prediction error,  $\epsilon$ , versus parameters to which the function is sensitive. An ideal prediction is characterized by  $\epsilon = 0.0$ . Accordingly, the prediction error is plotted as a function of [

] in Figures 5.2 through 5.8. The prediction error,  $\epsilon$ , is defined by Equation 5-1.

Figure 5.2 is a plot of the prediction error for the ABBD1.0 correlation relative to the entire [

.]

Figure 5.4 is a plot of the prediction error for the ABBD1.0 correlation relative to the entire [

.]

Figure 5.5 is a plot of the prediction error for the ABBD1.0 correlation relative to the [

.]

Figures 5.6 and 5.7 are plots of the prediction error for the ABBD1.0 correlation relative to the [

.]

Figure 5.8 is a plot of the prediction error for the ABBD1.0 correlation relative to the [

.]

In Summary, Figures 5.2 through 5.8 demonstrate that the ABBD1.0 correlation provides a good fit to the test data with no systematic biases which would limit the validity of the correlation to predict the bundle critical power performance in design and licensing applications.

Figure 5.9 is a frequency distribution of the prediction error for the SVEA-96 data base. [

.]

Figure 5.10 shows critical power dependence on axial power shape and mass flux predicted by ABBD1.0. Note that the intent of Figure 5.10 is to show the trends for various axial power shapes. A nominal condition is assumed for these correlation predictions. There are no measured data at these precise conditions for direct comparison. As shown in Figure 5.10, [

.]

Similarly, Figure 5.11 shows the ABBD1.0 critical power dependence on inlet subcooling for several different mass flux values. As shown in Figure 5.11, [

.]

Table 5.5 shows the mean error, standard deviation, number of data points and 95/95 tolerance limits [



.]

Figure 5.12 to Figure 5.14 present essentially the same information as Figure 5.2. Instead of the prediction error, the ratio of the predicted critical power to the measured critical power is plotted as a function of mass flux for each of the axial power profiles. Table 5.6 provides the mean, standard deviations and number of data points for the various mass flux ranges.

Additional plots of the prediction error as a function of mass flux, pressure, and inlet subcooling at selected regions covering the fringe area of operation are presented in Figures 5.15 through 5.32. As can be seen from these figures, with the exception of Figure 5.17, there are no significant trends or biases. These figures demonstrate that ABBD1.0 CPR correlation is applicable in the fringe area of operation (with sufficient data points) as well as near the nominal condition (with a majority of data points). Figure 5.17 shows a small bias. At high pressure (85 bar) and high mass flux ( $> 1400 \text{ kg/m}^2\text{-s}$ ), the prediction errors becomes more negative. However, this bias does not have any significant impact on reactor application since a negative error implies a more conservative (e.g., lower) lower prediction of critical power.

In summary, the following conclusions can be drawn from comparison of the ABBD1.0 correlation predictions with the 24-rod SVEA-96 data base:

1. All trends in the critical power data base discussed in Section 3 are adequately captured with the ABBD1.0 CPR correlation. Furthermore, predicted critical power trends with [ ] are consistent with previous dryout testing of earlier assembly designs.
2. The quality of the predictions of the ABBD1.0 CPR correlation does not show any evidence [ ]
3. Therefore, it is concluded that the ABBD1.0 CPR correlation provides a satisfactory fit to the data to justify its use for design and licensing applications. A normal uncertainty distribution with a mean error of [ ] provides a good characterization of the prediction error distribution for the SVEA-96 data base.

.]

## 5.2 Correlation Uncertainty and Range of the Correlation

Based on the evaluations in Section 5.1, it is concluded that the best estimate of the ABBD1.0 CPR correlation mean prediction error and standard deviation in the mean prediction error should be based on the [ ].  
Therefore, from Table 5.3, a mean prediction error and standard deviation of [ ] will be used for design and licensing applications. A detailed description of the treatment of the correlation uncertainty in a design and licensing application is provided in Reference 6 (See ABB Response to NRC Request Number 13).

The range over which the ABBD1.0 CPR correlation is valid is shown in Table 5.7. This range is based on the [ ]

.]

**TABLE 5.1****NUMBER OF DATA POINTS AND LOCAL POWER DISTRIBUTIONS  
(EVALUATION DATA SET)**


**TABLE 5.2****NUMBER OF DATA POINTS AND LOCAL POWER DISTRIBUTIONS  
(VALIDATION DATA SET)**


**TABLE 5.3****MEAN PREDICTION ERRORS AND STANDARD DEVIATIONS  
FOR ABBD1.0 CPR CORRELATION**


**TABLE 5.4****NUMBER AND PERCENT OF CALCULATED DATA POINTS  
EXCEEDING THE 5% BOUNDARY**


[illegible]**CE Nuclear Power LLC**

**TABLE 5.6**  
**MEAN AND STANDARD DEVIATIONS FOR ECPR AT VARIOUS MASS FLUX**  
**RANGES**



Range is defined as Lower Bound < Mass Flux ≤ Upper Bound  
ECPR = predicted critical power / measured critical power

**TABLE 5.7 RANGE OF VALIDITY OF ABBD1.0**




*Figure 5.1 ABBD1.0 predicted versus measured power, all sub-channel data points, The lines represent  $\pm 5\%$  error*



*Figure 5.2 ABBD1.0 prediction error as a function of mass flux, all sub-channel data points*





*Figure 5.3 ABBD1.0 prediction error as a function of mass flux, sub-channel validation data*

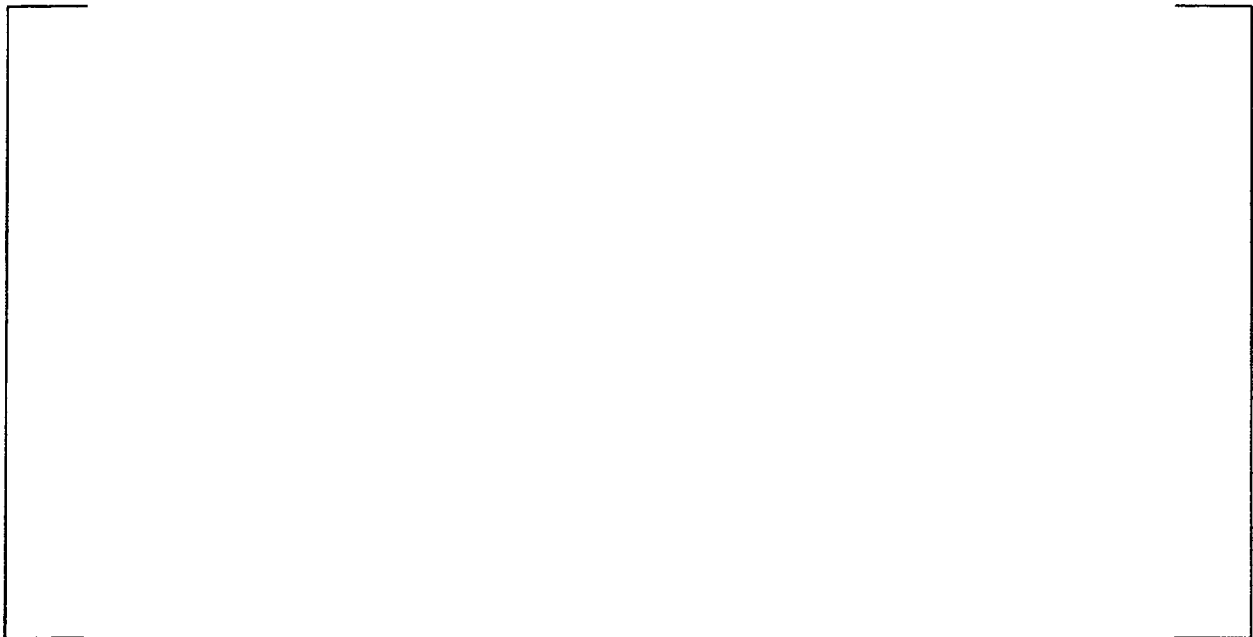


*Figure 5.4 ABBD1.0 prediction error as a function of outlet pressure, all sub-channel data points*



*Figure 5.5 ABBD1.0 prediction error as a function of inlet subcooling, all sub-channel data points*



*Figure 5.6 ABBD1.0 prediction error as a function of boiling length, all sub-channel data points*



*Figure 5.8 ABBD1.0 prediction error as a function of R-factor,  
all sub-channel data points*



**Figure 5.7 ABBD1.0 prediction error as a function of annular flow length,  
all sub-channel data points**



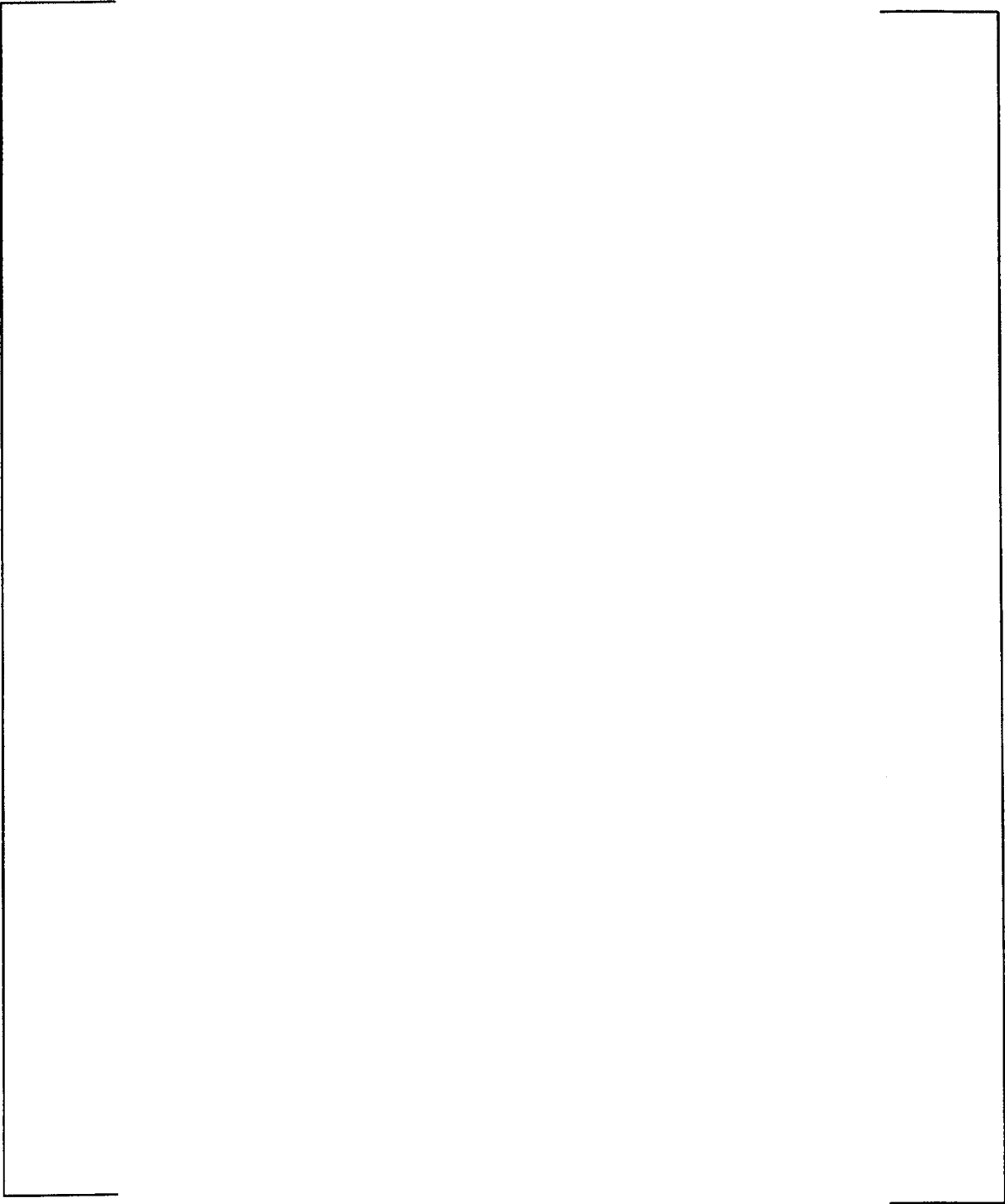
*Figure 5.9 ABBD1.0 for all sub-channel tests data, Histogram, frequency versus CPR error*



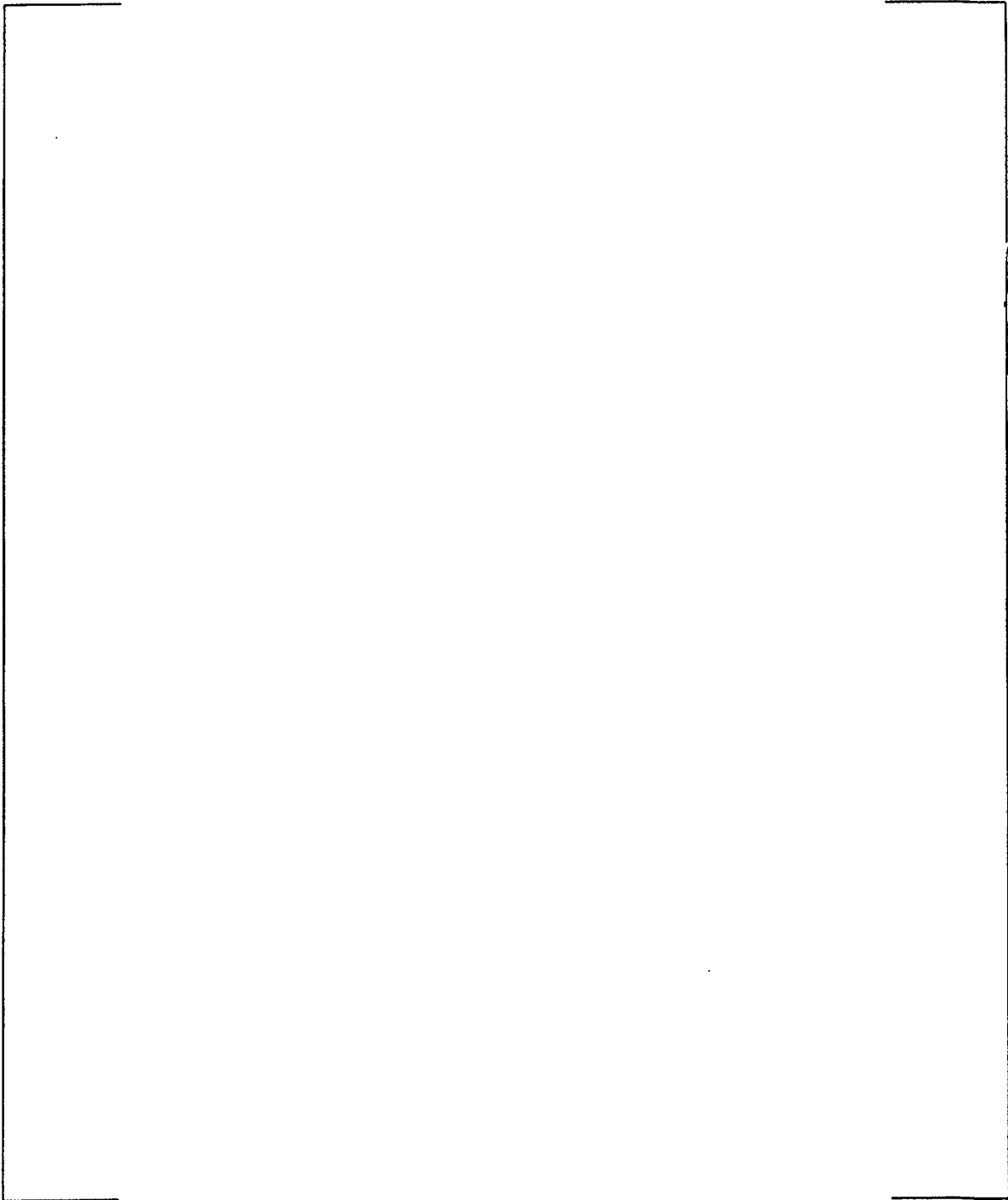
*Figure 5.10 ABBD1.0 critical power dependence on axial power shape  
(pressure =70 bar, subcooling =10K, R-factor =1.0)*



Figure 5.11 ABBD1.0 critical power dependence on subcooling



*Figure 5.12 ECPR versus Mass Flux (Cosine Axial Power Tests)*



*Figure 5.13 ECPR versus Mass Flux (Bottom-peaked Axial Power Tests)*

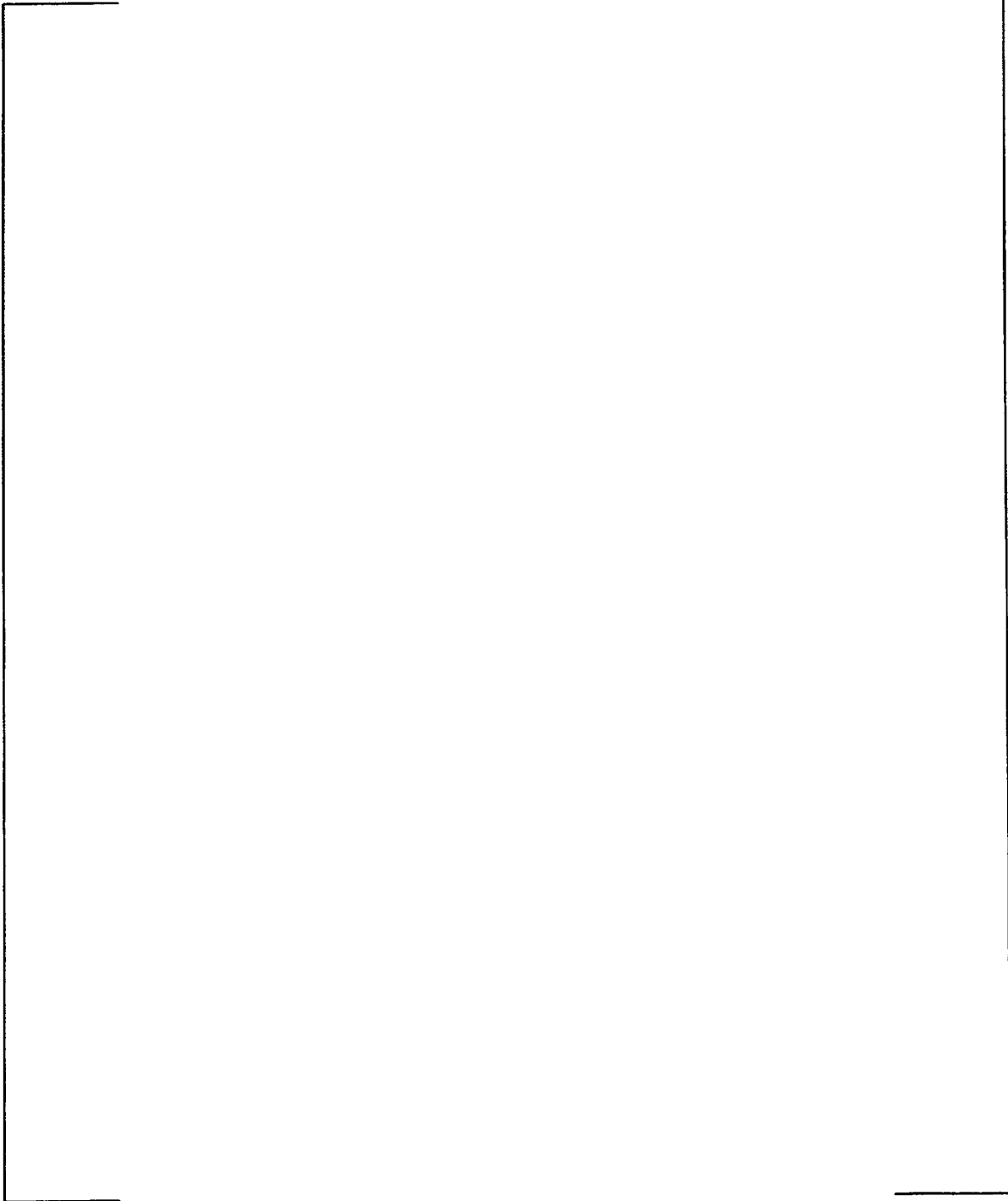


***Figure 5.14 ECPR versus Mass Flux (Top-peaked Axial Power Tests)***



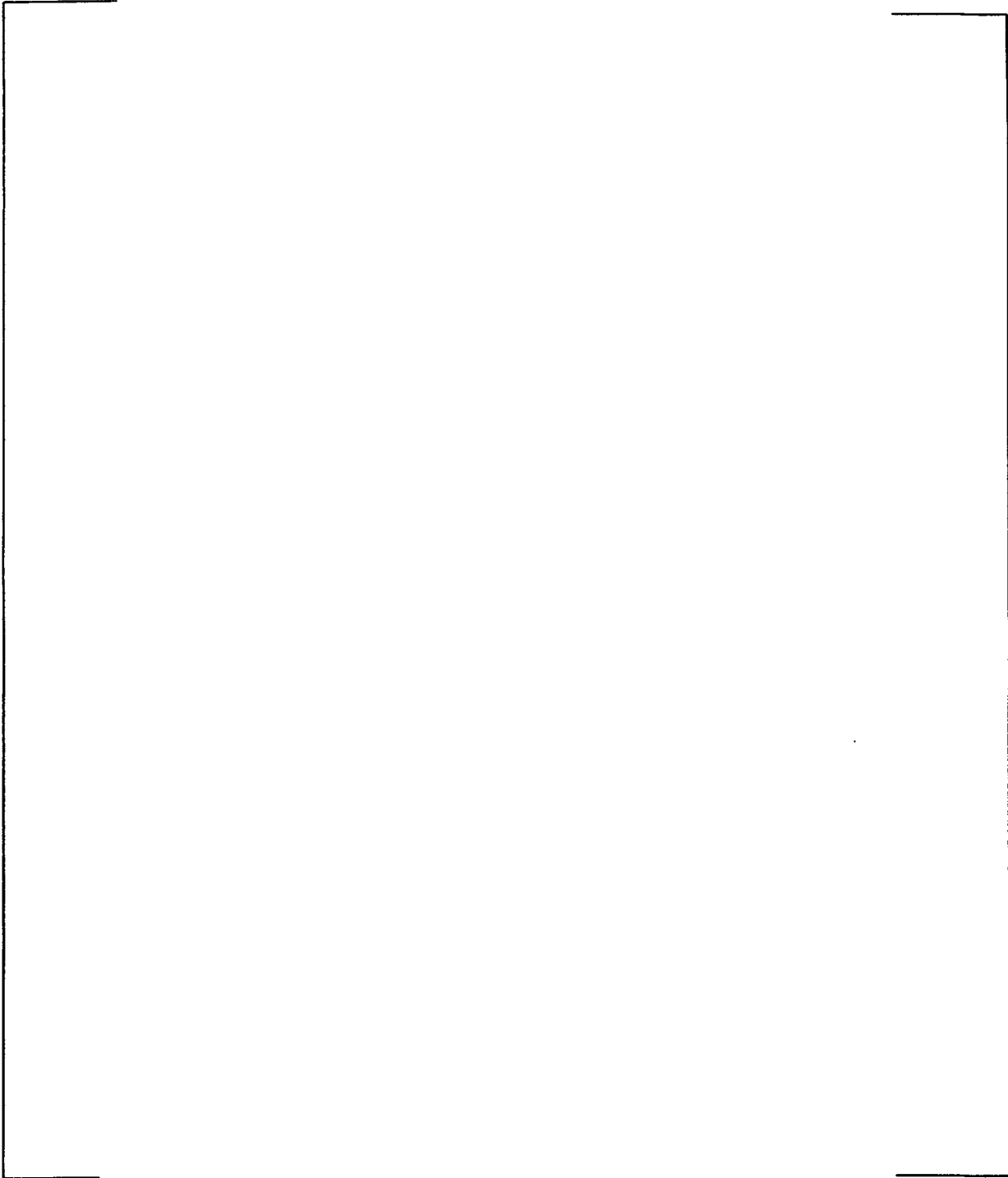


*Figure 5.15 Prediction Error versus Mass Flux at 25 bar*

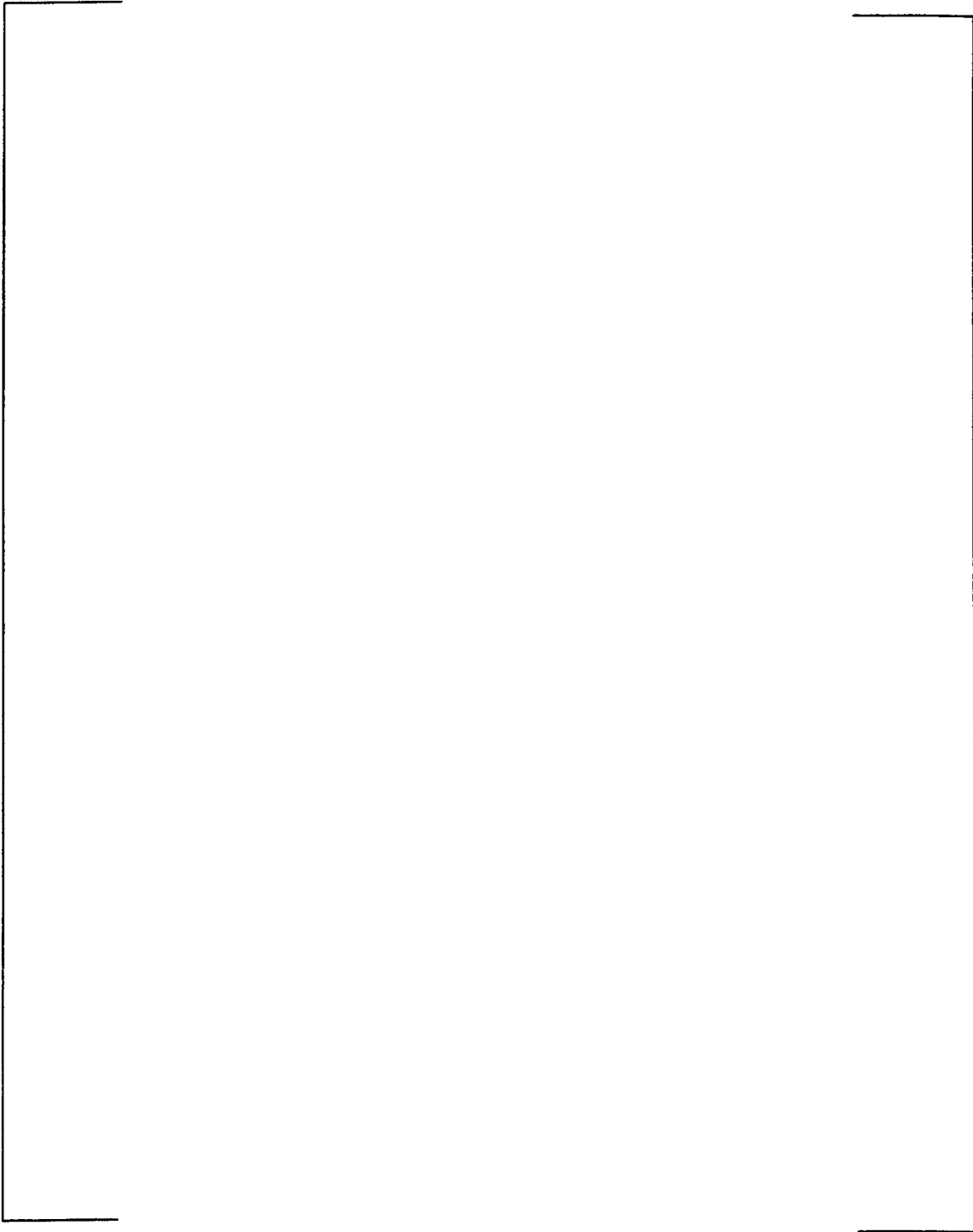


***Figure 5.16 Prediction Error versus Mass Flux at 70 bar***

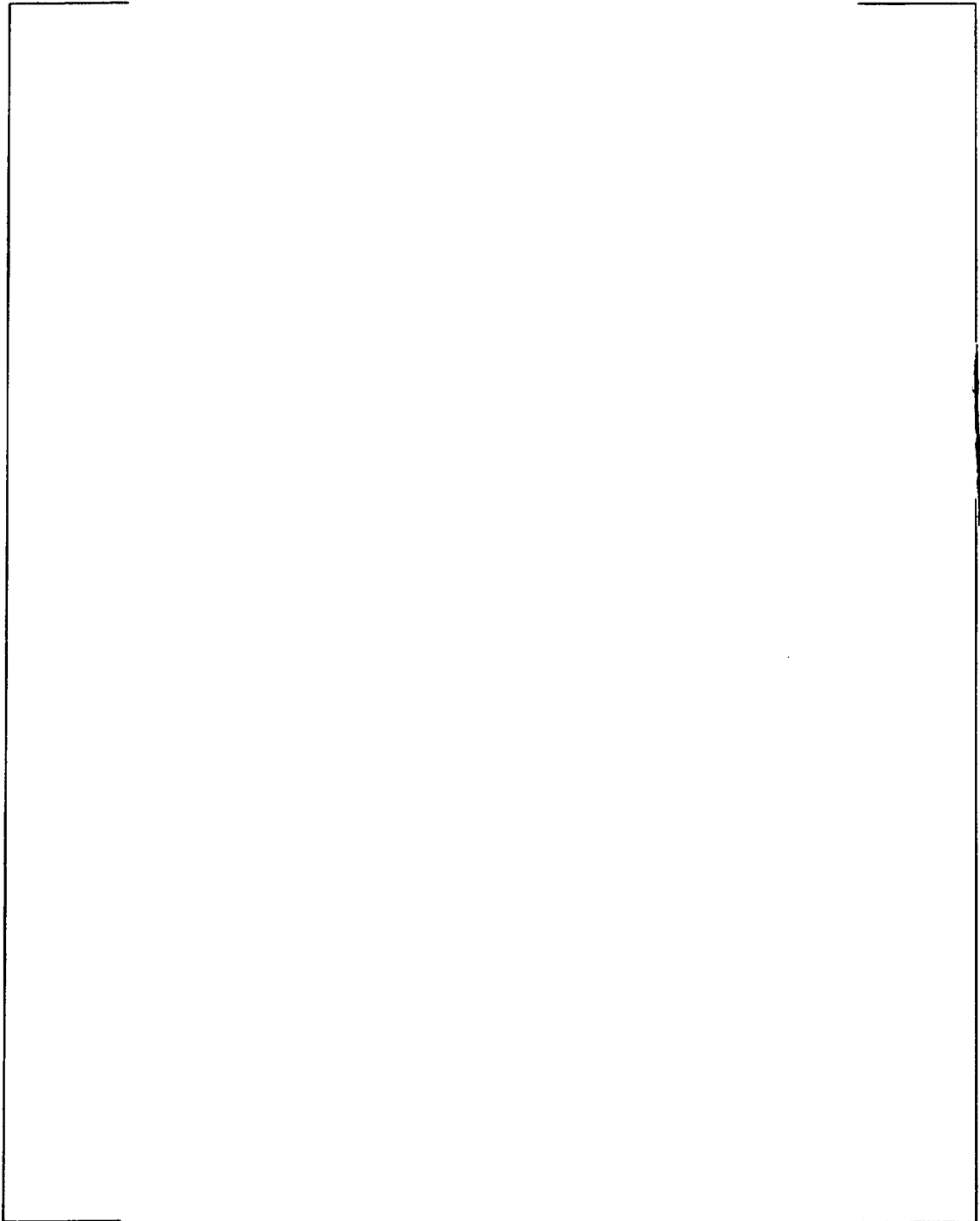


*Figure S.17 Prediction Error versus Mass Flux at 85 bar*

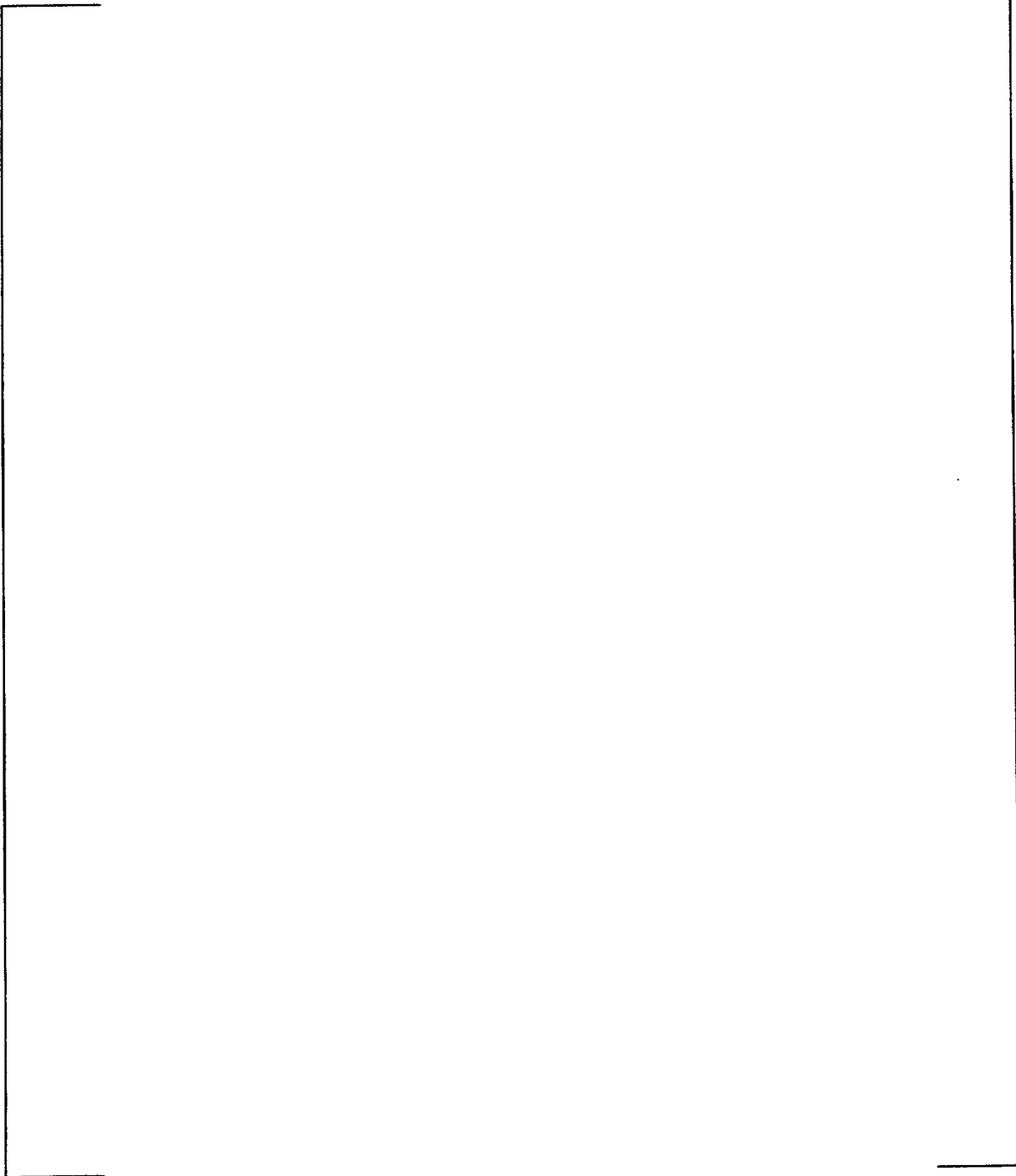


*Figure 5.18 Prediction Error versus Subcooling at 25 bar*

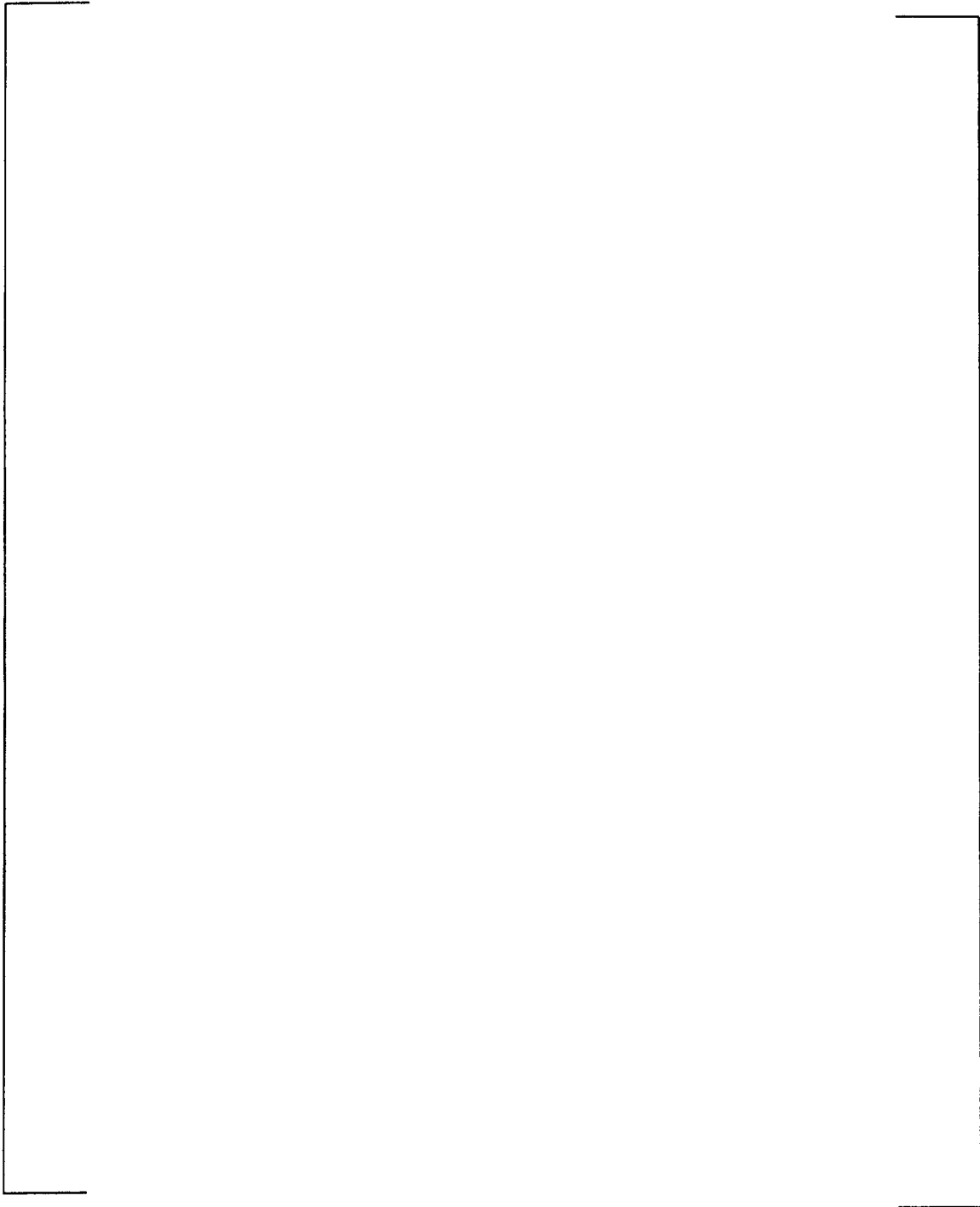


*Figure 5.19 Prediction Error versus Subcooling at 70 bar*

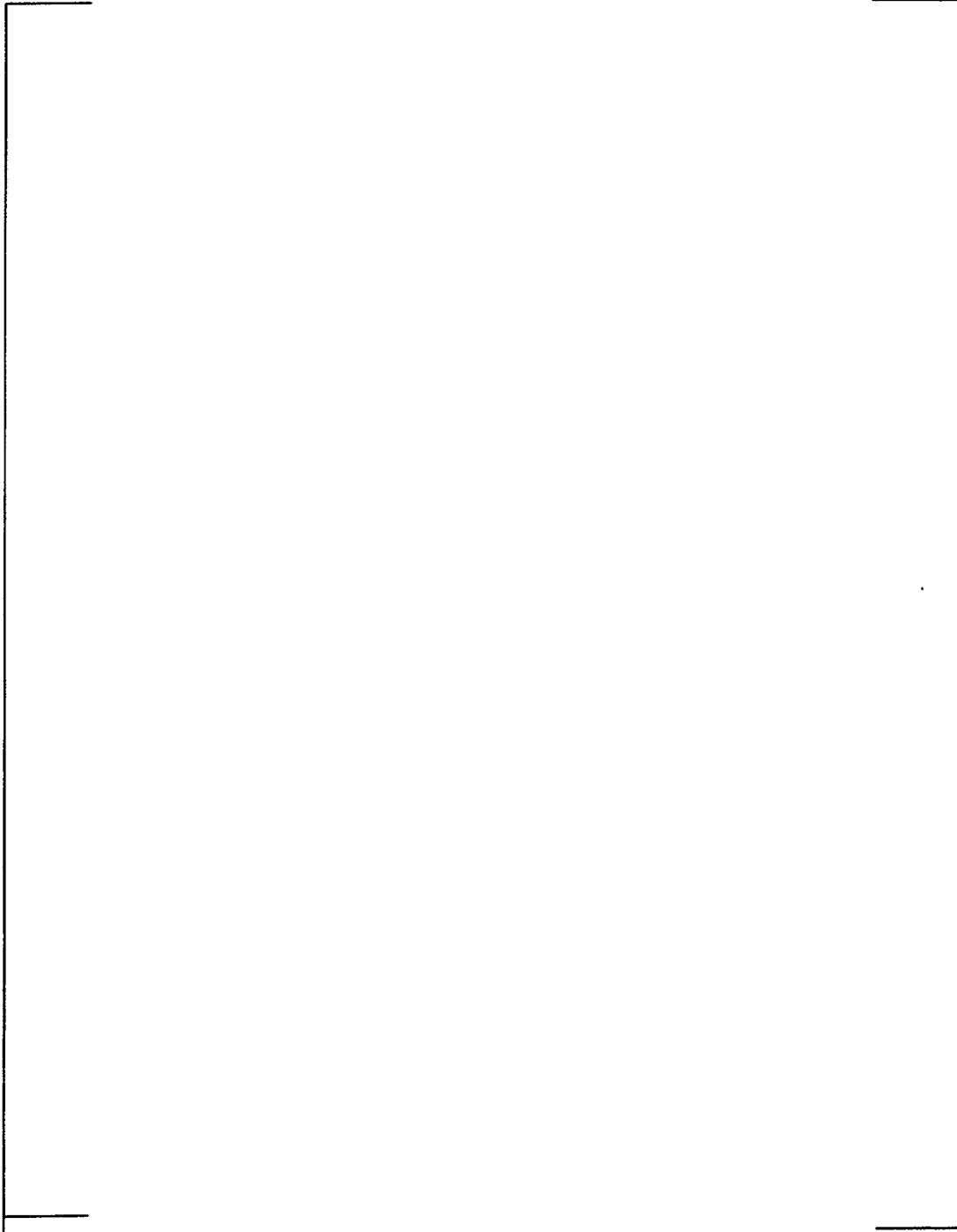


*Figure 5.20 Prediction Error versus Subcooling at 85 bar*

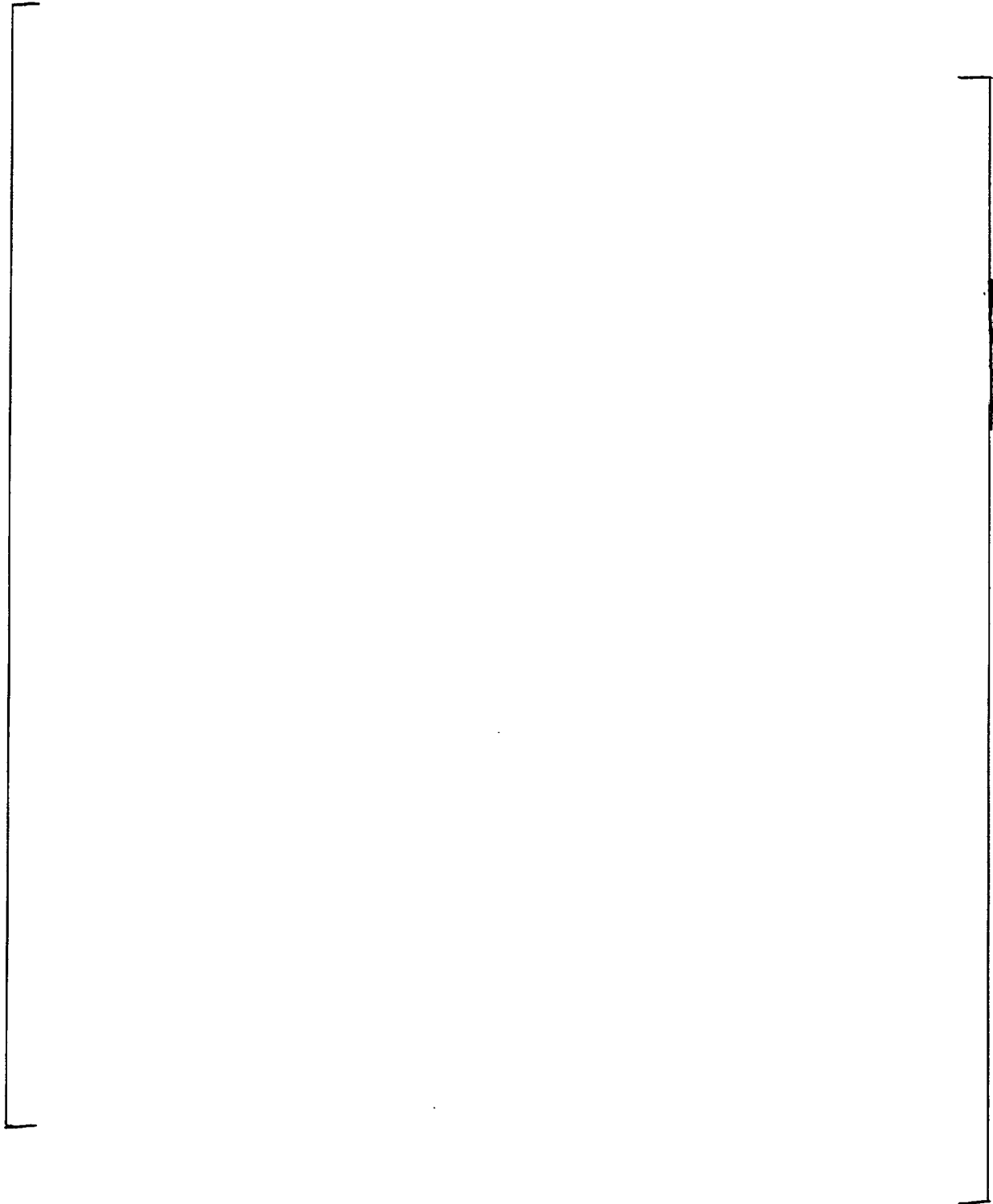


*Figure 5.21 Prediction Error versus Mass Flux at 10 Degree C subcooling*

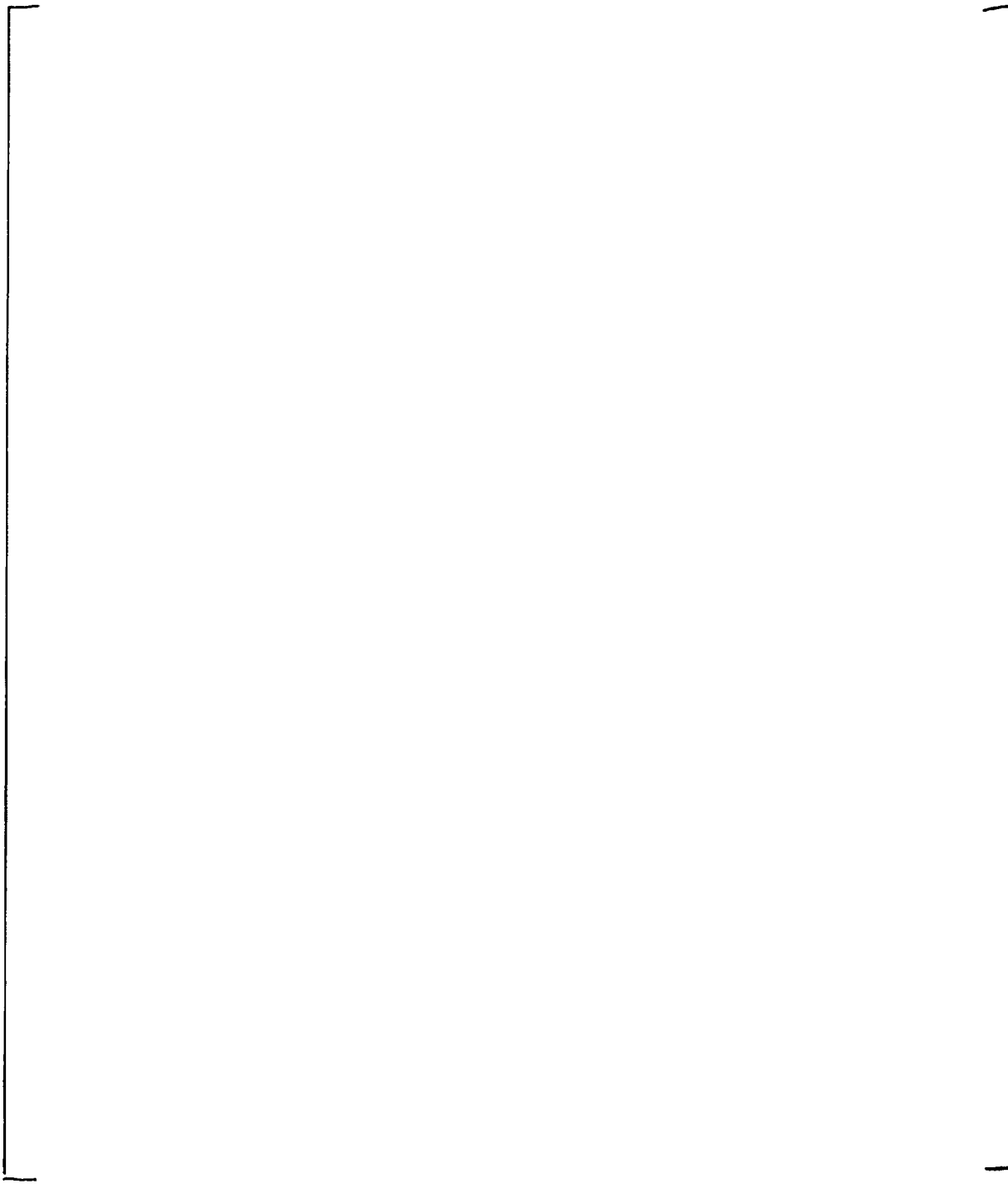


*Figure 5.22 Prediction Error versus Mass Flux at 20 Degree C subcooling*



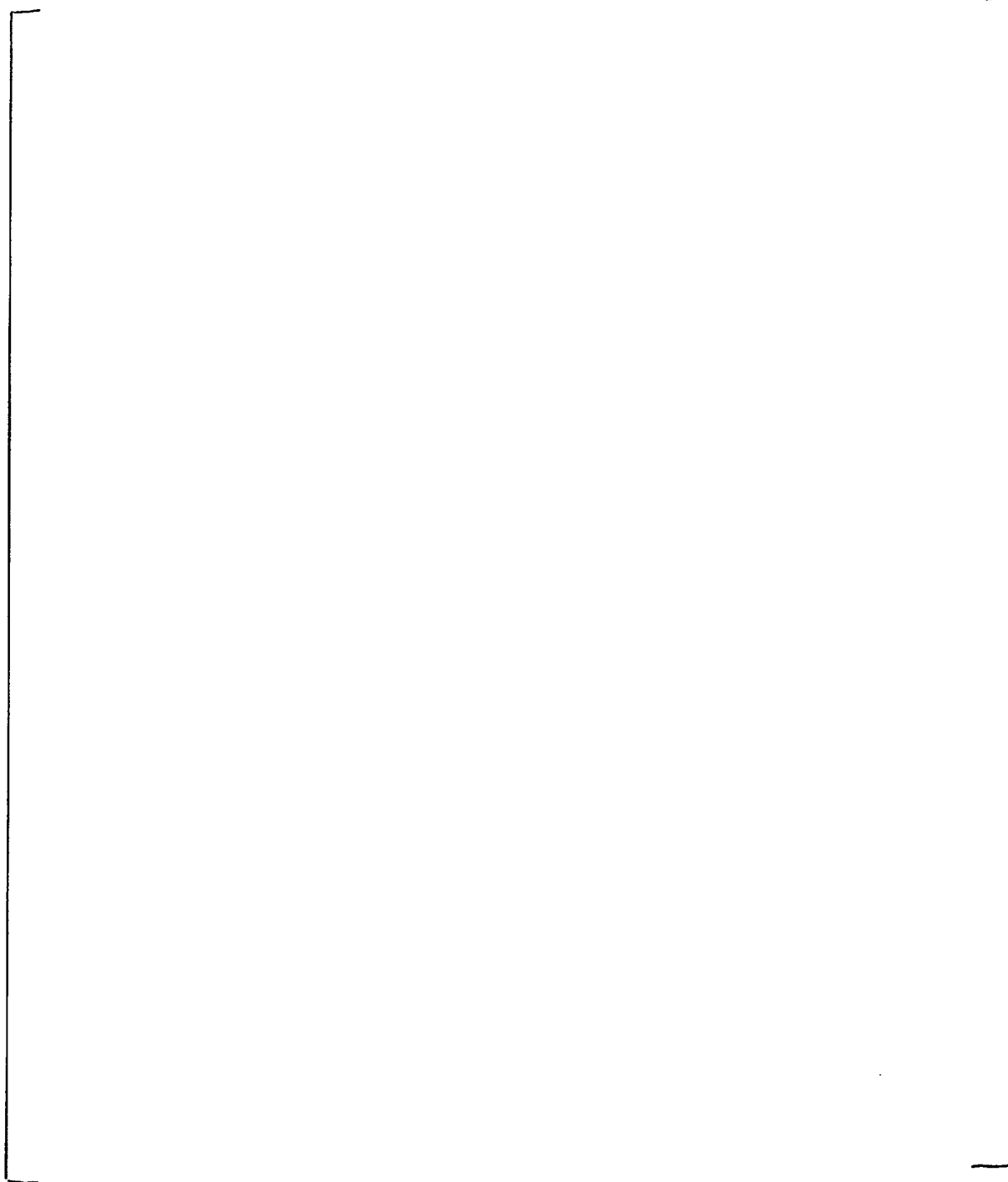


***Figure 5.23 Prediction Error versus Mass Flux at 30 Degree C subcooling***

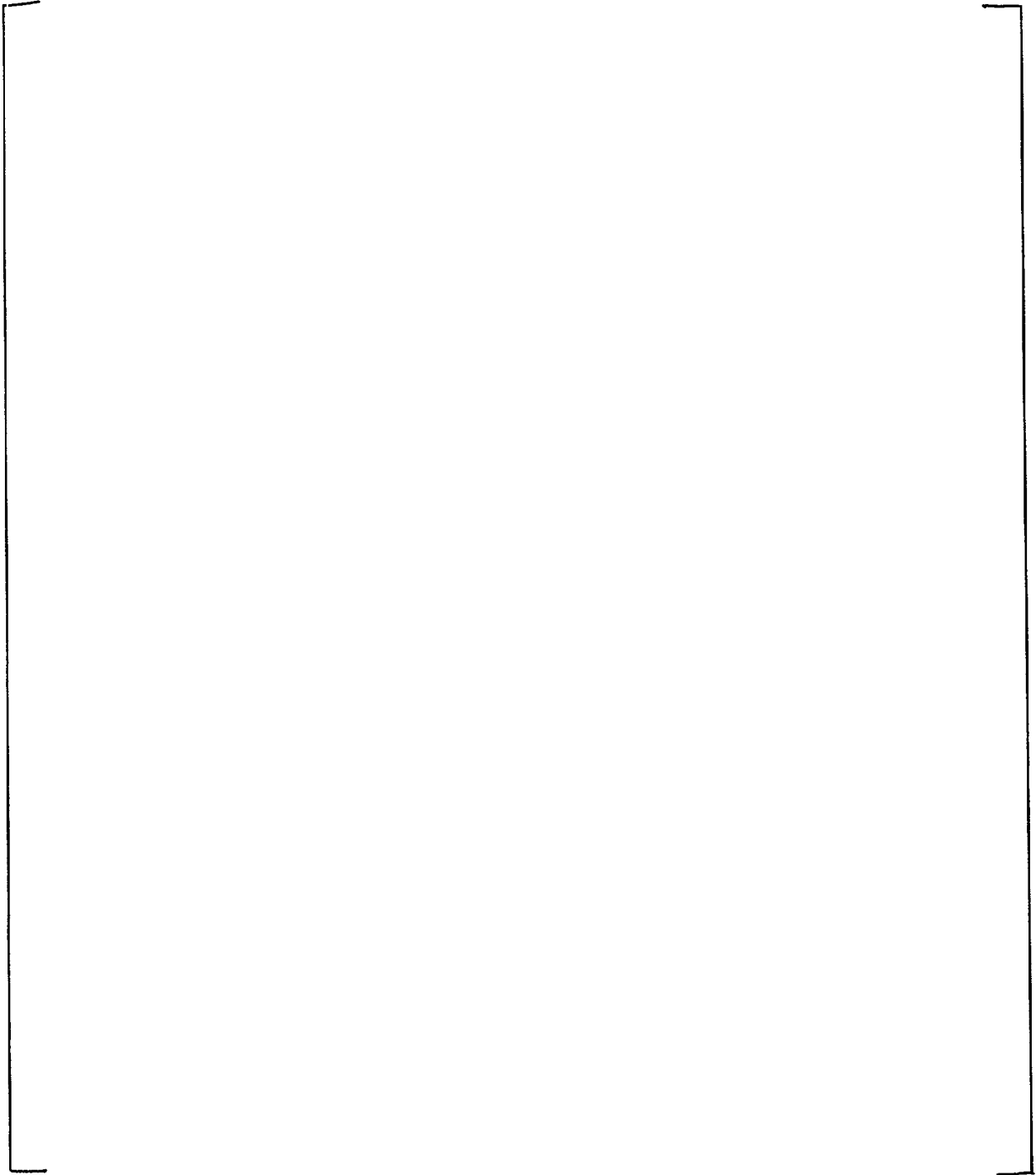


*Figure 5.24 Prediction Error versus Mass Flux at R-factor of 1.0*

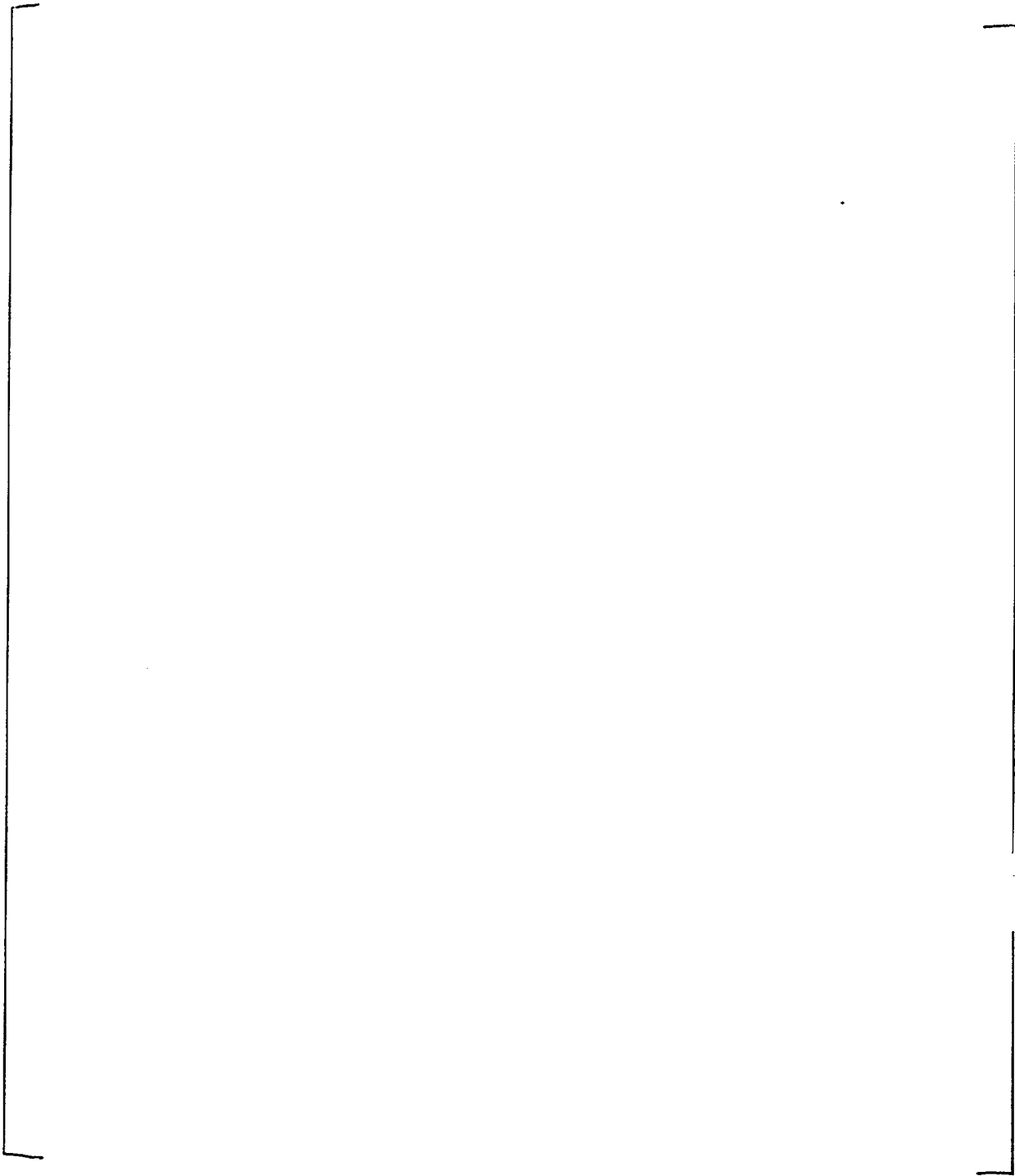


*Figure 5.25 Prediction Error versus Mass Flux at R-factor of 1.04*

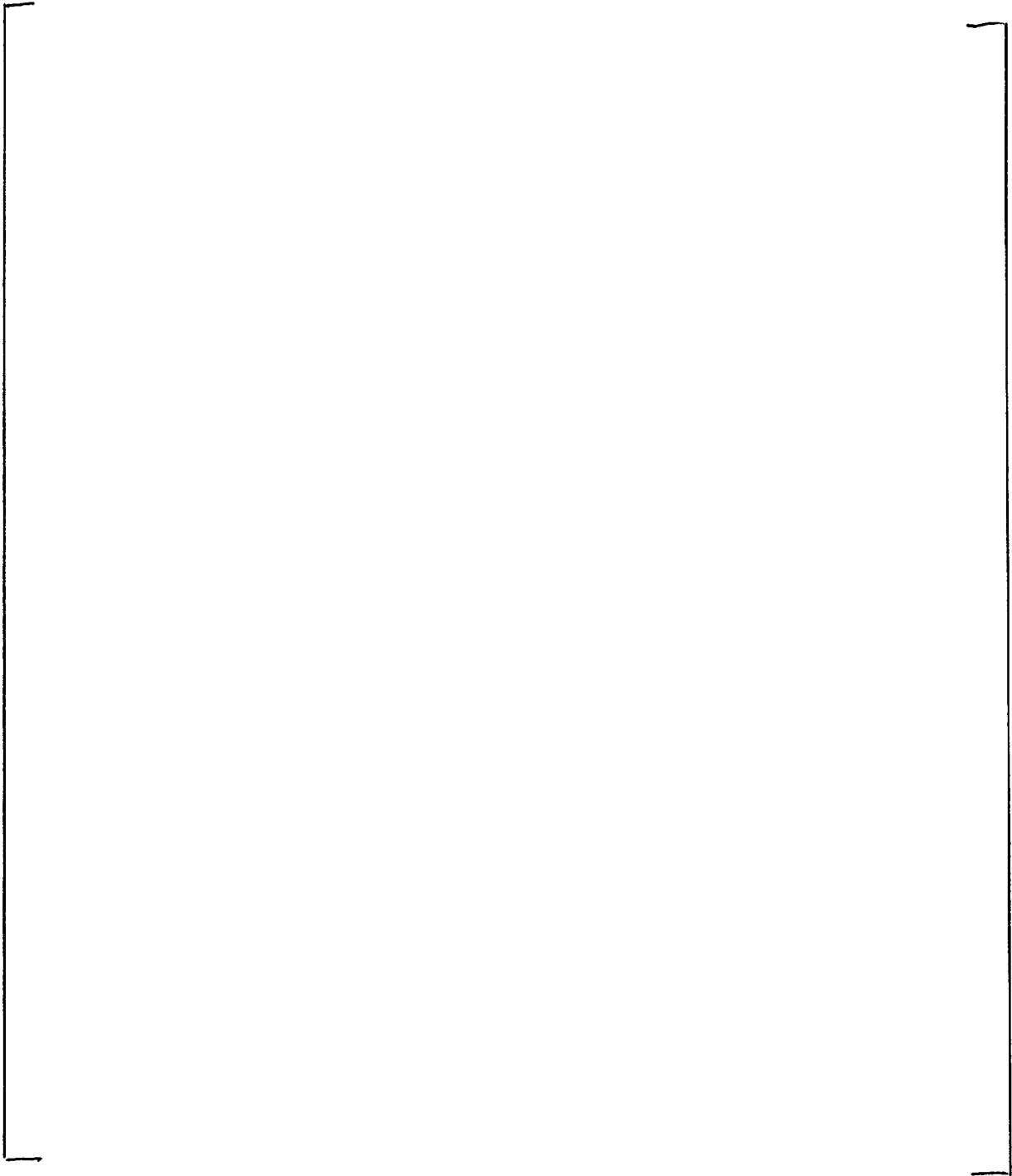


*Figure 5.26 Prediction Error versus Mass Flux at R-factor of 1.08*

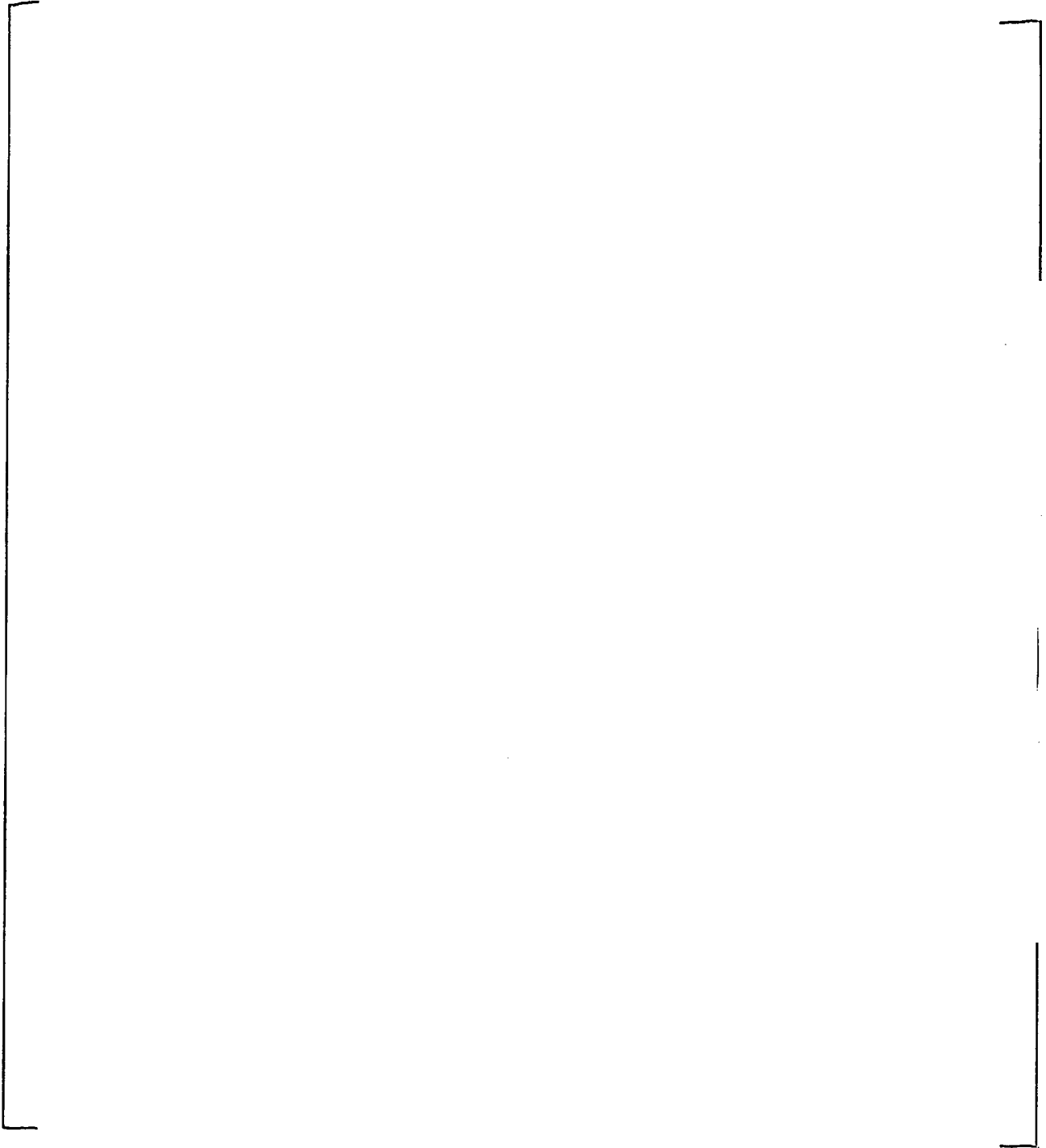


*Figure 5.27 Prediction Error versus Pressure at R-factor of 1.0*

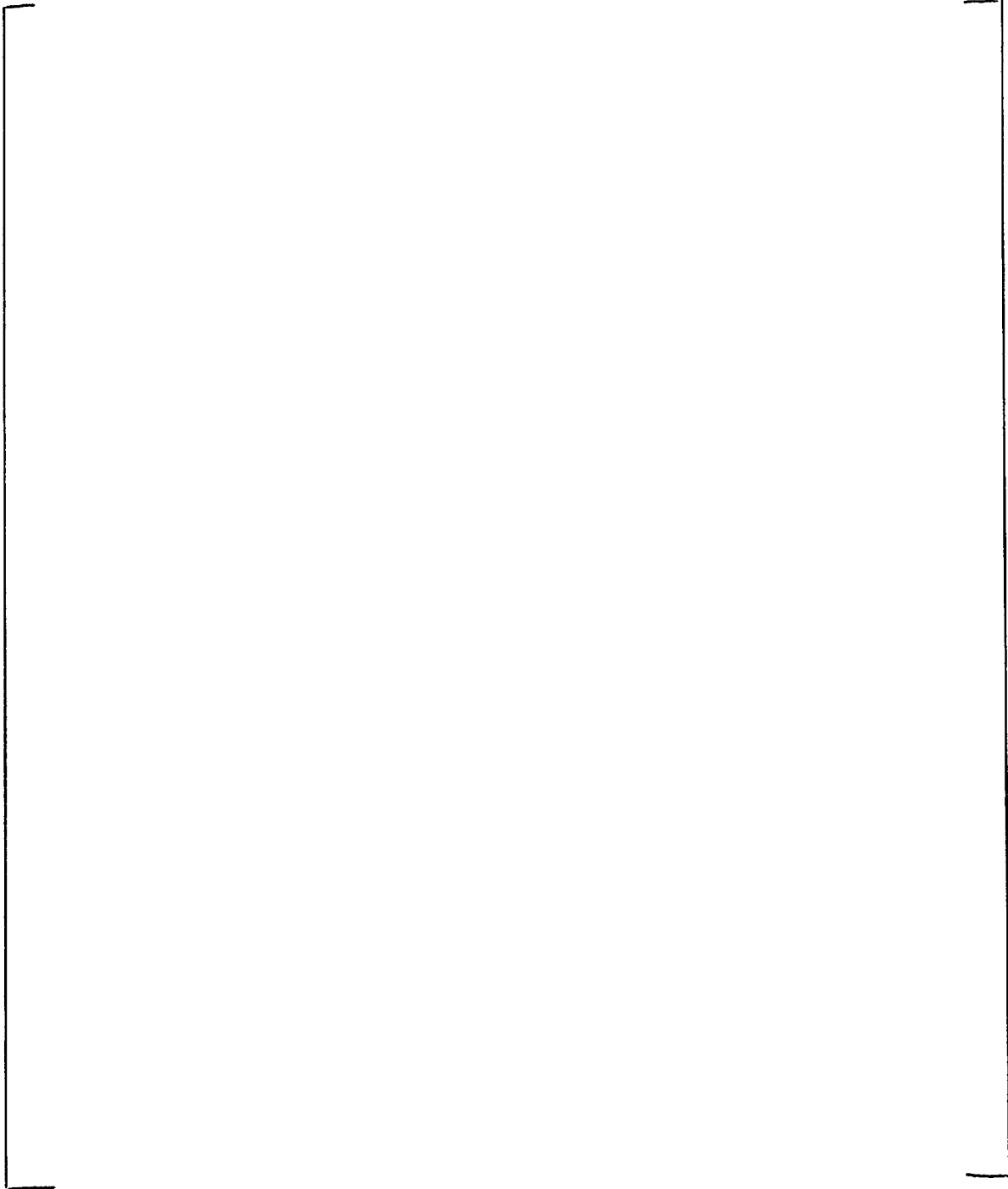


***Figure 5.28 Prediction Error versus Pressure at R-factor of 1.04***

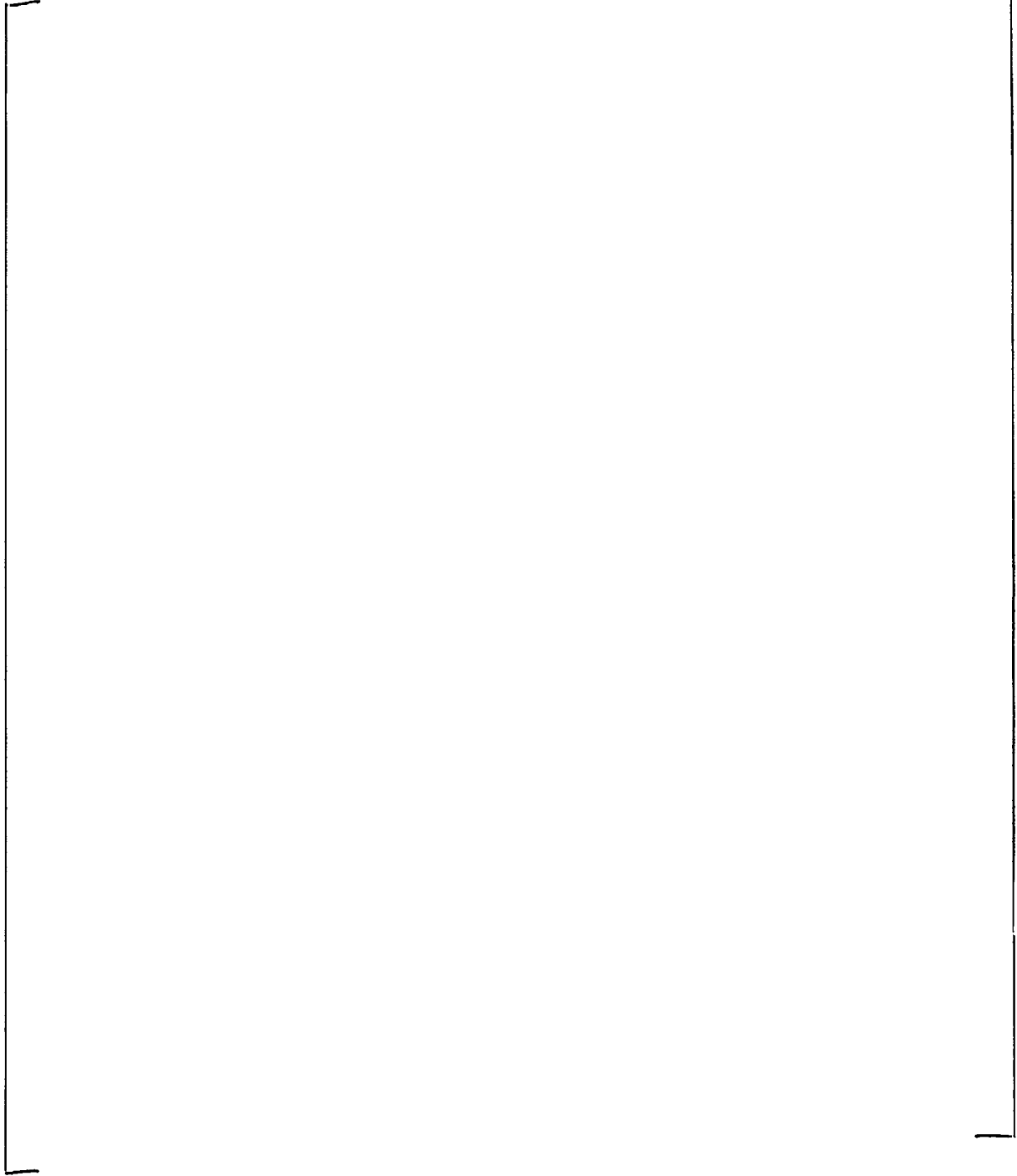


*Figure 5.29 Prediction Error versus Pressure at R-factor of 1.08*

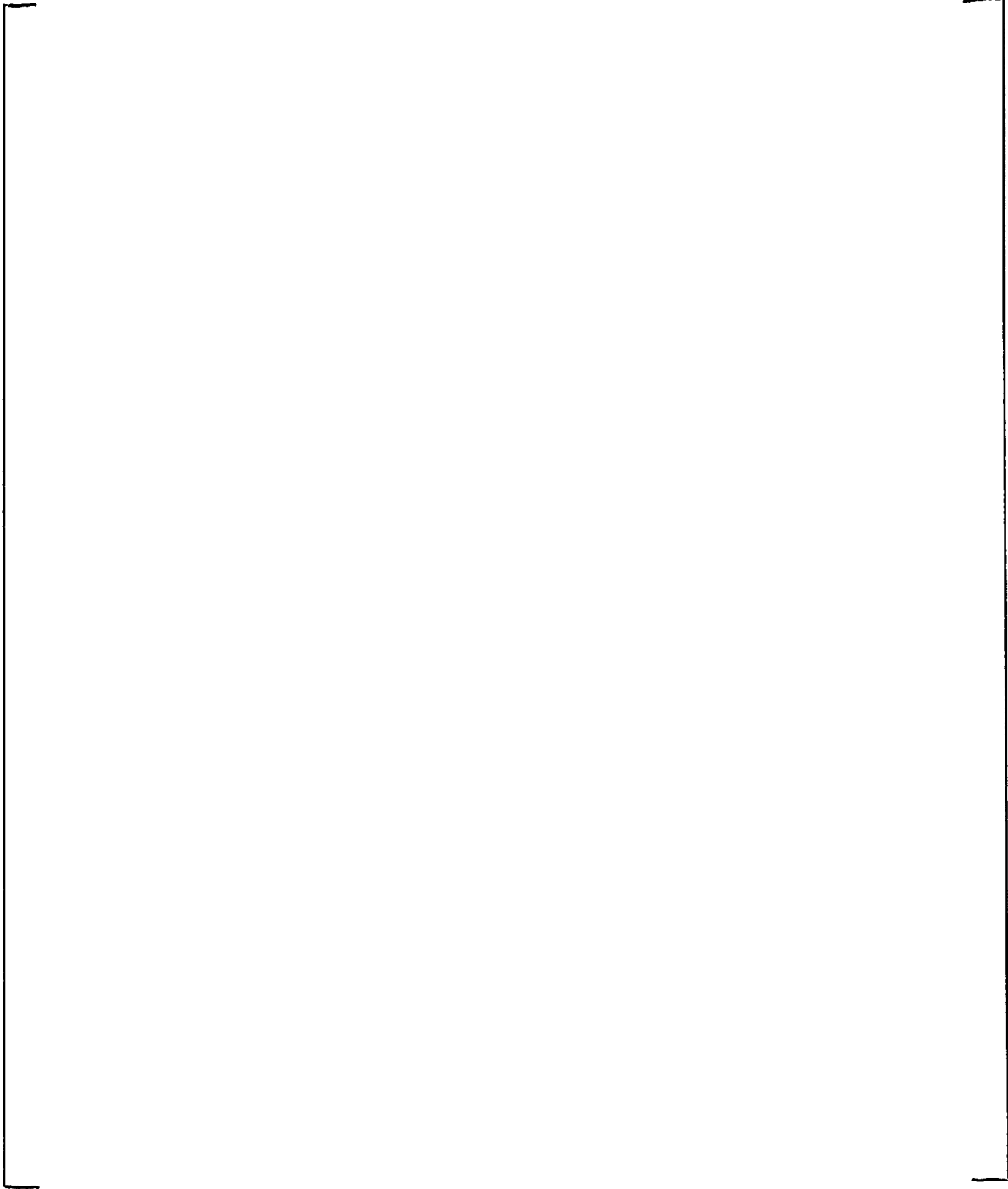


*Figure 5.30 Prediction Error versus Subcooling at R-factor of 1.0*



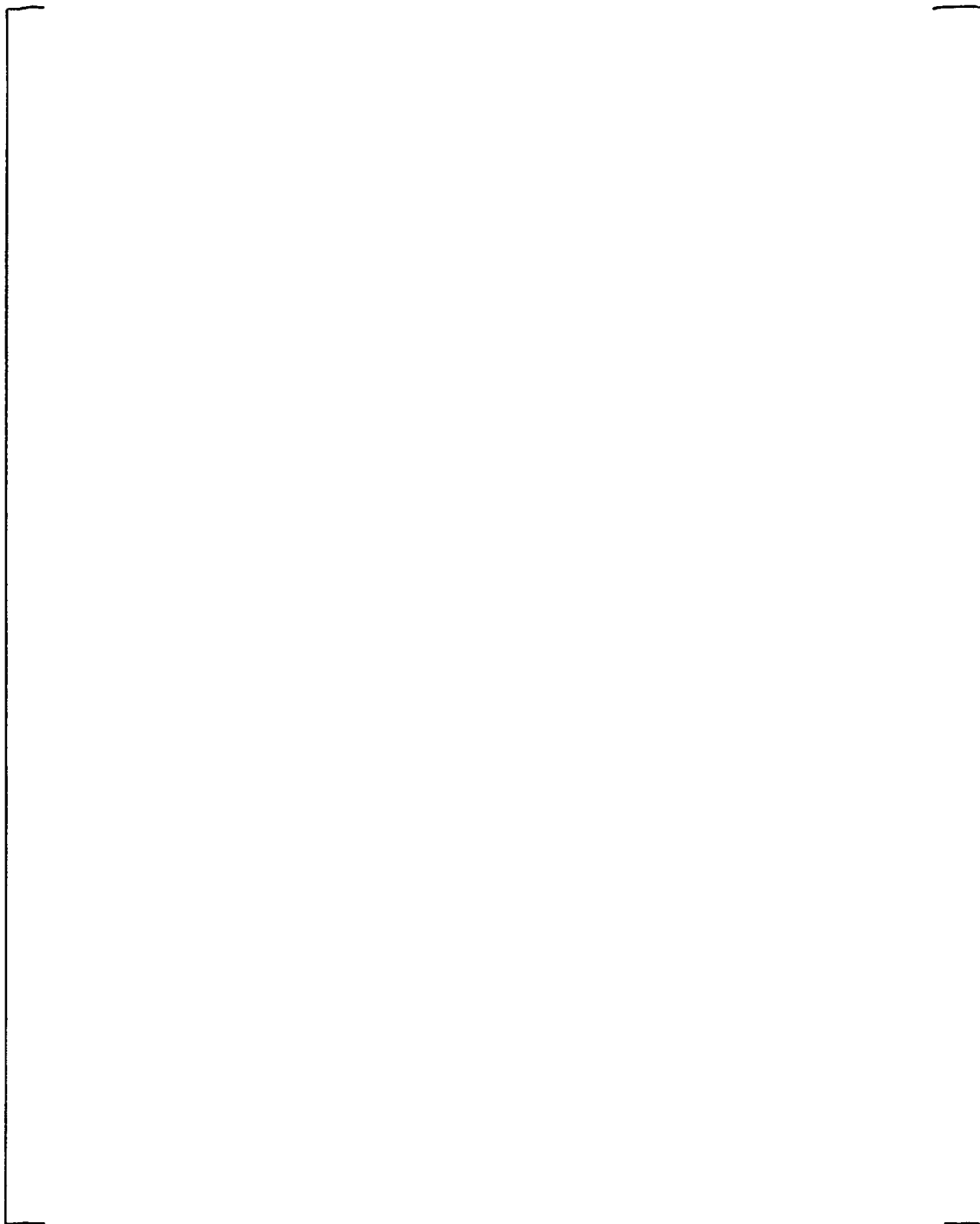


*Figure 5.31 Prediction Error versus Subcooling at R-factor of 1.04*

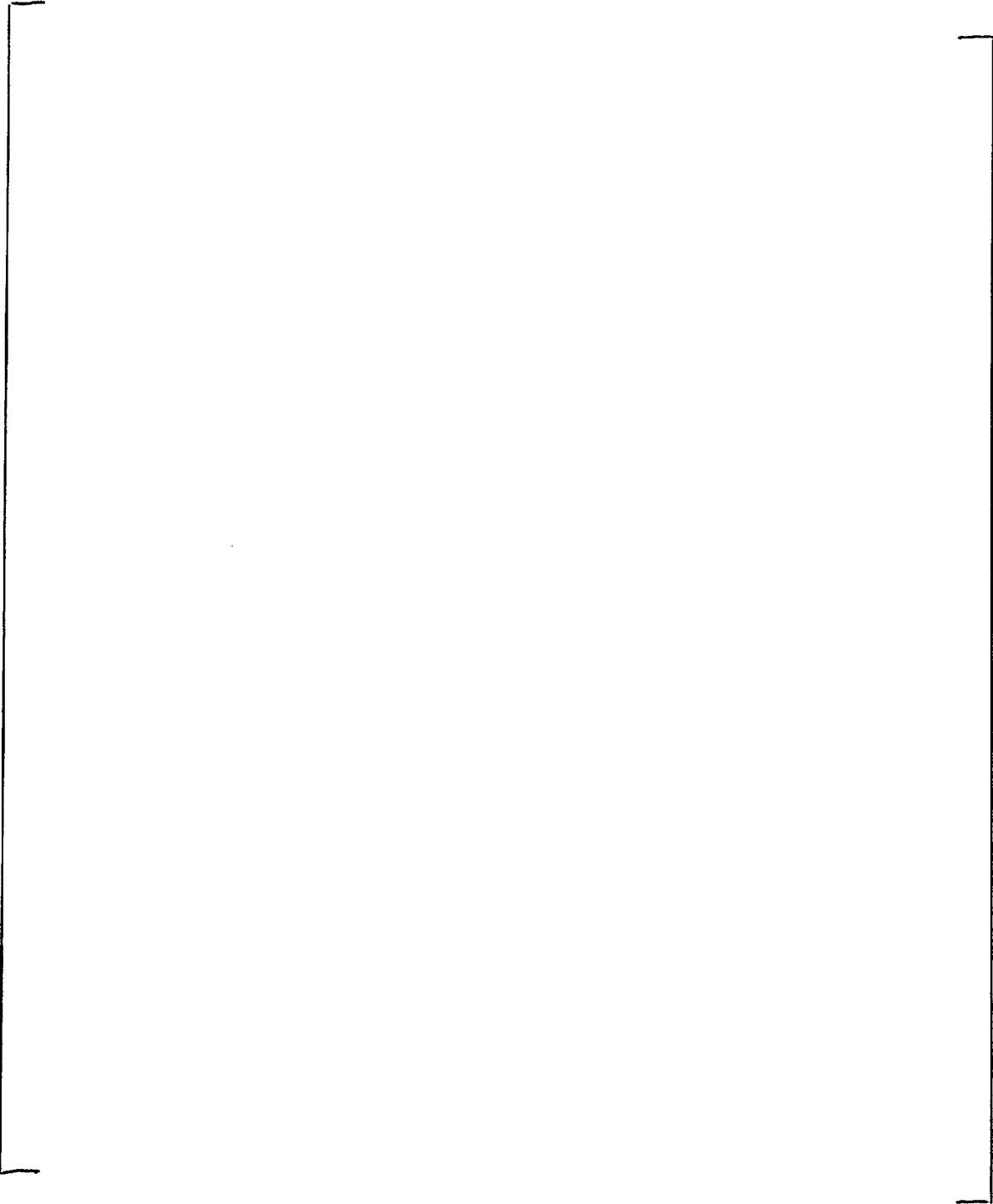


***Figure 5.32 Prediction Error versus Subcooling at R-factor of 1.08***

## 6 CONFIRMATION FOR TRANSIENT APPLICATION

### 6.1 Introduction

One specified acceptable fuel design limit (SAFDL) is that no more than 0.1% of the fuel rods in the core experience boiling transition under normal operation and anticipated operational occurrences. This requirement is equivalent to maintaining a certain transient Critical Power Ratio (CPR).

Transient CPR predictions involve evaluation of the flow, enthalpy, and pressure in the fuel assembly at each axial node as a function of time during the transient. A transient systems analysis code is used to calculate the transient fluid parameters. These parameters are then used with the steady-state CPR correlation for an assembly to evaluate transient CPR. One transient systems analysis code used by ABB for CPR predictions is the BISON-SLAVE channel model of the BISON transient analysis code (Reference 2). In licensing analysis applications the plant Operating Limit Minimum Critical Power Ratio (OLMCPR) is determined based, in part, on calculations with a transient systems analysis code. The OLMCPR is established to ensure that the Safety Limit Minimum Critical Power Ratio (SLMCPR) is not violated.

Two transient test programs are available to confirm that the ABBD1.0 CPR correlation in conjunction with the BISON-SLAVE channel model provides conservative  $\Delta$ CPR predictions during transient applications. The first program is the qualification of the ABBD2.0 CPR correlation for transient applications described in Reference 5. [ ] flow reduction transient tests and [ ] power increase transient tests were used to confirm that the ABBD2.0 CPR correlation for SVEA-96+ fuel in conjunction with the BISON-SLAVE channel model provide conservative CPR results during transient applications. Specifically, it was demonstrated in Reference 5 that transient CPR results were conservatively predicted in over 98% of the cases. The three non-conservative results were only marginally non-conservative and were well within the measurement uncertainty. These results for ABBD2.0 in Reference 5 are considered to provide confirmation that the ABBD1.0 CPR correlation in conjunction with the BISON-SLAVE code will also predict conservative results. Both correlations use [ ]

. ] Therefore, the program described in Reference 5 to qualify the ABBD2.0 CPR correlation for transient application for the SVEA-96+ assembly is considered to provide confirmation that the ABBD1.0 CPR correlation with the BISON-SLAVE code will predict conservative CPR results during a transient involving the SVEA-96 assembly.

The second test program confirming that the ABBD1.0 CPR correlation in conjunction with the BISON-SLAVE channel model provides conservative

transient  $\Delta$ CPR predictions is described in Section 7 of Reference 1. This program validated the application of the XL-S96 CPR correlation in conjunction with the BISON-SLAVE code for transient applications using the same process as used for the ABBD2.0 CPR correlation in Reference 5. Use of these SVEA-96 tests described in Section 7 of Reference 1 to confirm that the ABBD1.0 CPR correlation in conjunction with the BISON-SLAVE code provides an additional confirmation of the conservative treatment of CPR during transient application. This additional verification is described in this section.

The methodology for confirming that the application of the ABBD1.0 correlation in transient calculations will provide conservative predictions of  $\Delta$ CPR is summarized in this section. Specifically, the process for qualifying implementation of the ABBD1.0 correlation in transient codes is described. Then, the transient experiments performed in the FRIGG test loop and described in Section 7 of Reference 1 are summarized. Finally, the ABBD1.0 correlation validation in the BISON-SLAVE transient code is presented. The methodology used to confirm the adequacy of the ABBD1.0 correlation for transient applications described in this section is the same as the illustration for ABBD2.0 described in Reference 5.

## 6.2 Transient Implementation Validation Methodology

The two objectives of the transient systems analysis code implementation validation are to:

1. Confirm proper implementation of the steady state CPR correlation in the transient code.
2. Confirm the capability of the steady-state CPR correlation implemented in the transient code to calculate dryout during transients with adequate accuracy to provide conservative predictions of  $\Delta$ CPR.

Transient code implementation of the ABBD1.0 CPR correlation is validated for each code application by [

- a.
- b.

. ]

### 6.3 Transient Dryout Experiments

The transient tests used to validate the XL-S96 correlation were described in detail in Section 7 of Reference 1. The use of these tests to validate the ABBD1.0 correlation for transient applications is described in this section.

#### 6.3.1 FRIGG Loop

The transient tests were performed with the same test facility used in the steady-state experiments described in Section 2 of Reference 1.

As discussed in Reference 1, flow reduction transients with a SVEA-96 test assembly were simulated in the FRIGG loop transient tests. The FRIGG loop transients cases [

.] These flow reduction transients were performed by varying the speed of the recirculation pump positioned in the main circulation loop as well as the heater rod power.

Dynamic heater rod thermocouple responses are recorded during the transient tests. In addition, transient test system response data are recorded in order to provide time-dependent boundary conditions for the transient system code calculations. The test section inlet coolant flow, pressure, temperature and the total power production are recorded.

#### 6.3.2 Test Section

The test section used for the transient tests is identical to the test section (SF24A) used for steady state tests. The local power distribution used in the transient tests is shown in Figure 6.1.

#### 6.3.3 Transient Tests Description

Flow reduction event simulations were used for the XL-S96 CPR correlation validation for transient applications in Reference 1. The same data discussed in Reference 1 were used to validate the use of ABBD1.0 for transient applications. The flow reduction transient is characterized as follows:

1. The mass flow to the test section was reduced from about 3 kg/s to 1 kg/s (6.6 lb/s to 2.2 lb/s) in about 4 seconds.
2. The reduction in flow rate was followed by a reduction of the power supplied to the heater rods. The heater rod power reduction was initiated between 0.5 to 2.5 seconds after the flow reduction was initiated.

The general transient behavior is shown schematically in Figure 6.2.

#### 6.3.4 Dryout Threshold Temperature

The dryout threshold temperature is the temperature increase during the transient which is assumed to indicate dryout (e.g., CPR equals 1.0). As described in Reference 1, a dryout threshold temperature [

. ]

#### 6.3.5 Transient Data

Five transient tests were performed in Reference 1 and used for the transient CPR performance evaluation. All five cases have the same general transient behavior as shown in Figure 6.2.

The initial test section conditions (power and mass flow) and the delay between the start of flow coastdown and the start of power reduction were varied. These data, as well as the power and mass flow conditions in the final state of the transient, are summarized in Table 6.1. The pressure was maintained at about 7 MPa (1015 psia), and the inlet subcooling was maintained at about 10 °C (18 °F) in all the 5 cases.

Boundary conditions for these five flow reduction tests are shown in Figures 6.3 through 6.7. Figures 6.3 through 6.7 show heater rod power level, inlet coolant flow, test section inlet pressure, and inlet coolant temperature applied to the test section as a function of time.

Table 6.2 summarizes the lead thermocouple readings. Based on the dryout threshold temperature of [ , ] dryout was detected in cases 1435, 1437 and 1440. No indication of dryout was detected during test numbers 1394 and 1395.

#### 6.4 Implementation Validation for BISON Code

The BISON-SLAVE channel model of the time domain reactor dynamics code BISON (Reference 2) will be used in conjunction with the ABBD1.0 CPR correlation to predict transient CPR behavior for reload fuel licensing analysis applications and other operational transient simulations. The BISON-SLAVE simulations presented in this section are an illustration of the methodology described in Section 6.2 for confirming that the use of a CPR correlation based on steady-state data is acceptable for transient application.

An overview of the BISON code and test section model is described below. Then, the transient test simulation results for the flow reduction tests are presented. It will be shown that the BISON-SLAVE predictions of transient dryout are conservative for all tests confirming the conservative calculation of transient CPR performance.

### 5.4.1 BISON Code

BISON is a time domain BWR dynamics code used for analyzing operational and safety related transients. The code simulates the hydraulics of the entire primary core coolant loop including the recirculation pumps. A two-group diffusion theory model describes the axial distributions of neutron flux and power in the reactor core. Heat conduction in the fuel is solved in the radial direction at each axial segment. The influence from external systems such as the turbine, control systems, scram signals, and relief valves can also be simulated in BISON.

A BISON-SLAVE version of the code is used for simulation of a single bundle in the core by utilizing boundary conditions from a previous BISON calculation for the entire reactor. It can also be used in a stand-alone mode to study heated bundles in loop experiments. External boundary conditions in the form of inlet mass flow and temperature, inlet pressure, and assembly power are supplied as input to the code. This option was used in the present evaluation to calculate the transient critical power ratio (CPR) for the experiments performed.

The ABBD1.0 CPR correlation is incorporated in the BISON-SLAVE code. Instantaneous fluid properties [ ] are used in evaluating the CPR correlation under transient conditions.

### 5.4.2 BISON Model

[ ] are modeled in the BISON simulations of the tests. The heated part of the test section is simulated with the BISON-SLAVE channel model. The heater rod is modeled with the same radial nodal divisions typically used in plant calculations. The radial representation and material compositions of the heater rod are shown in Figure 6.8.

The experimental conditions described in the previous sections were used as input to the BISON-SLAVE model. [ ]

[ ] The power is provided as a boundary condition for the heater rods in the test assembly. The axial and local rod radial power distributions are [ ]

[ ] The outlet pressure and inlet flow and subcooling are also provided as boundary conditions.

The R-factors for the local power distributions (Figure 6.1) used in the flow reduction tests were determined [ ]

[ ]

### 6.4.3 BISON Test Simulation Results

All five tests were simulated with the BISON-SLAVE code. The calculated transient CPR results are shown in Table 6.3. [

. ]

The predicted times to dryout [ ] are compared with the measured times to dryout [ ] in Table 6.4. [

. ]

### 6.5 Summary

The systematic ABB methodology used to confirm the conservative application of a CPR correlation for transient CPR code applications is illustrated in this section for the ABBD1.0 CPR correlation. The results in Reference 5 and the comparisons of BISON-SLAVE code predictions with SVEA-96 sub-bundle test results in this section demonstrate that the ABBD1.0 CPR correlation is capable of providing conservative estimates of the onset of dryout during fast transients.



**TABLE 6.1 INITIAL AND FINAL EXPERIMENTAL BOUNDARY CONDITIONS**


**TABLE 6.2 MEASURED DRYOUT TEMPERATURE RESULTS**


**TABLE 6.3 CALCULATED DRYOUT PERFORMANCE**


**TABLE 6.4 MEASURED AND PREDICTED TIMES TO DRYOUT**

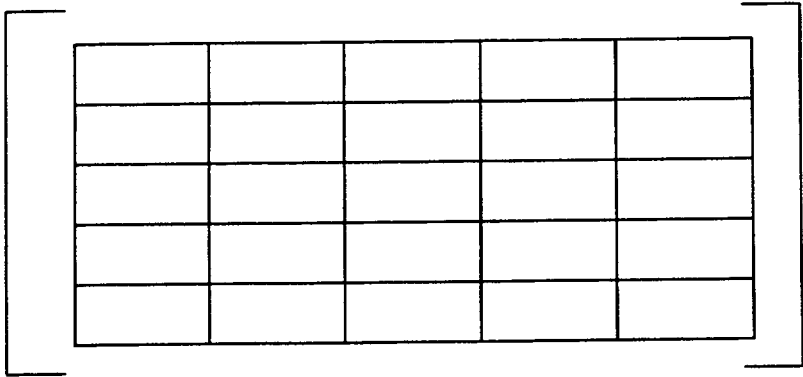



Figure 6.1 Flow reduction tests local power distribution

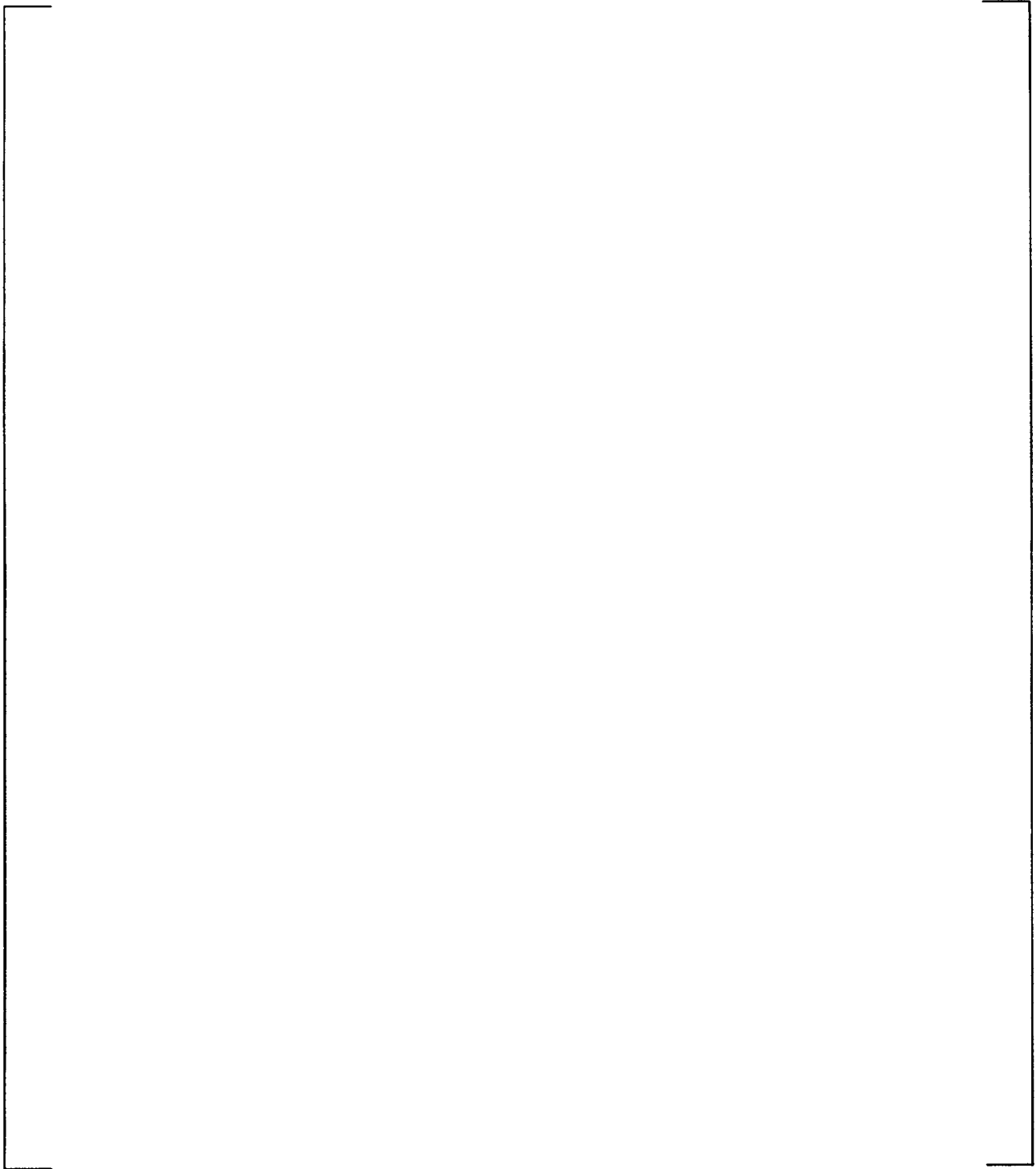


Figure 6.2 Schematic transient behavior

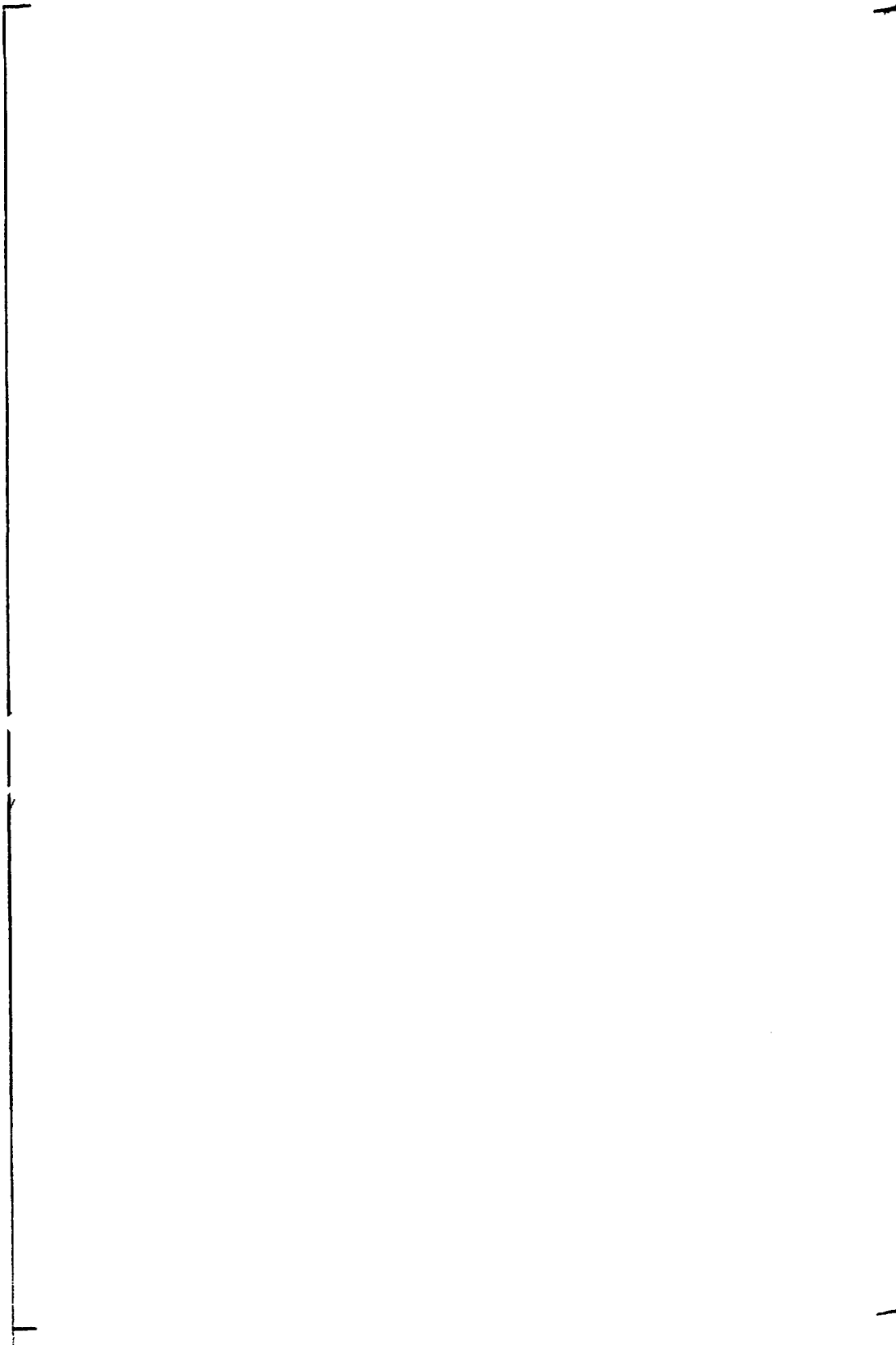


Figure 6.3 Boundary conditions for flow reduction transient test 1394

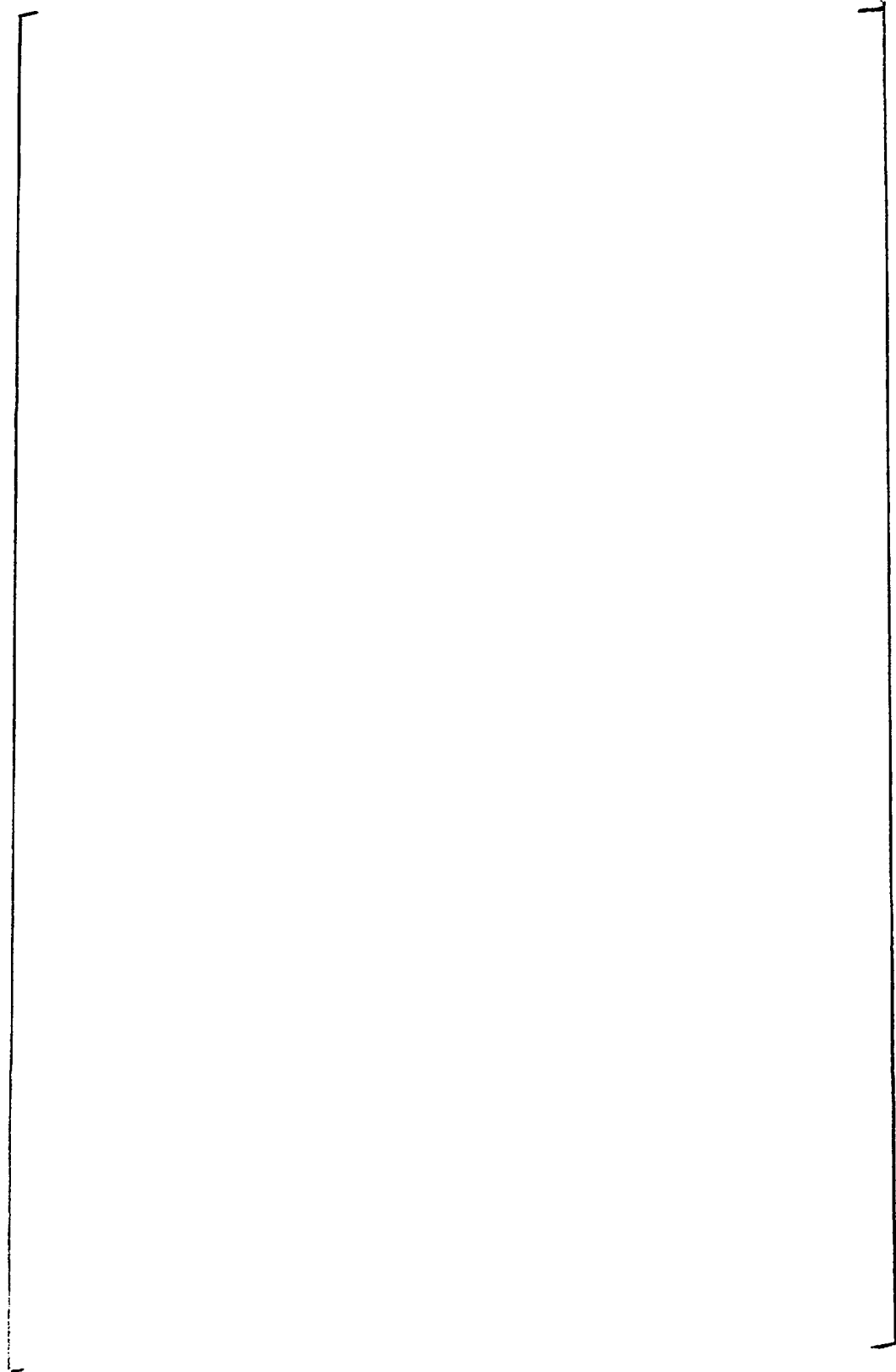


Figure 6.4 Boundary conditions for flow reduction transient test 1395

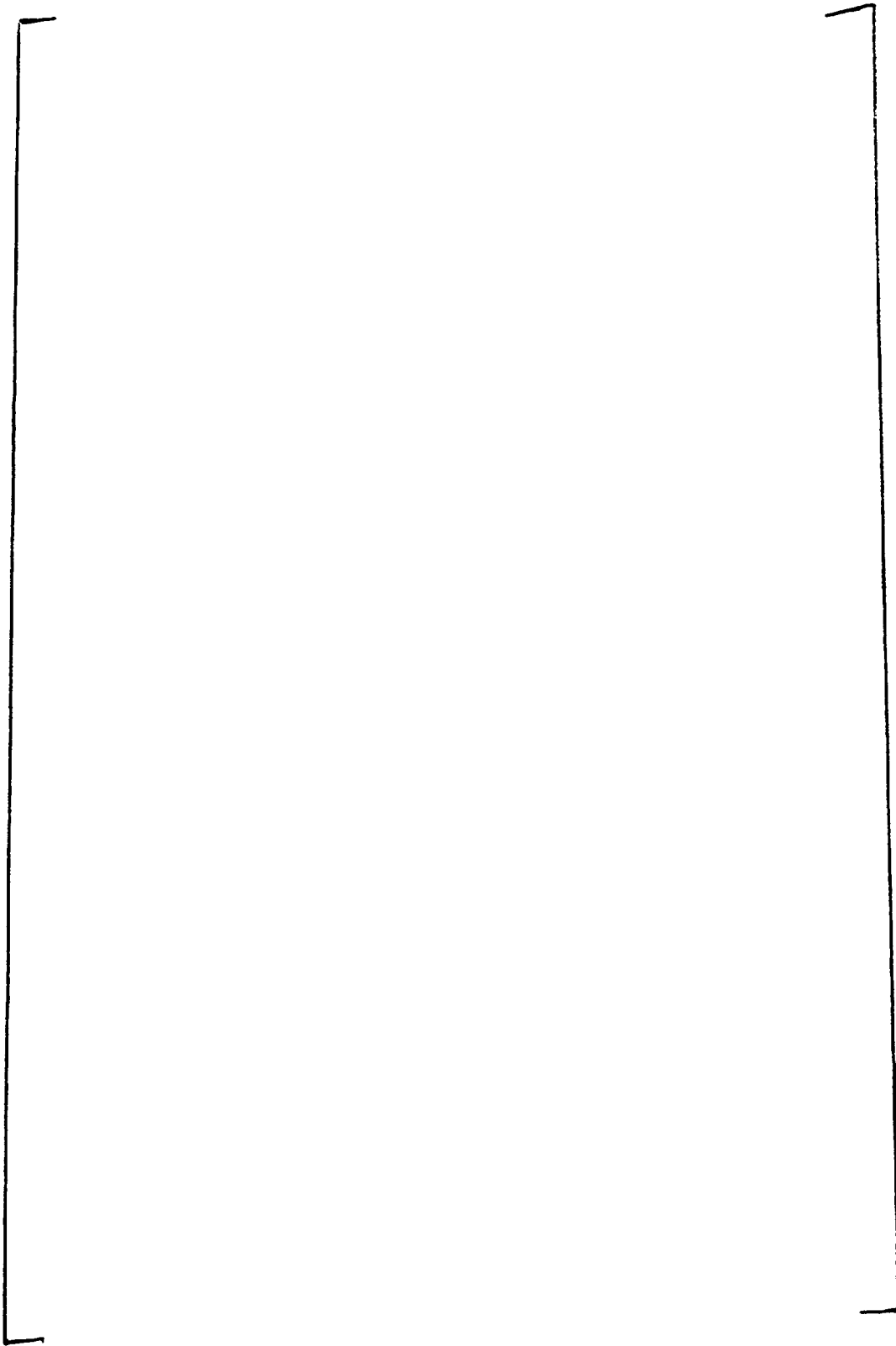


Figure 6.5 Boundary conditions for flow reduction transient test 1435

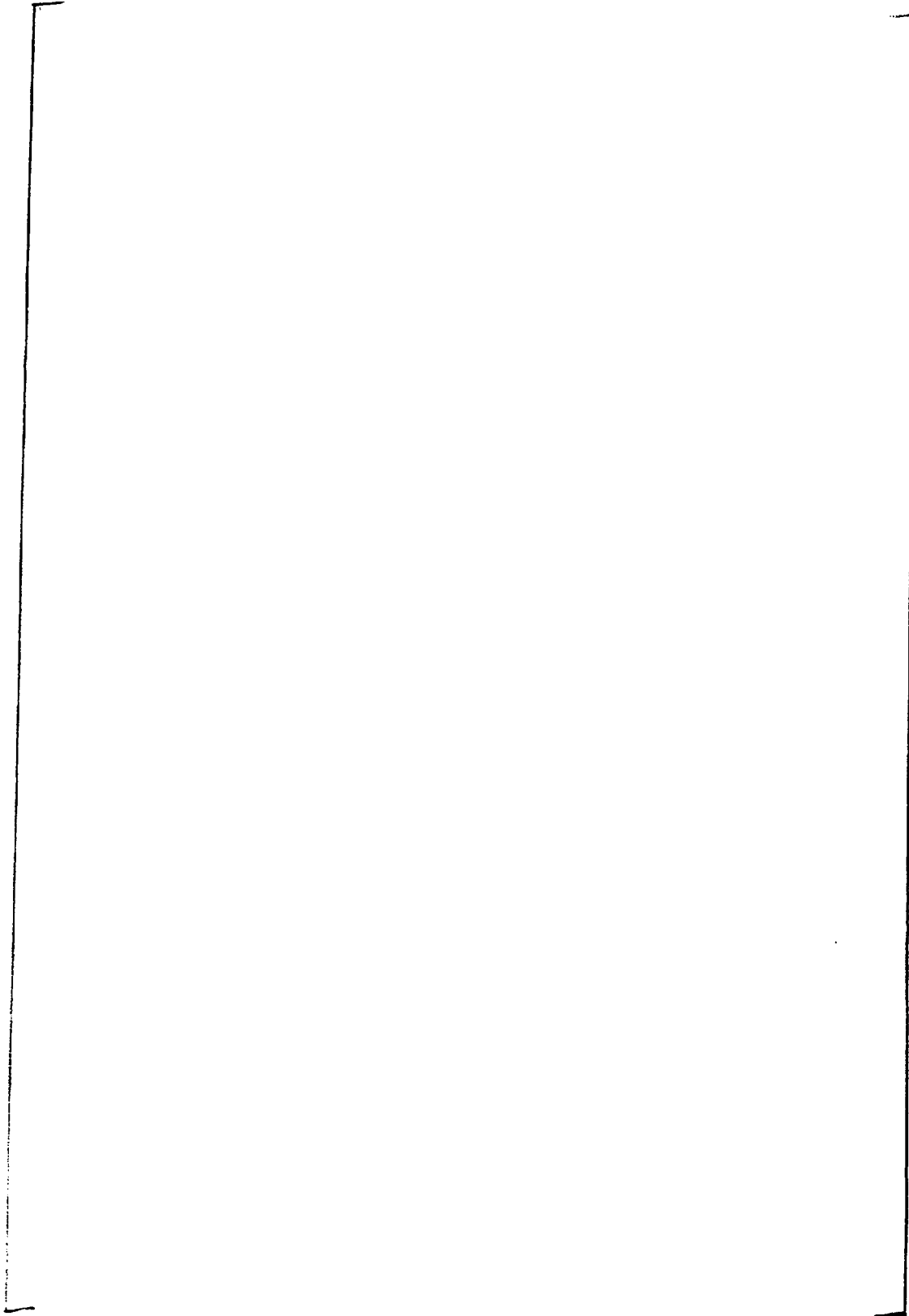


Figure 6.6 Boundary conditions for flow reduction transient test 1437

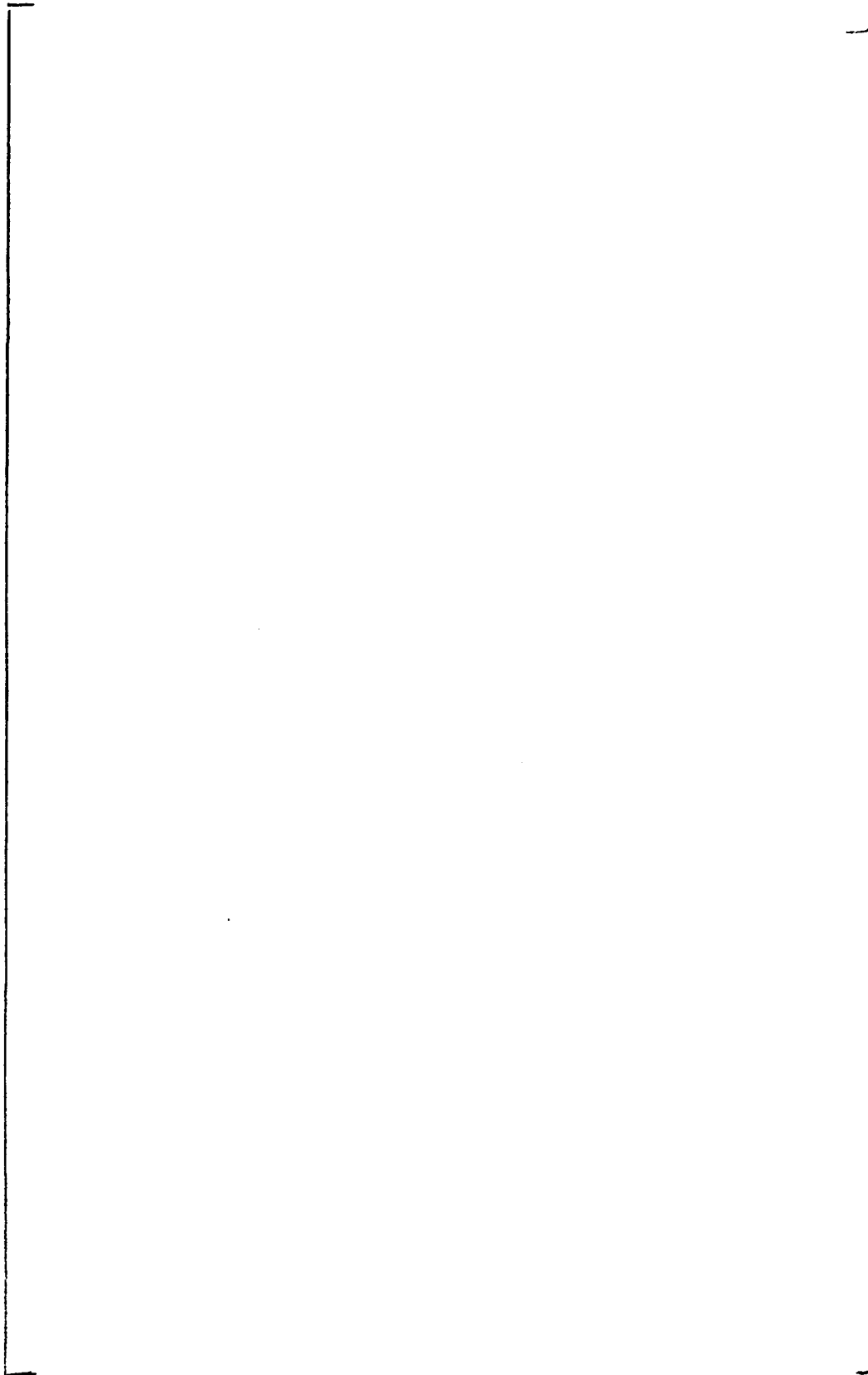


Figure 6.7 Boundary conditions for flow reduction transient test 1440



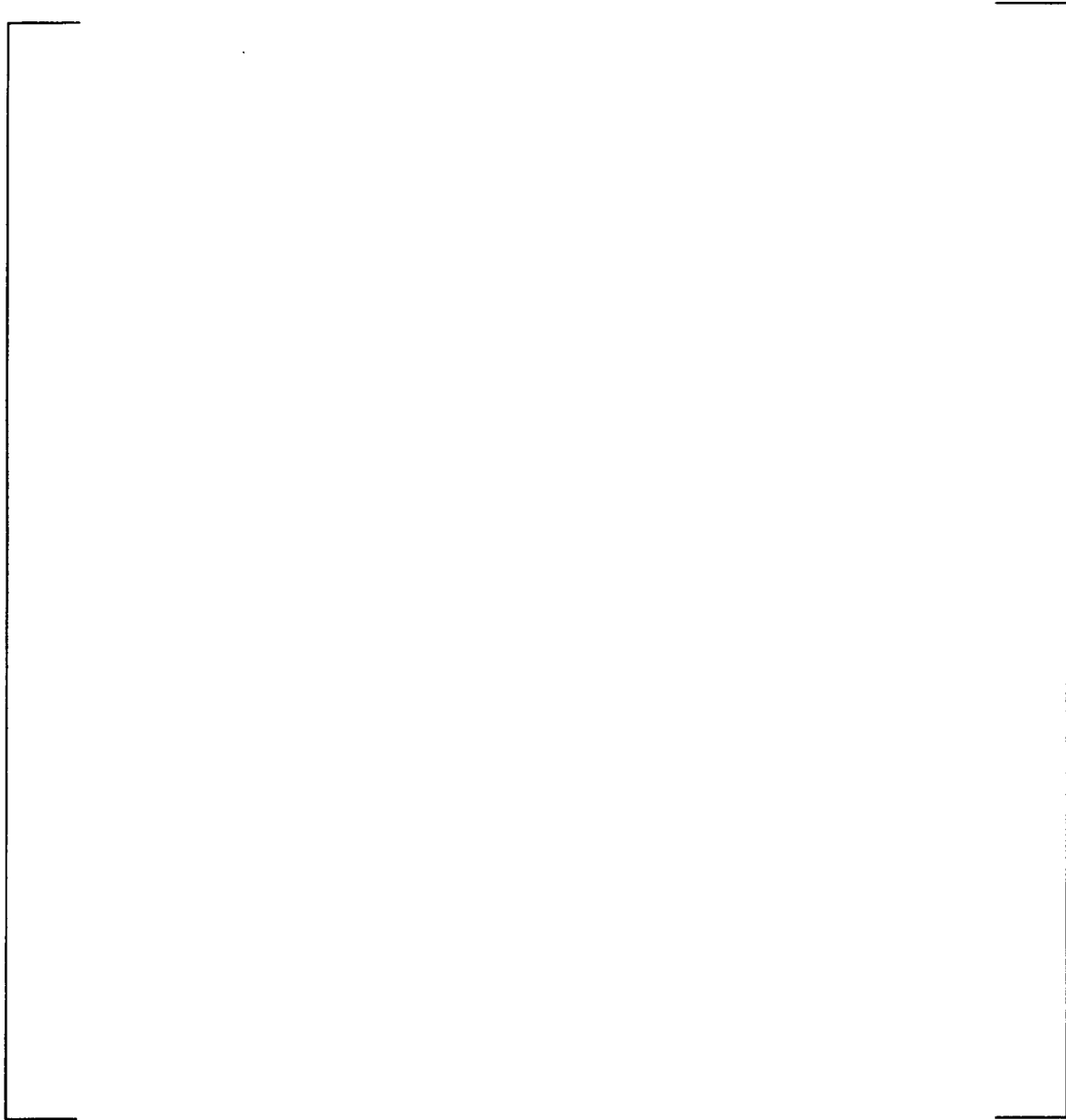


Figure 6.8 BISON-SLAVE model for test heater rod

## 7 CONCLUSIONS

The critical power measurements described in this report provide an accurate simulation of the SVEA-96 fuel assembly. A total of [ ] 24-rod sub-bundle data points covering the entire range expected during reactor operation were obtained. The ABBD1.0 critical power ratio correlation was developed to correlate this critical power data. The correlation was developed to provide best estimate predictions of critical power for a SVEA-96 fuel assembly. The mean prediction error and standard deviation over the entire range of validity are [ ].

Based on the critical power data for SVEA-96 and the evaluations of the data presented in this report, the following conclusions can be drawn:

1. Sufficient data have been obtained to justify the use of the correlation over the following ranges for design and licensing applications:

TABLE 7.1


These ranges cover the operating conditions expected during U.S. BWR steady-state, transient, or accident conditions over which CPR calculations are expected to be required.

2. The correlation provides a best estimate of the bundle Critical Power Ratio over the range of validity and, is, therefore, acceptable for evaluations of Critical Power Ratios for design and licensing purposes over this range.
3. The mean prediction error and standard deviation to be utilized for the correlation for design and licensing applications is [

]

are appropriate for computing core Safety Limit Minimum Critical Power Ratios (SLMCPR).

4. The correlation has been demonstrated to be capable of providing conservative estimates of the onset of dryout during fast transients. The capability of the correlation to provide conservative estimates of the onset of dryout during fast transients is demonstrated for each transient system code application. An illustration of the ABB methodology for confirming the capability of the correlation to conservatively treat transient applications is provided for the BISON-SLAVE code documented in Reference 2. It is demonstrated in this illustration that the correlation, in conjunction with the BISON-SLAVE code, is acceptable for the calculation of changes in CPR during transient events for design and licensing applications.

## 8 REFERENCES

1. "SVEA-96 Critical Power Experiments on a Full Scale 24-Rod Sub-Bundle", ABB Report UR-89-210-P-A, October 1993.
2. "BISON - A One Dimensional Dynamic Analysis Code for Boiling Water Reactors", ABB Report RPA 90-90-P-A, December 1991.  
  
"BISON - One Dimensional Dynamic Analysis Code for Boiling Water Reactors: Supplement 1 to Code Description and Qualification", ABB Report CENPD-292-P-A, July 1996.
3. "General Electric BWR Thermal Analysis Basis (GETAB): Data, Correlation and Design Application", NEDO-10958, November 1973.
4. "CONDOR: A Thermal-Hydraulic Performance Code for Boiling Water Reactors", ABB Report BR 91-255-P-A, Rev. 1, (Proprietary), BR 91-262-NP-A (Non-proprietary), May 1991.
5. "10x10 SVEA Fuel Critical Power Experiments and CPR Correlations: SVEA-96+", ABB Report CENPD-389-P, June 1998.
6. "Response to Request for Additional Information Regarding CENPD-389-P", Letter, I. C. Rickard (ABB) to USNRC Document Control Desk, LD-99-019, April 9, 1999.
7. "Acceptance for Reference of Licensing Topical Report CENPD-389-P, 10x10 SVEA Fuel Critical Power Experiments and CPR Correlations: SVEA-96+", Letter, C. A. Carpenter (NRC) to I. C. Rickard (ABB), May 8, 1999.

## **APPENDIX A**

### **SVEA-96 Assembly Description**

The SVEA96 assembly is shown in Figures A-1 and A-2. The fuel assembly consists of 96 fuel rods arranged in four subbundles, each with a 5x5-1 lattice. Each subbundle is a separate unit with top and bottom tie plates. The fuel rods are supported laterally by six spacers, distributed uniformly along the bundle. The channel has a cruciform internal structure (watercross) with a square center channel and cross wings with gaps for non-boiling water during normal operation.

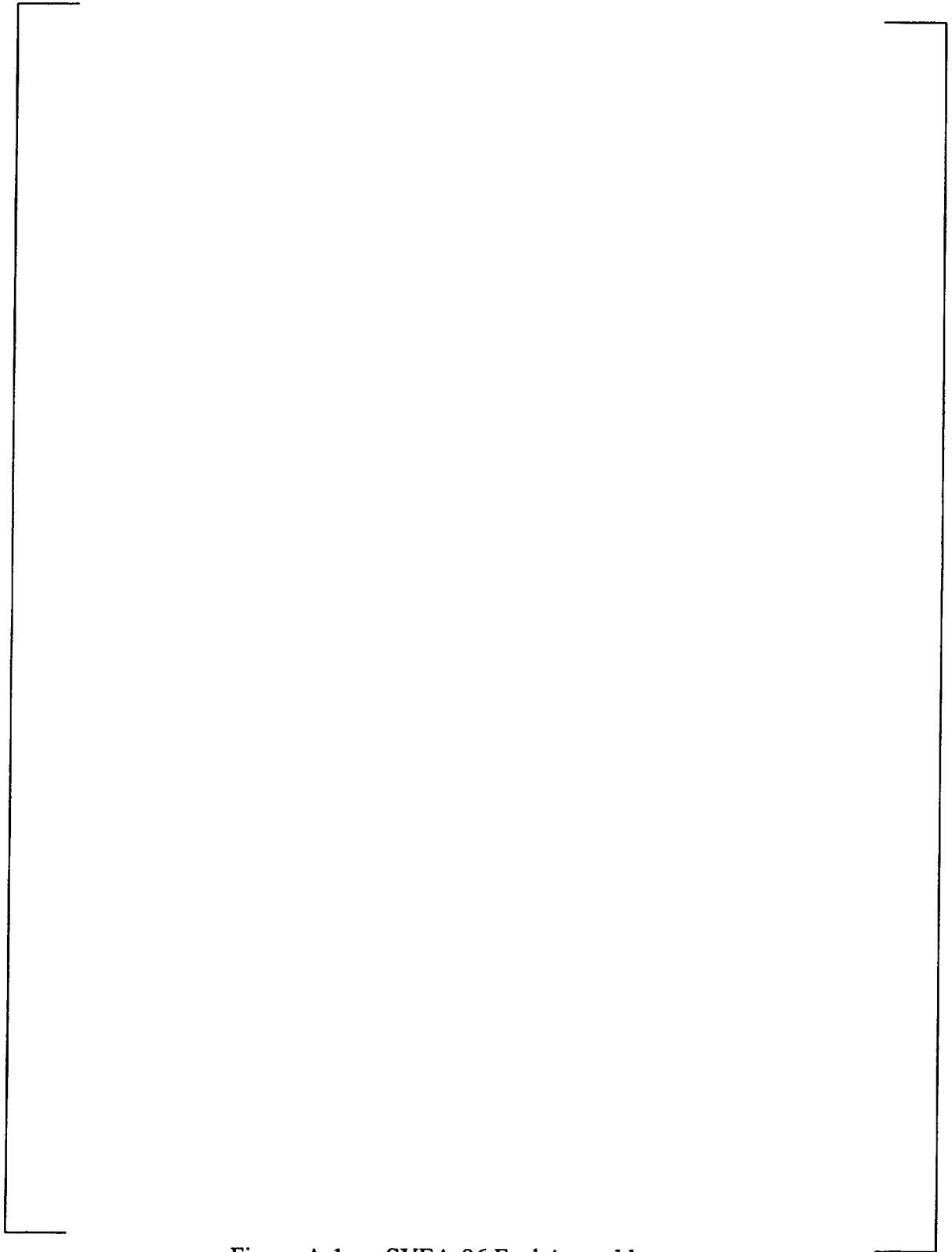


Figure A-1 SVEA-96 Fuel Assembly

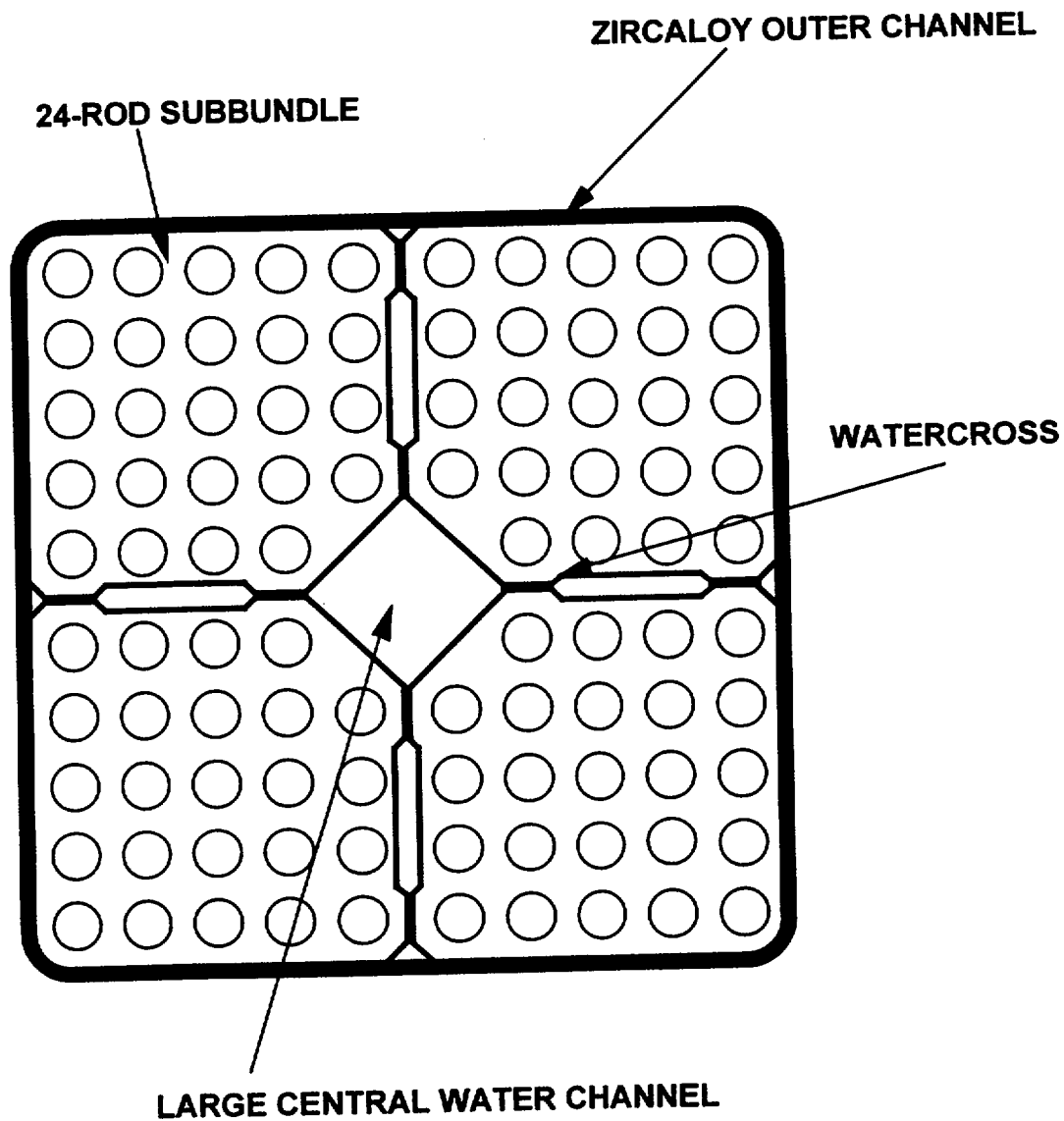


Figure A-2 SVEA96 Fuel Assembly Cross Section

**APPENDIX B****SVEA 96 Steady State Critical Power Test Data**  
**(Bottom-Peaked Axial Power Shape)**

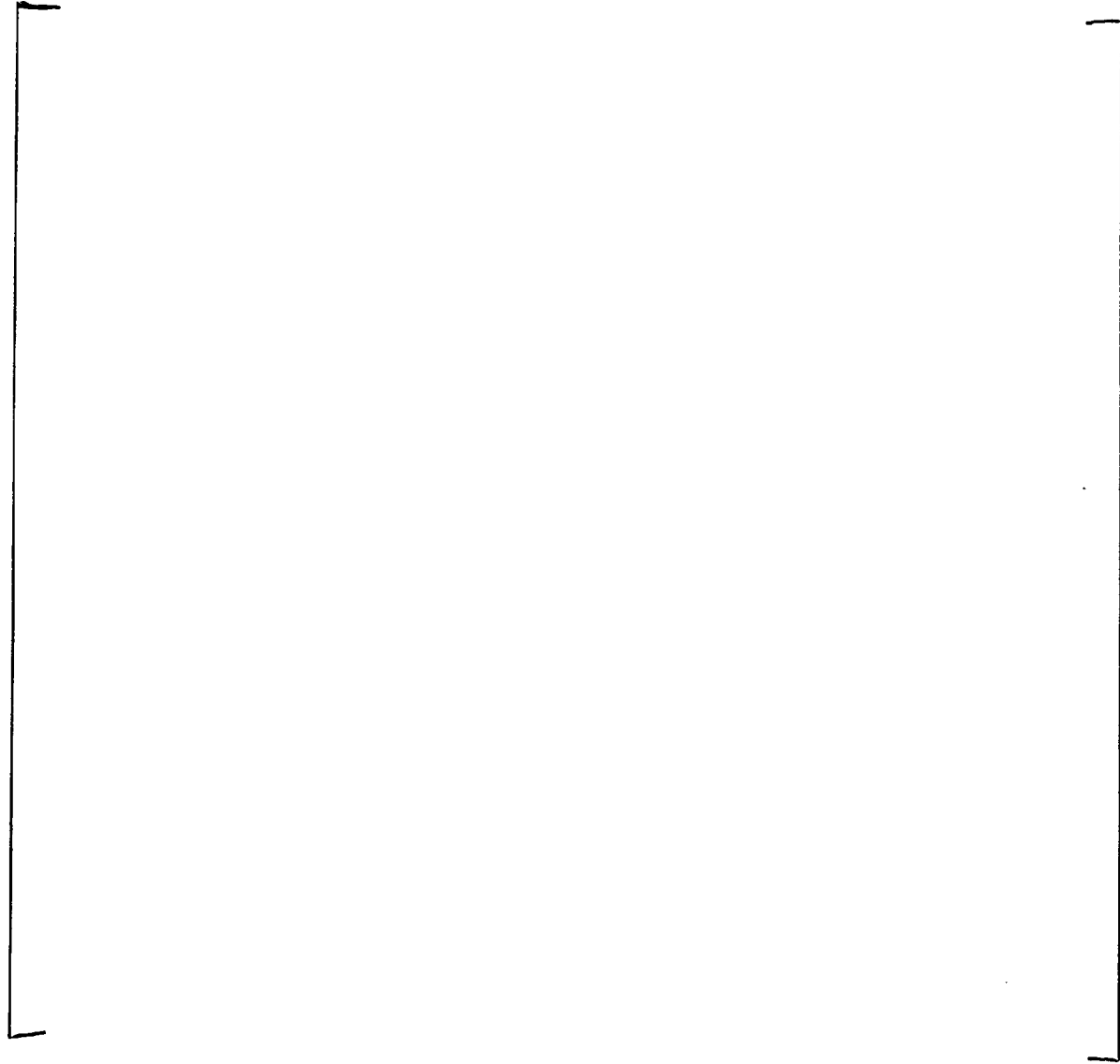
The data in this Appendix are provided as follows:

ID	The identity of the measurement point
P	The system pressure (bar)
T <sub>sub</sub>	Subcooling temperature (K)
Flow	Mass flow (kg/s)
Power	Bundle power at dryout (kW)
Y/I	The ratio between the average local power for the 15 peripheral rods and the average local power for the 9 central rods
Rod	The rod(s) and its/their thermocouples indicating dryout (refer to Figure 2.3 for rod location and Figure 2.6 for thermocouple location, e.g. 107.14 means rod 7 in Figure 2.3 and T/C level 14 in Figure 2.6)

The local power distribution map at about 3 kg/s flow is printed on each page together with a critical power versus mass flow plot with all separate dryout points. When the local power distribution map is not printed, it has been shown for a previous test series.

It must, however, be noted that the local power distribution may differ slightly for different points intended to have the same nominal distribution (e.g. AA4, AA5, etc.). The actual measured local power distributions were used for all points in the correlation development and validation process.

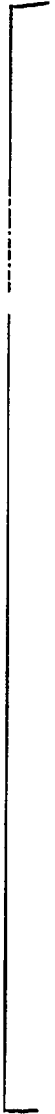






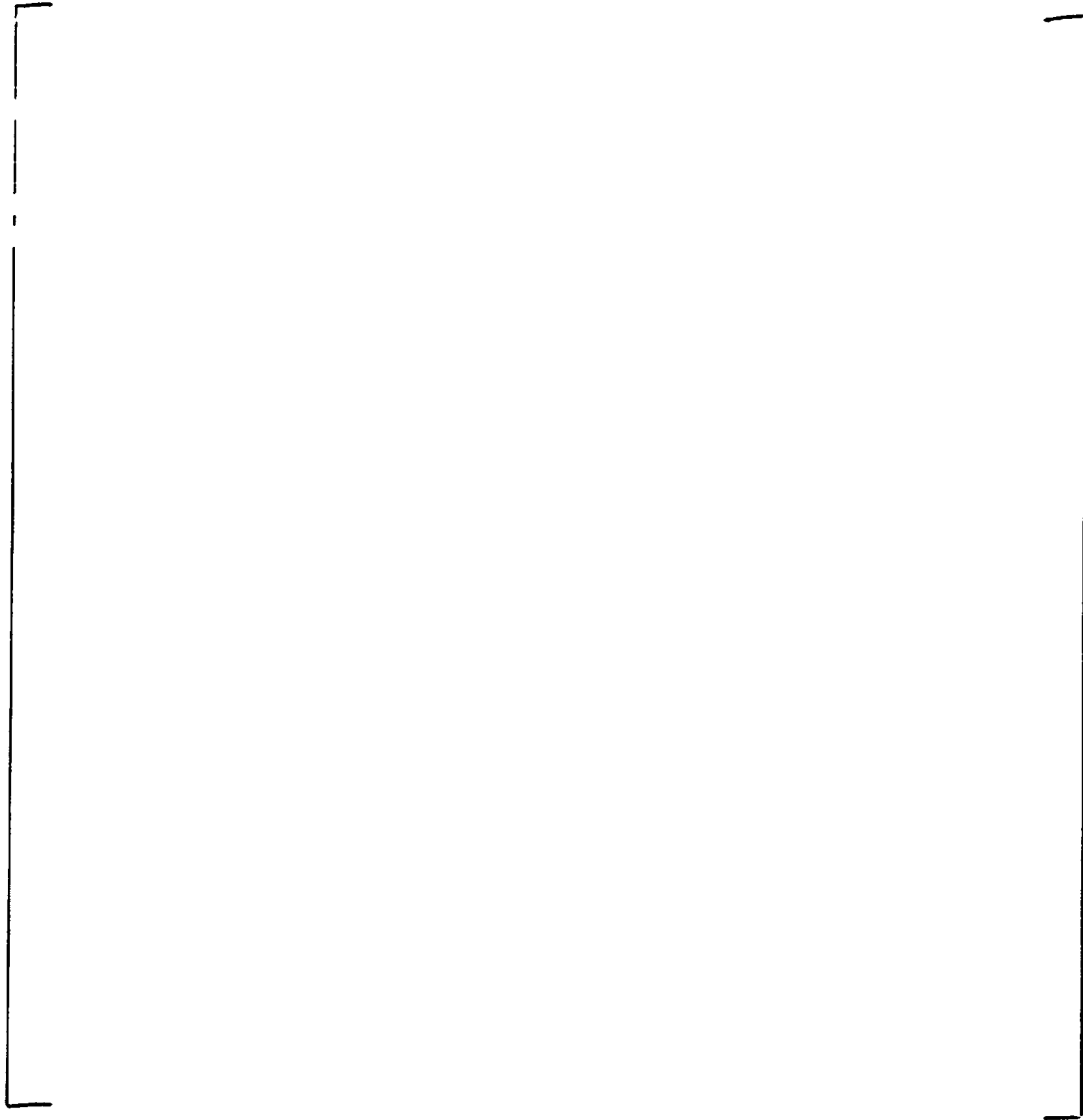


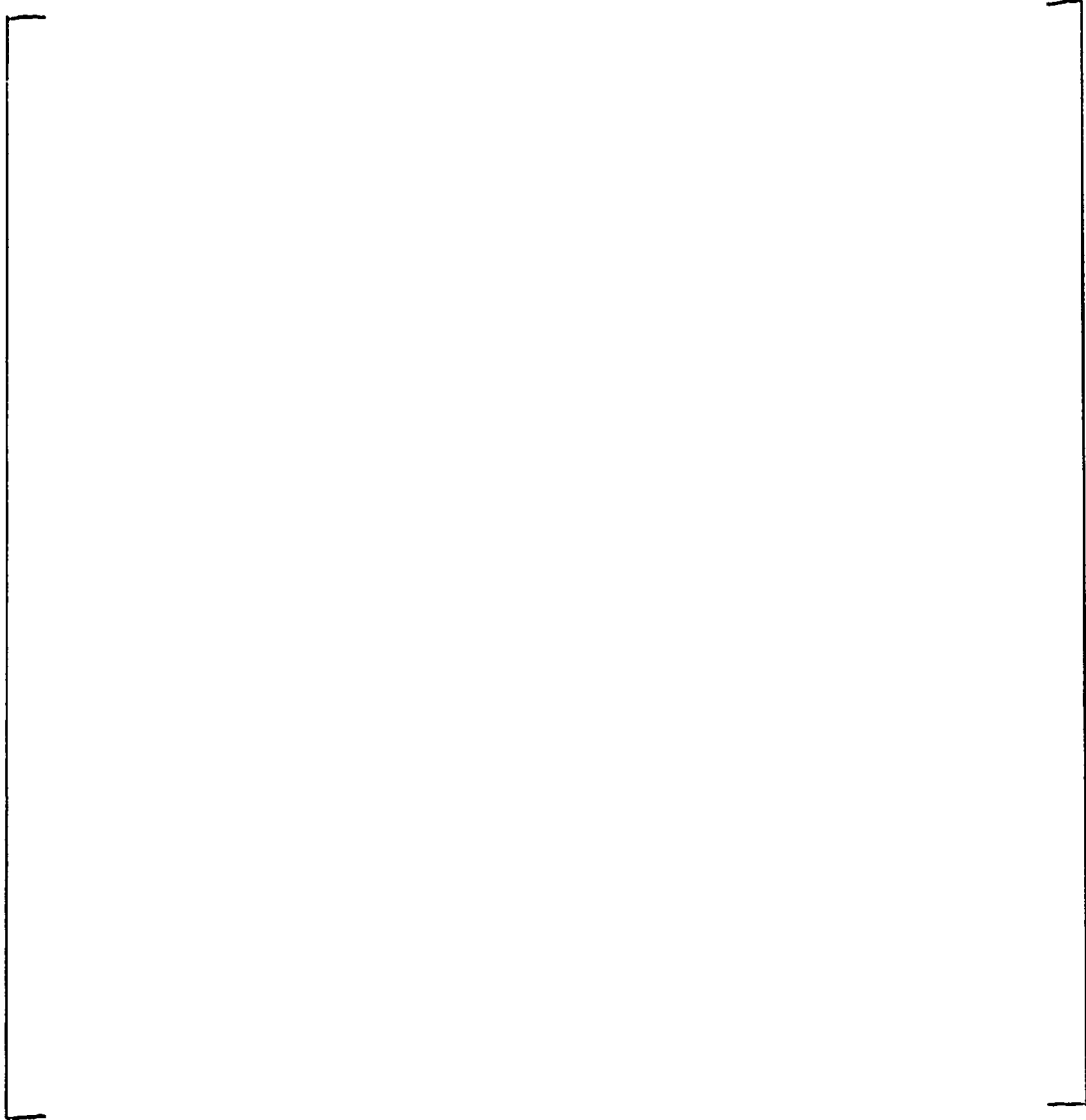




[

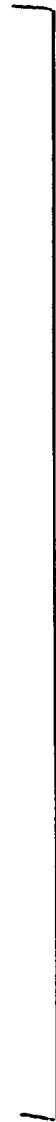
]









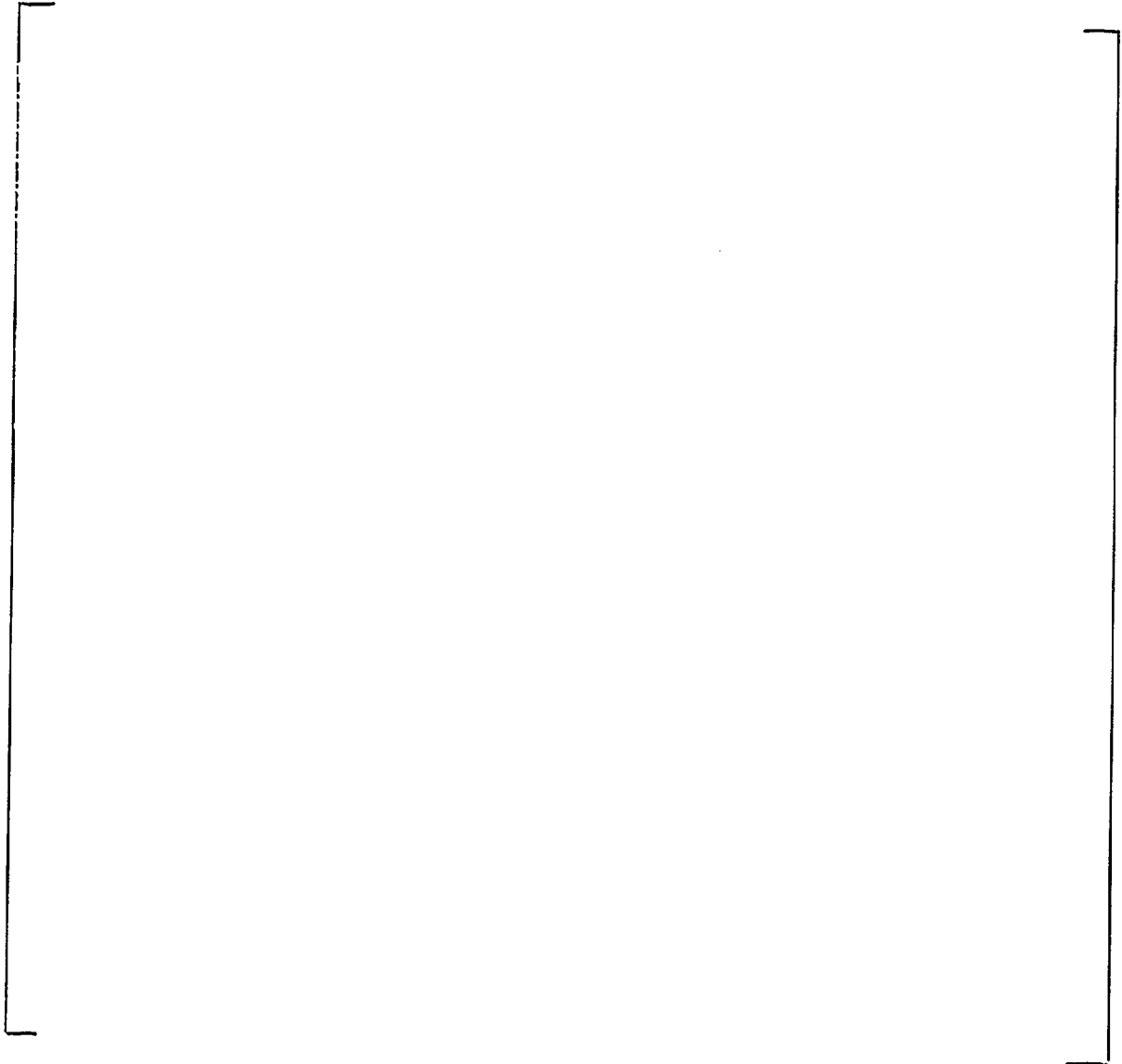






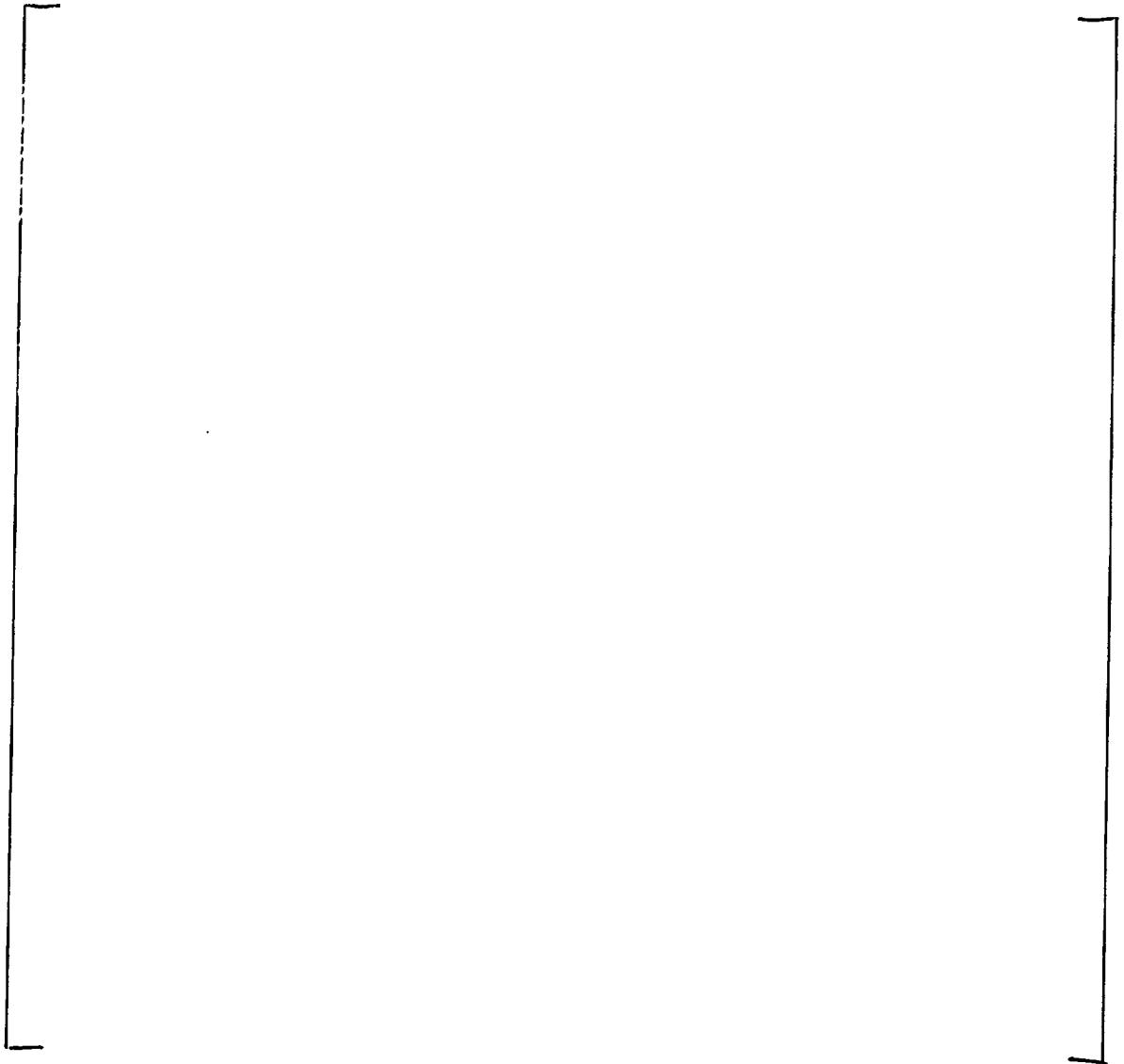


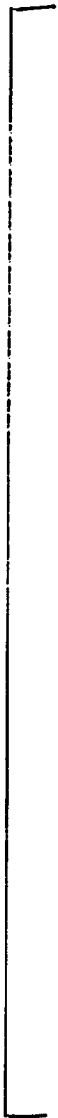


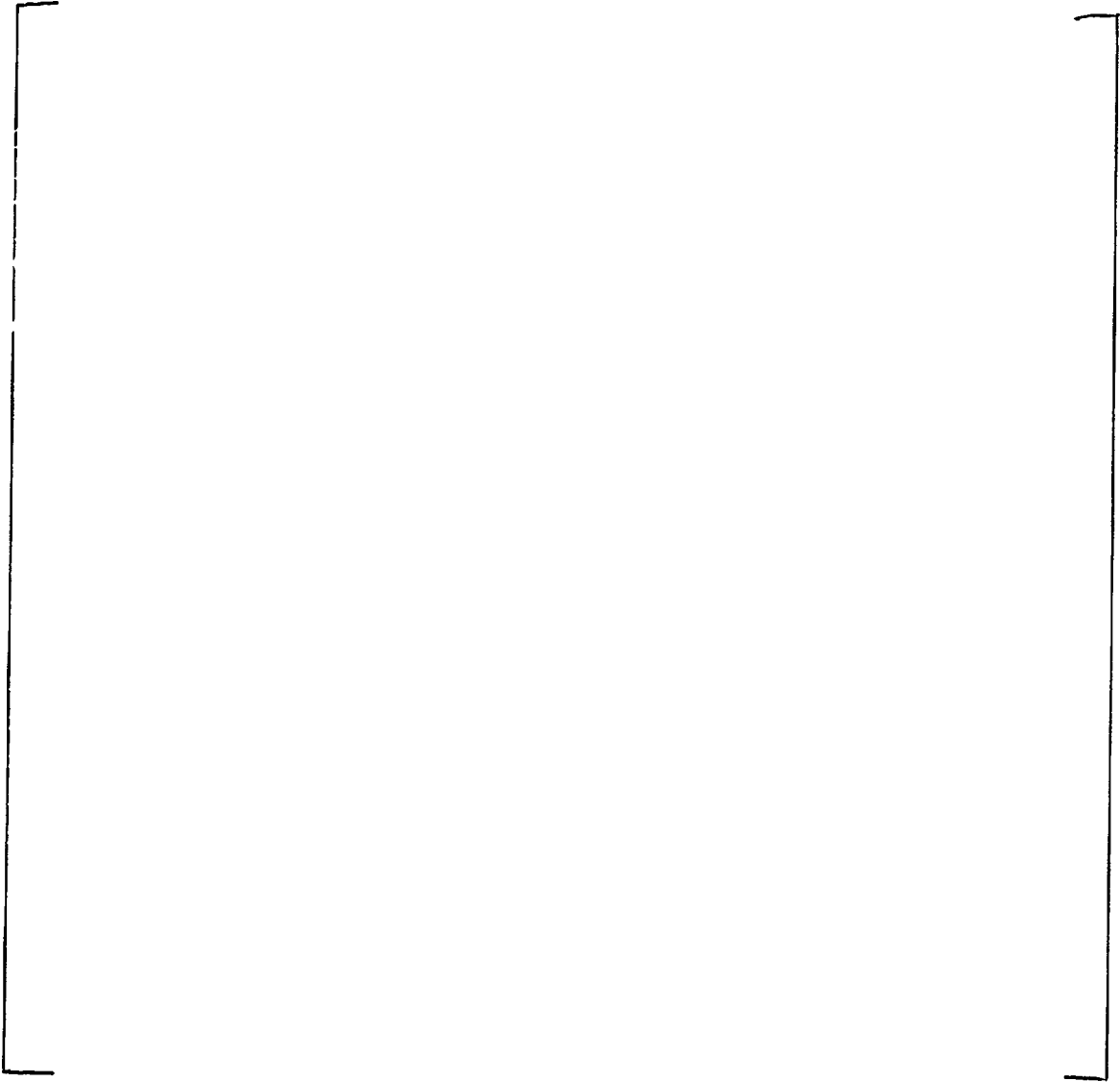




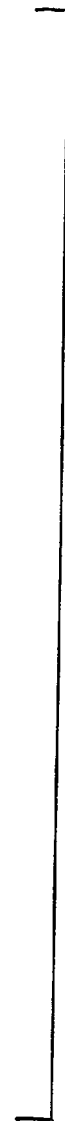


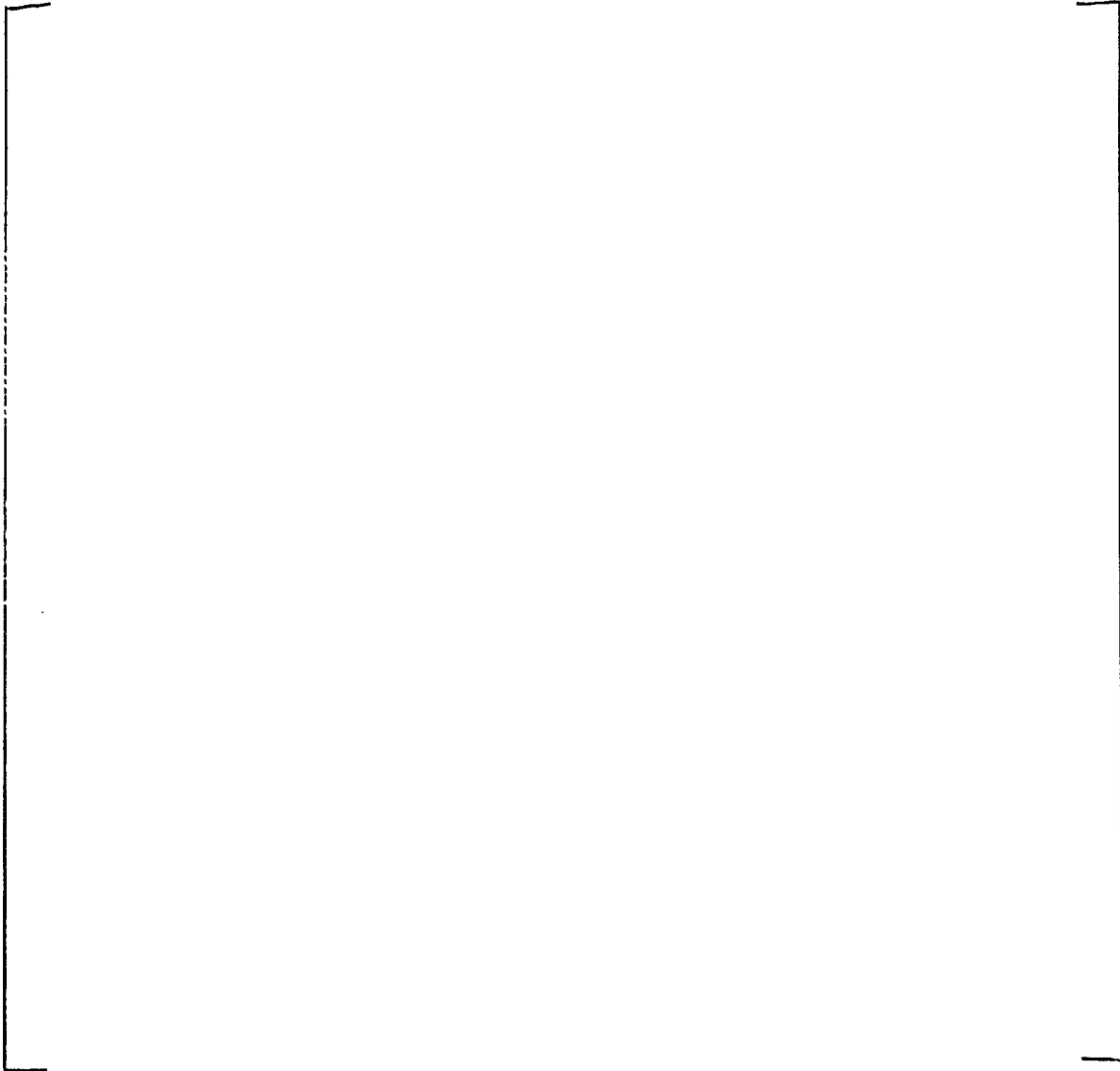


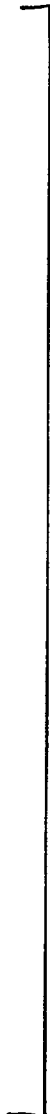






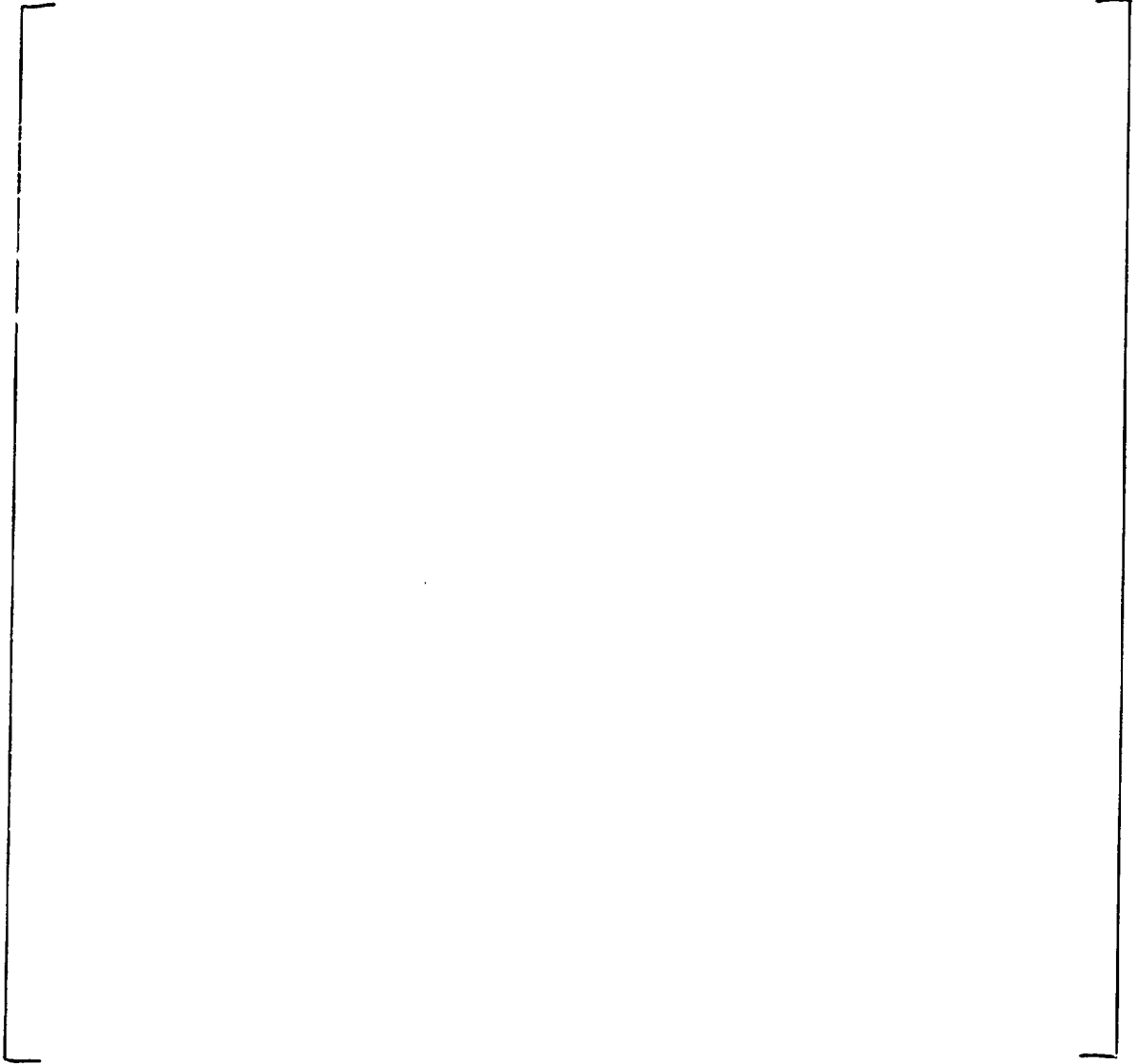






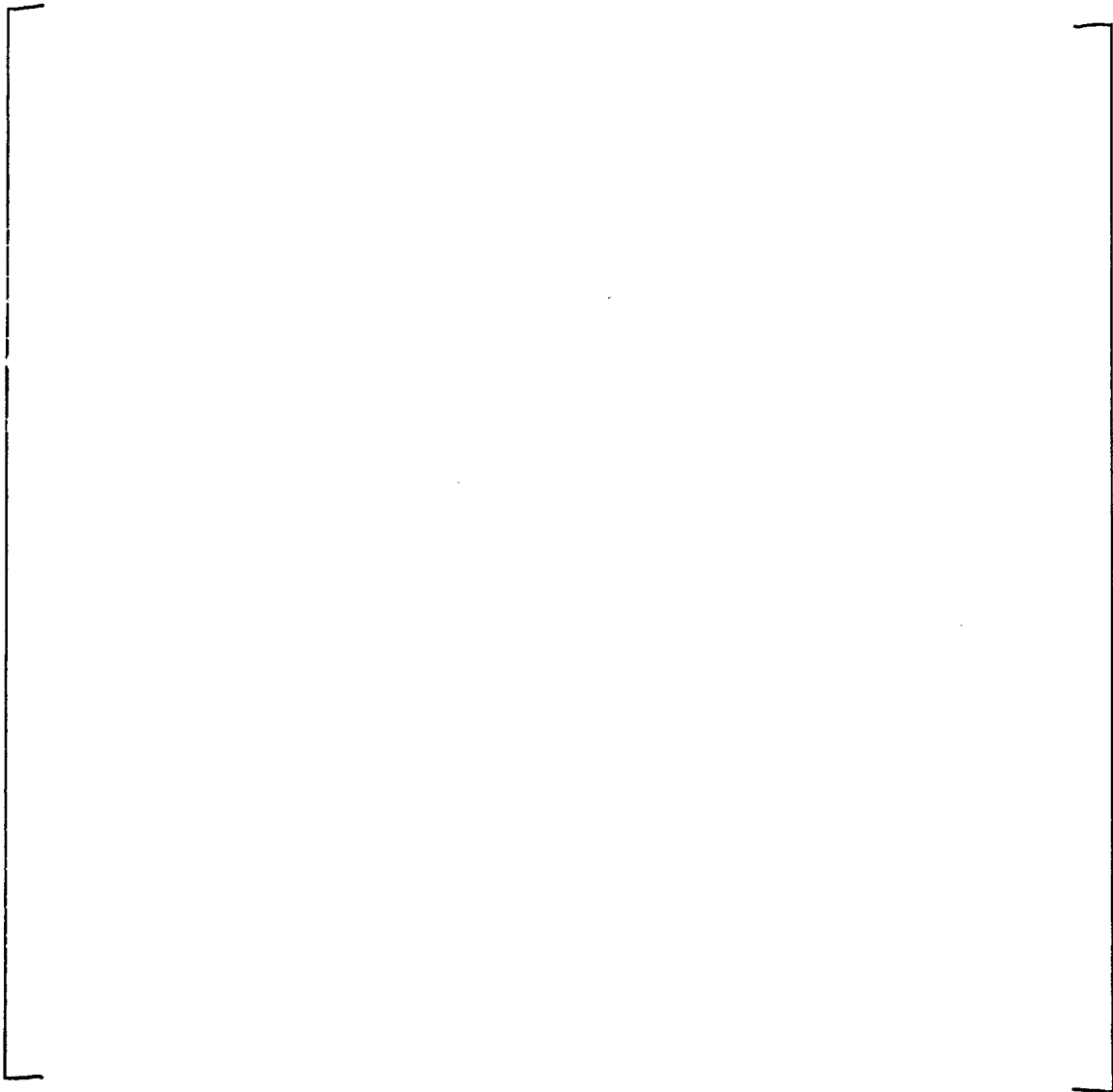






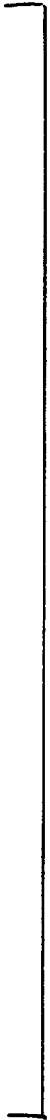






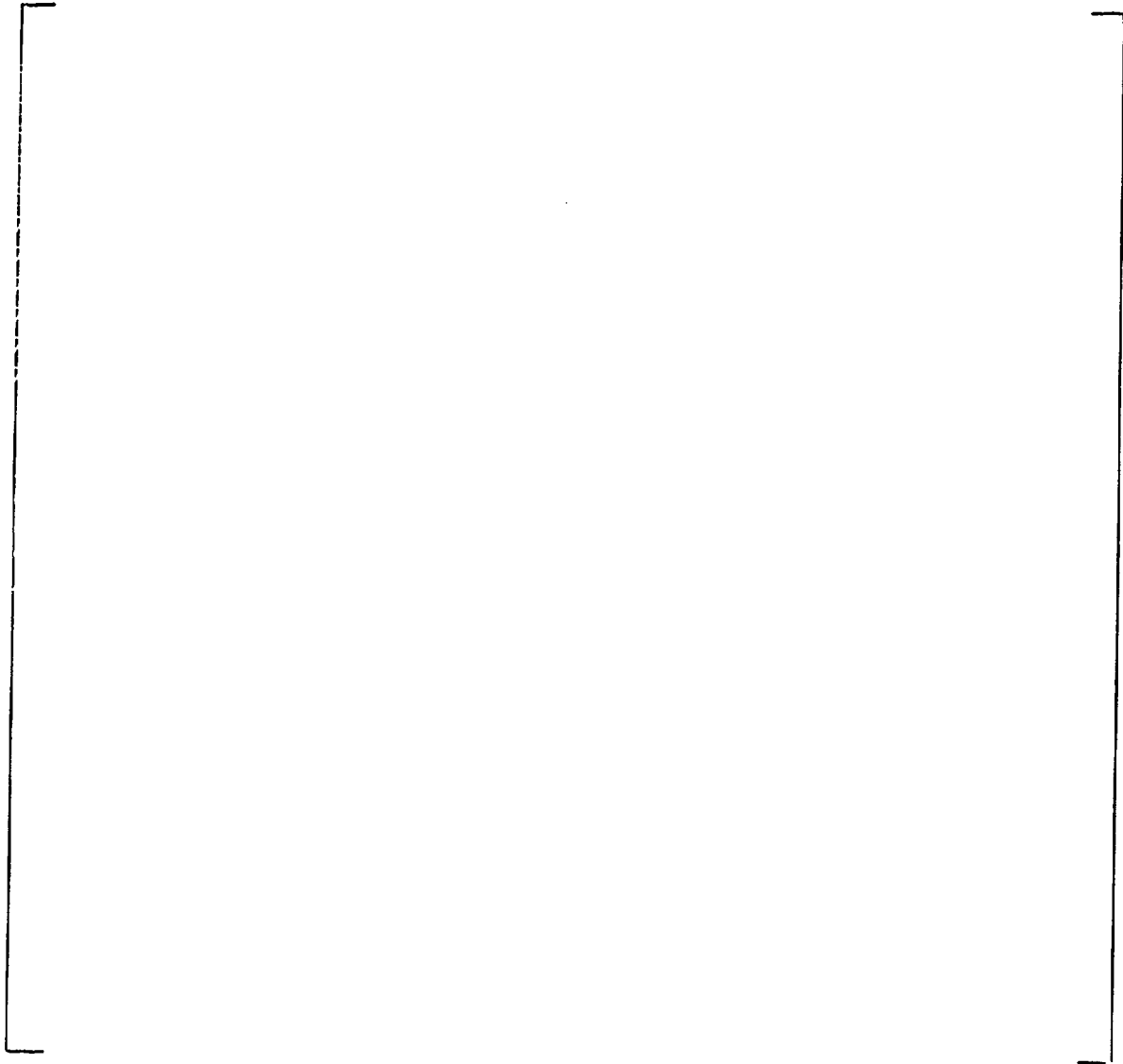


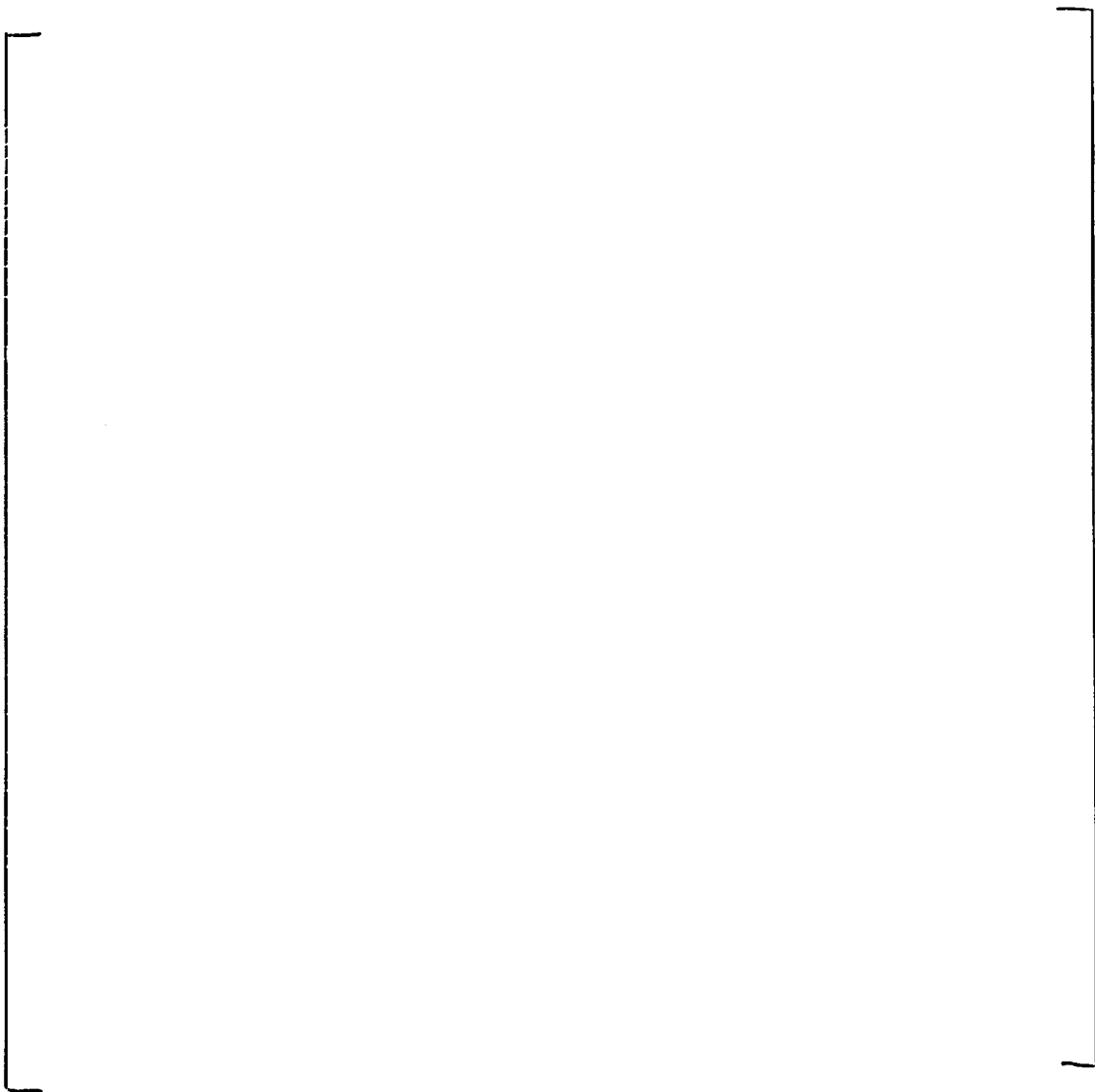


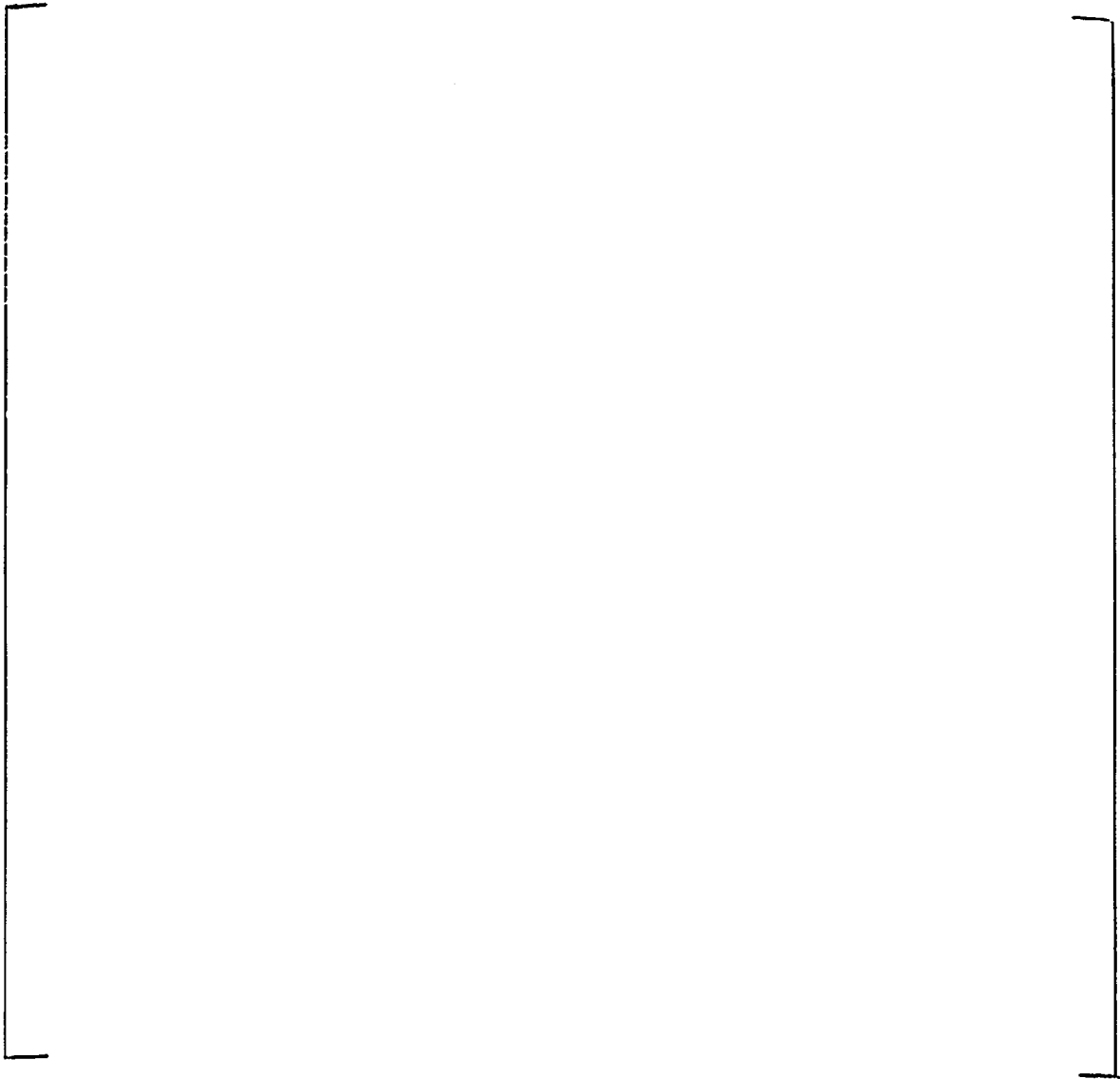


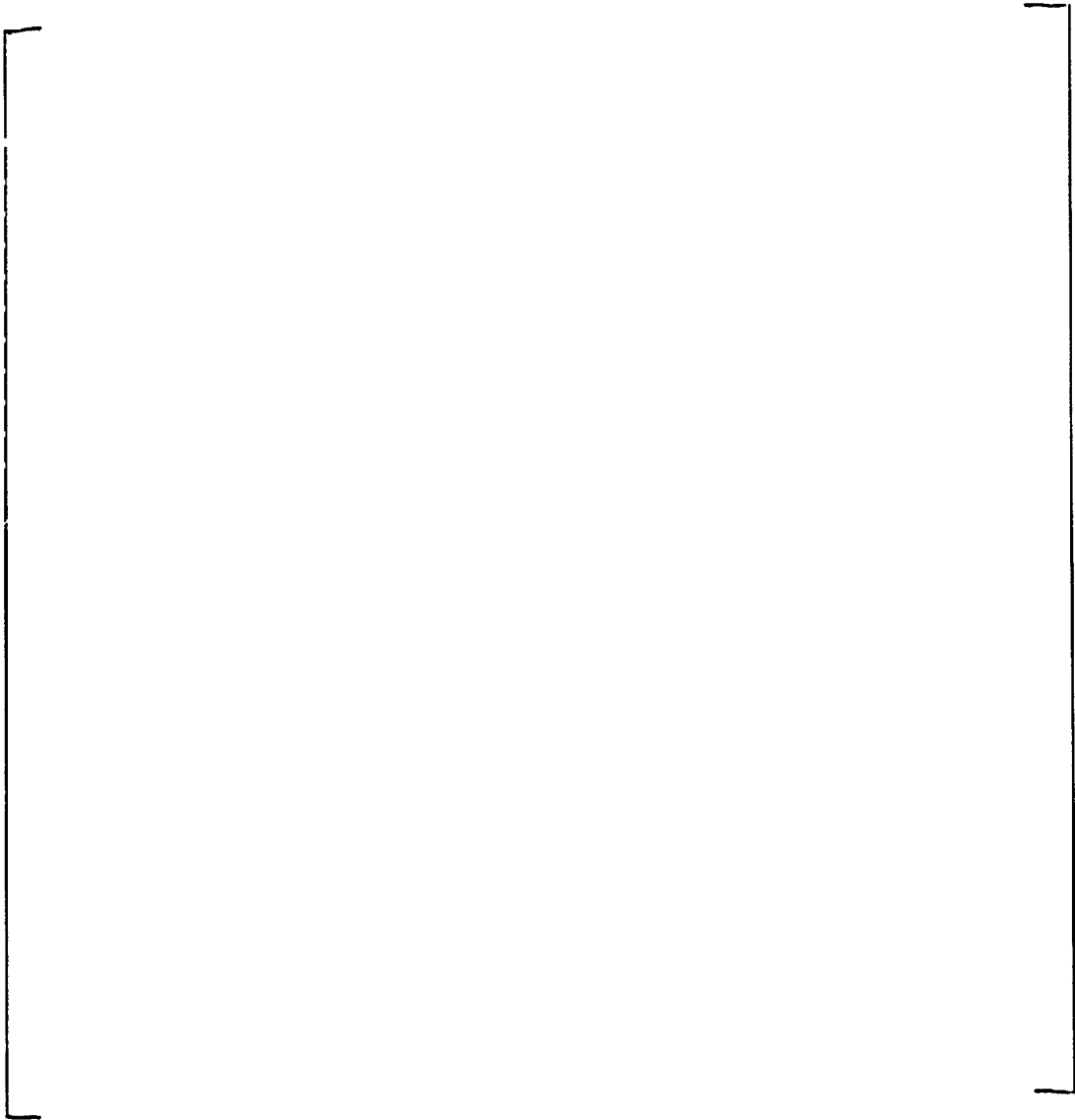














## APPENDIX C

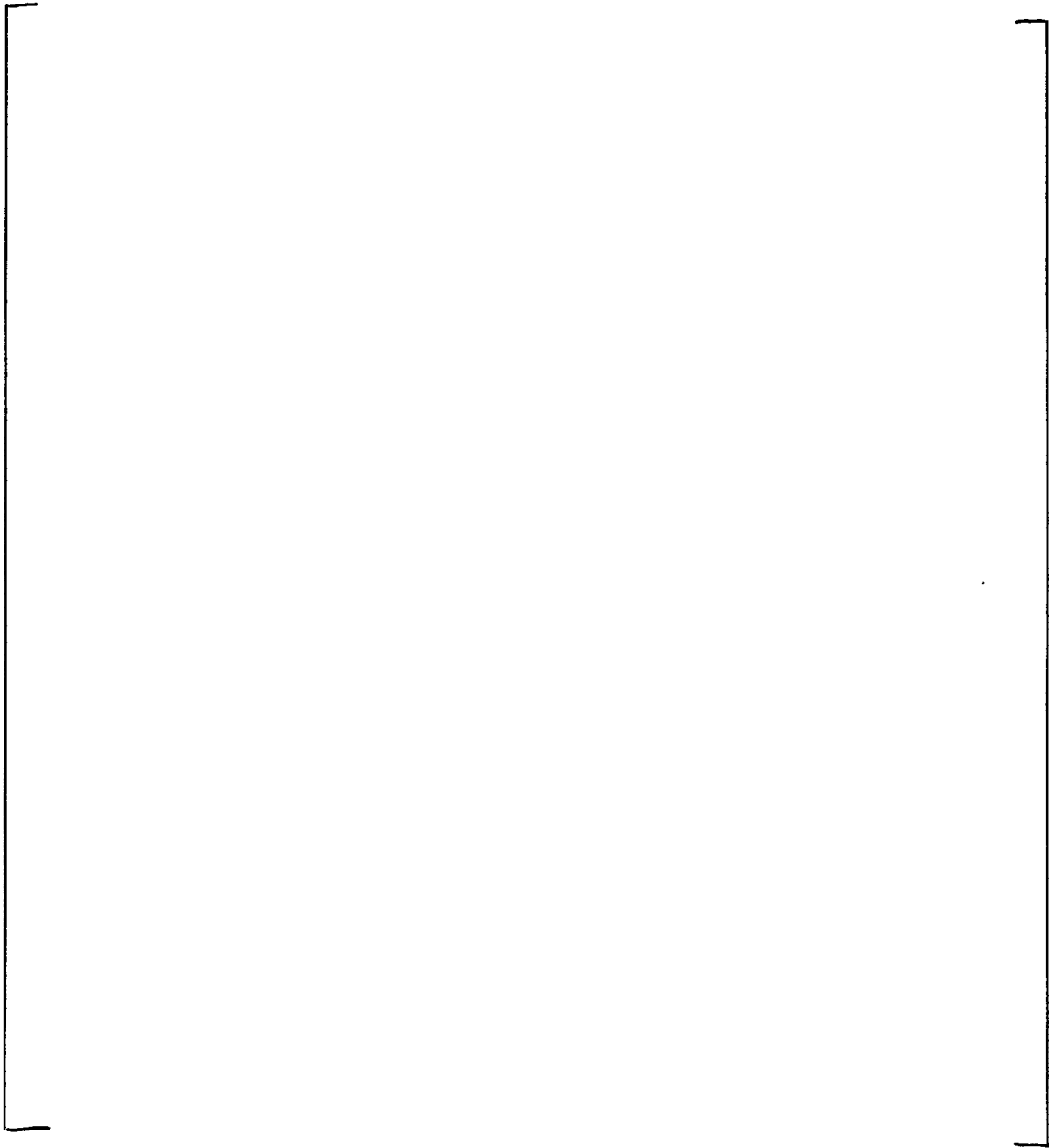
### **SVEA 96 Steady State Critical Power Test Data** **(Top-Peaked Axial Power Shape)**

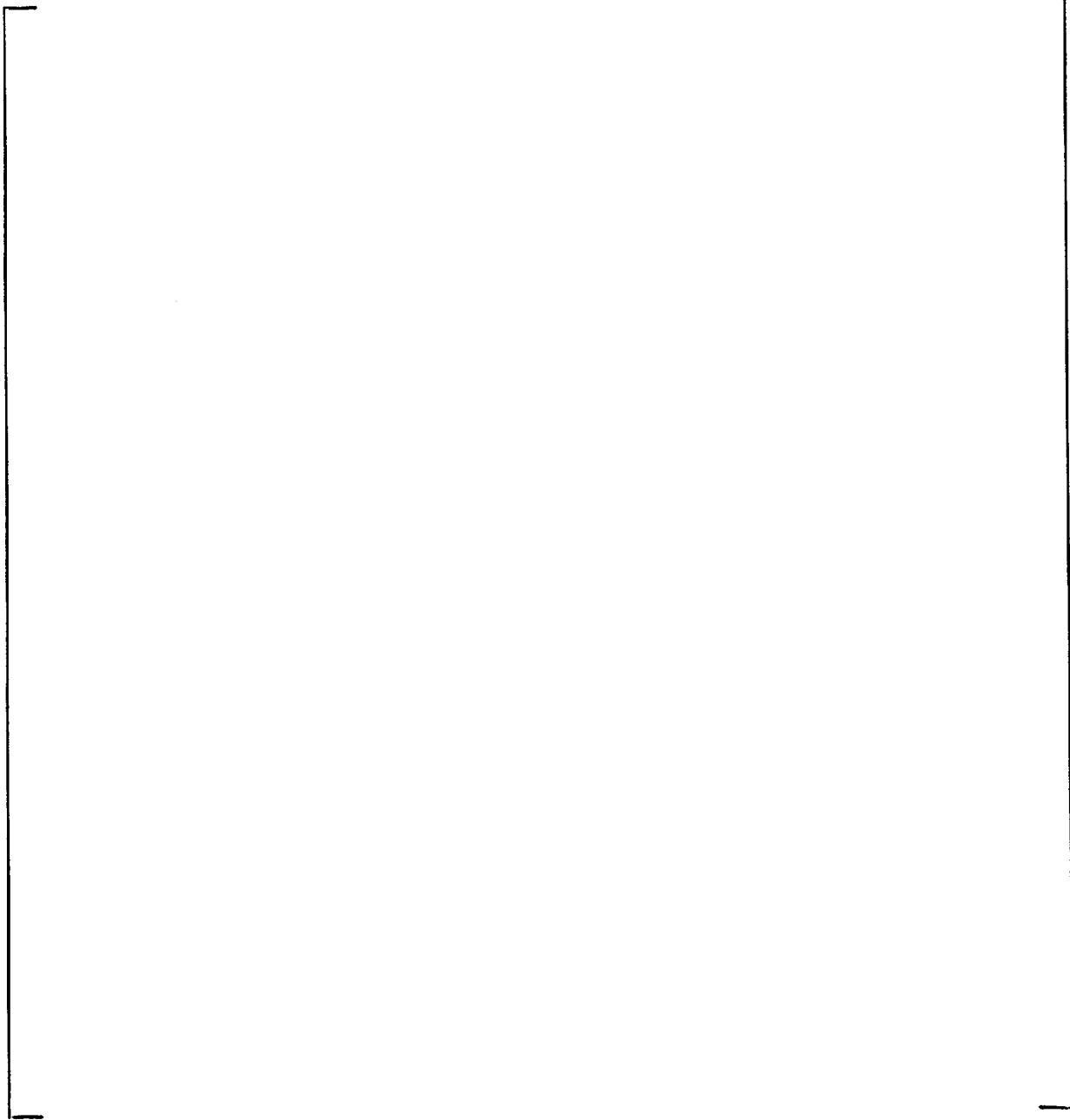
The data in this Appendix are provided as follows:

ID	The identity of the measurement point
P	The system pressure (bar)
T <sub>sub</sub>	Subcooling temperature (K)
Flow	Mass flow (kg/s)
Power	Bundle power at dryout (kW)
Y/I	The ratio between the average local power for the 15 peripheral rods and the average local power for the 9 central rods
Rod	The rod(s) and its/their thermocouples indicating dryout (refer to Figure 2.3 for rod location and Figure 2.7 for thermocouple location, e.g. 107.01 means rod 7 in Figure 2.3 and T/C level 1 in Figure 2.7)

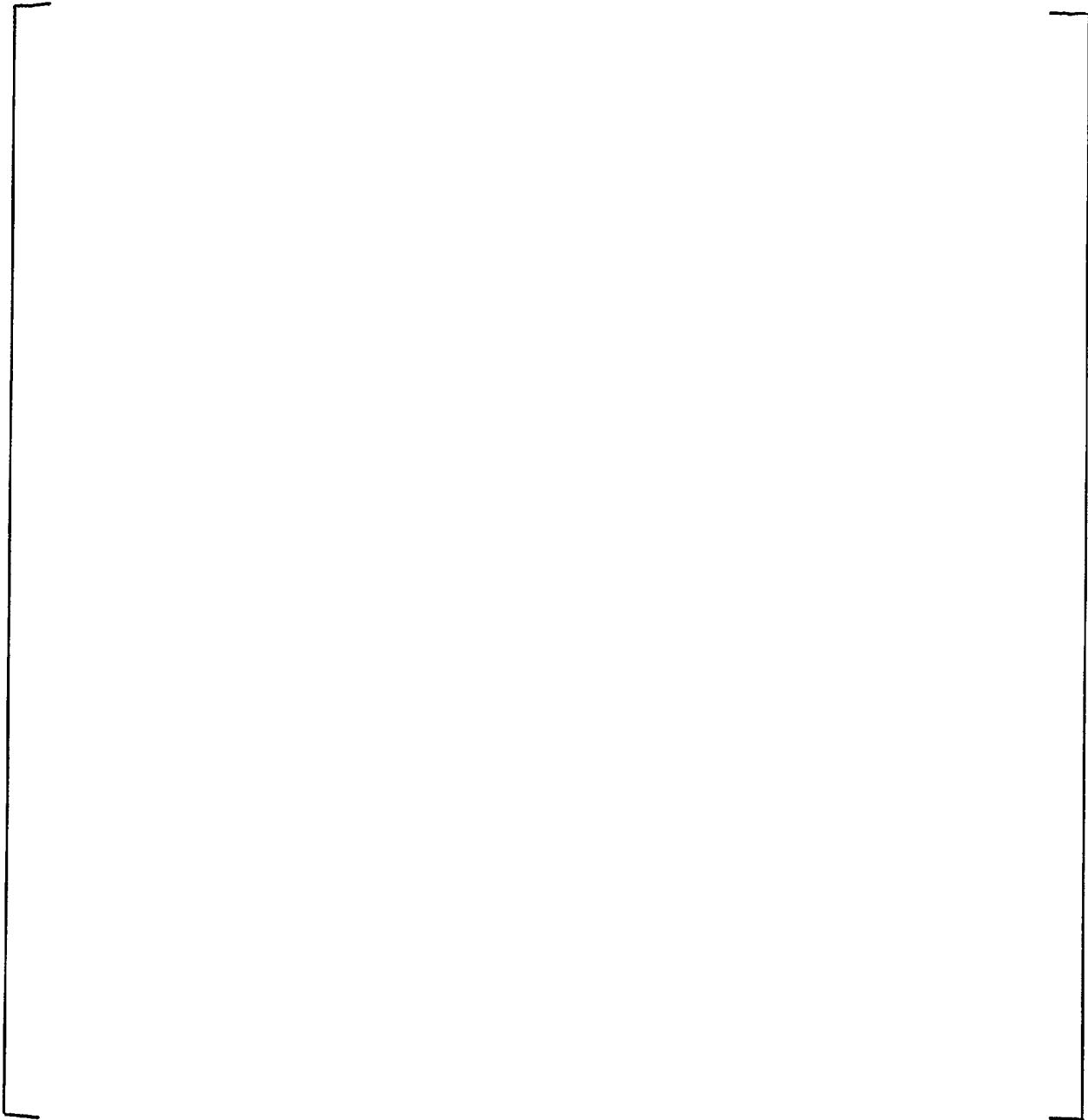
The local power distribution map at about 3 kg/s flow is printed on each page together with a critical power versus mass flow plot with all separate dryout points. When the local power distribution map is not printed, it has been shown for a previous test series.

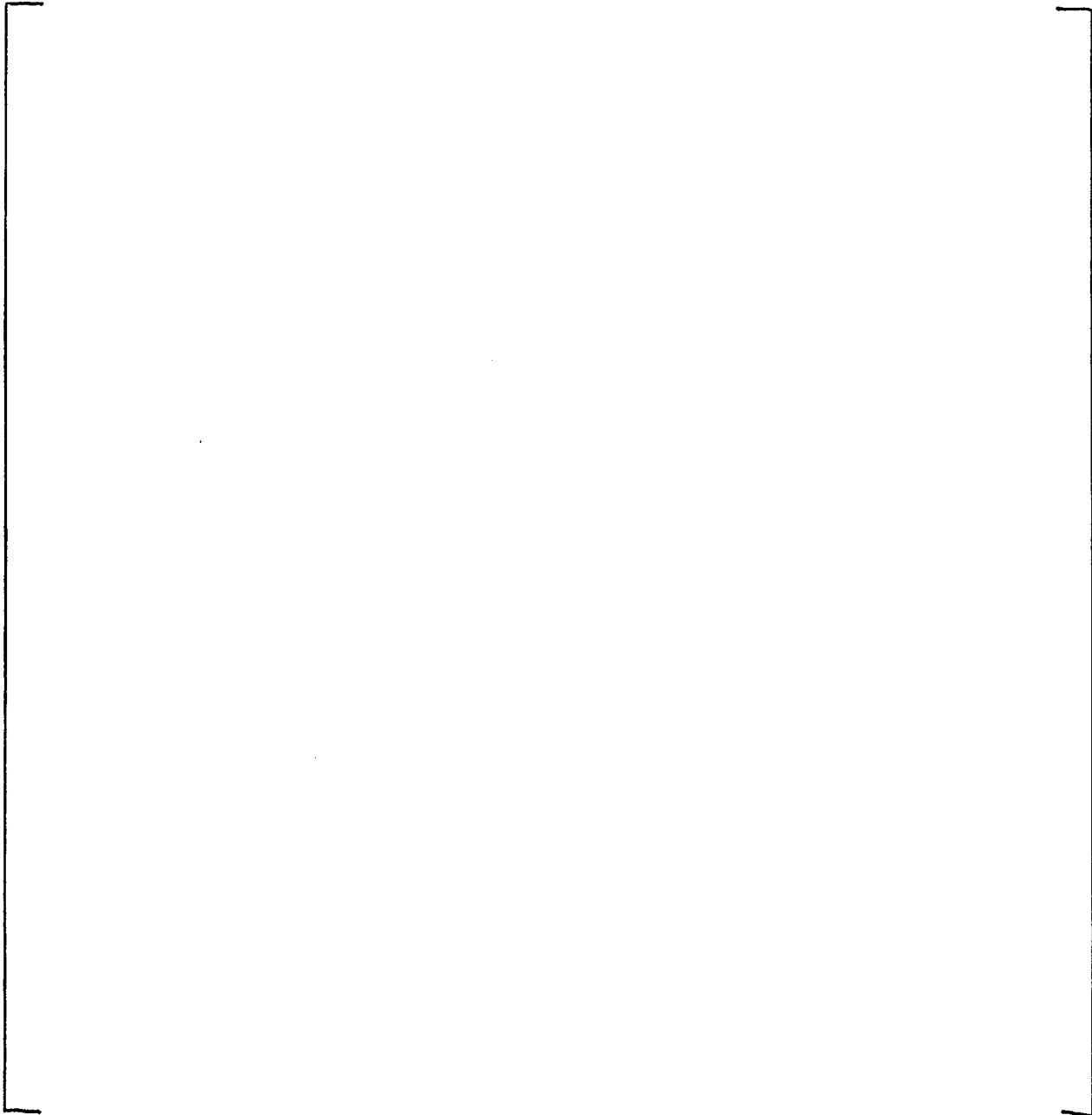
It must, however, be noted that the local power distribution may differ slightly for different points intended to have the same nominal distribution (e.g. AA4, AA5, etc.). The actual measured local power distributions were used for all points in the correlation development and validation process.

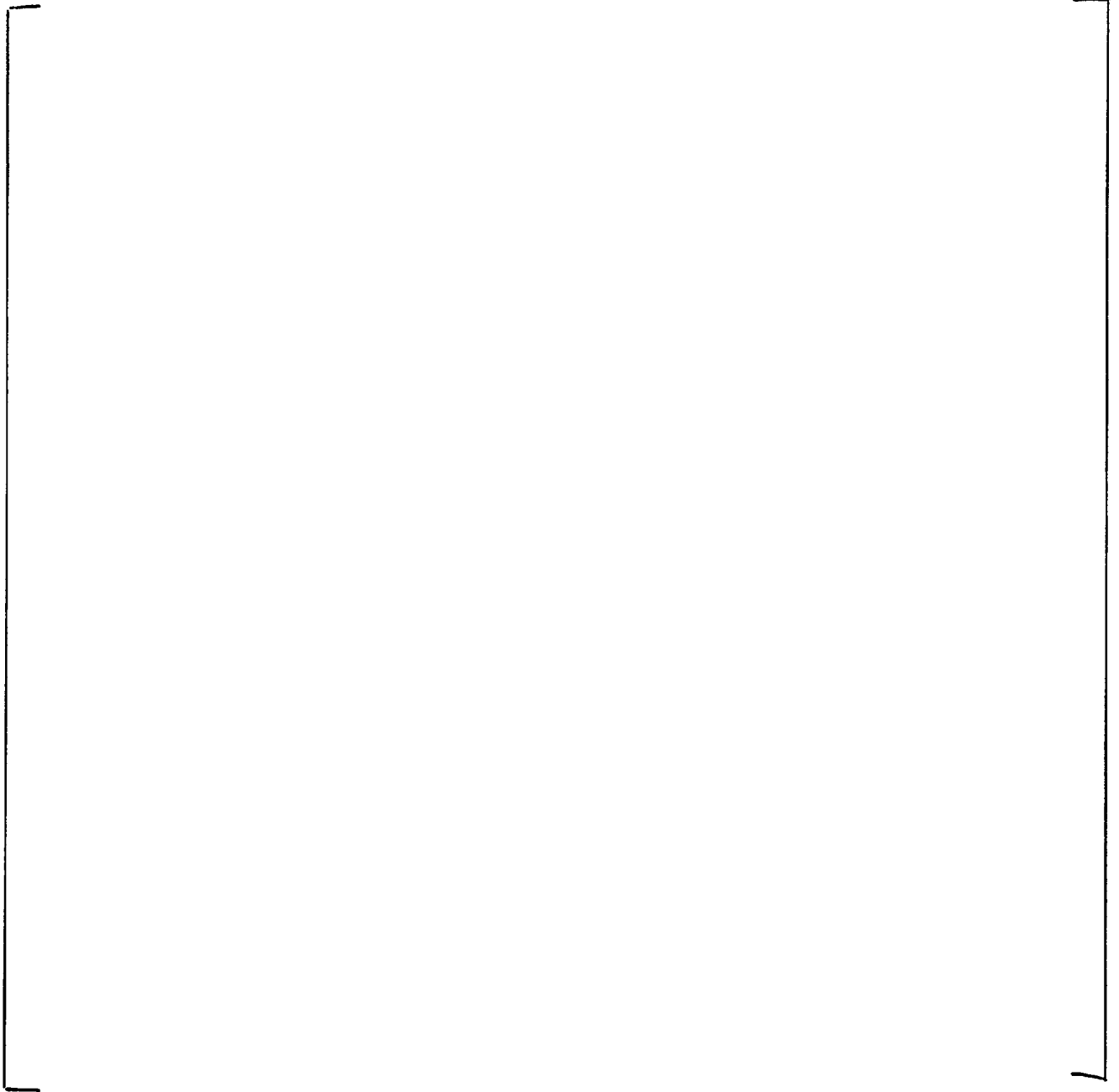


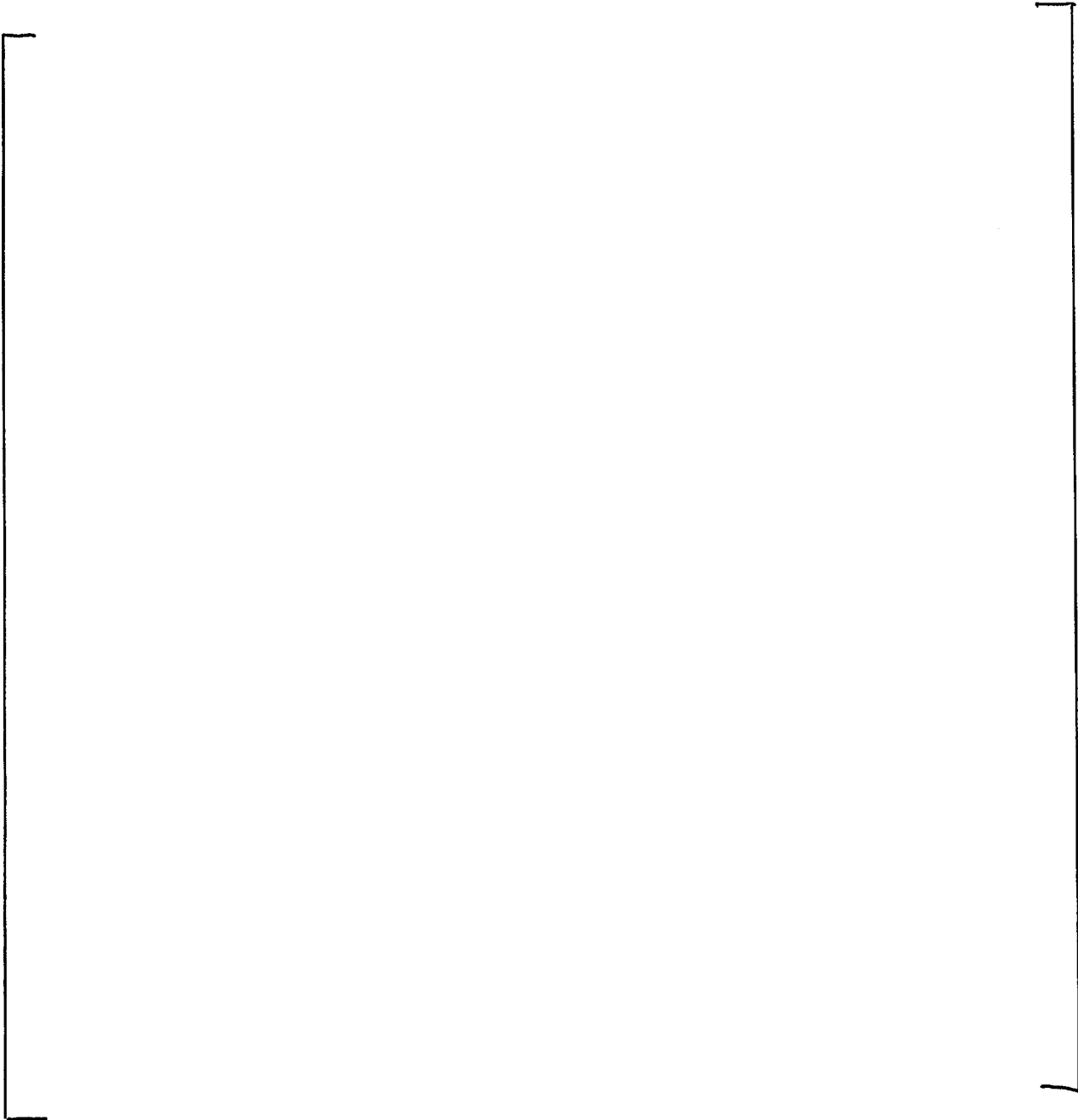


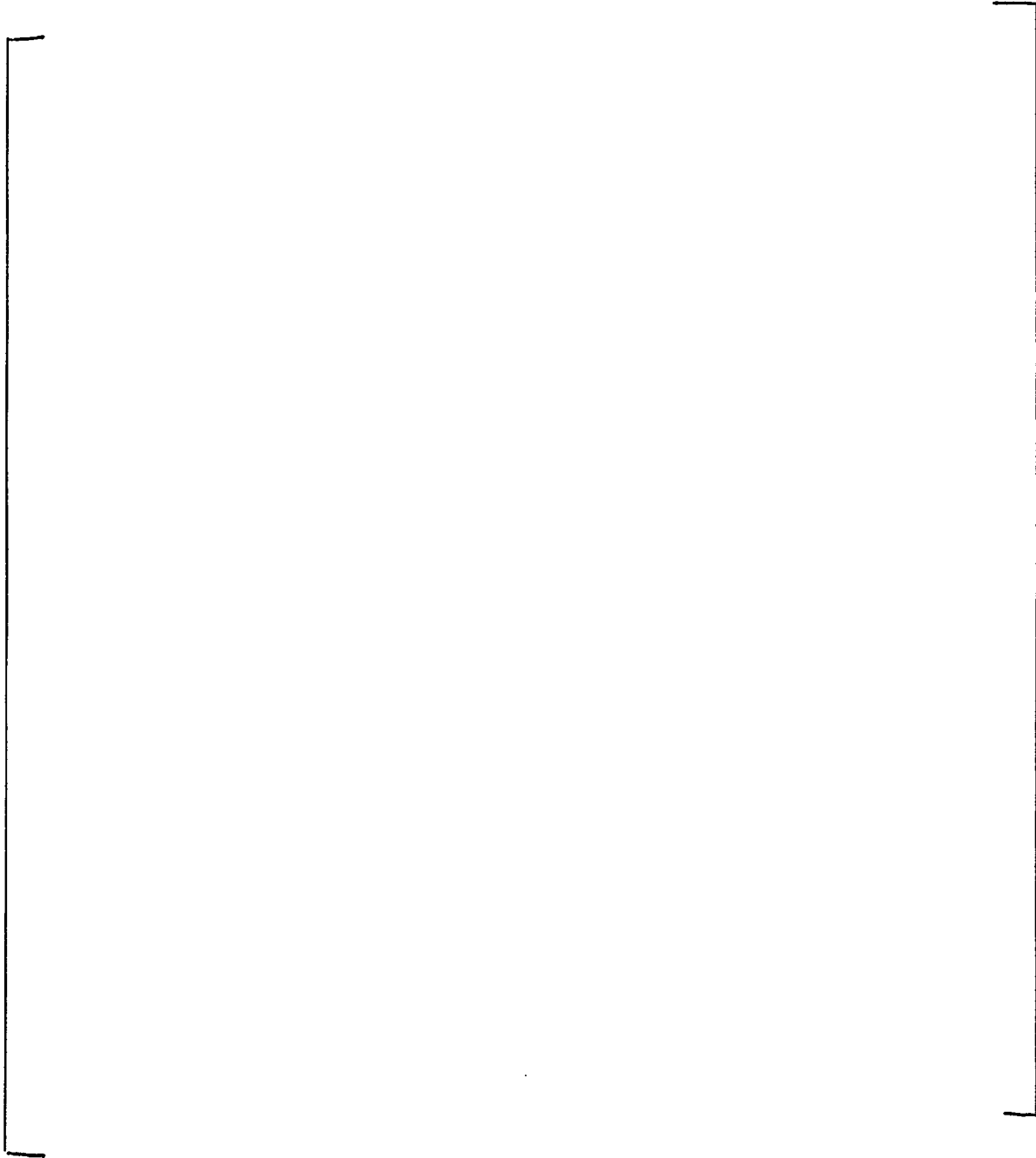


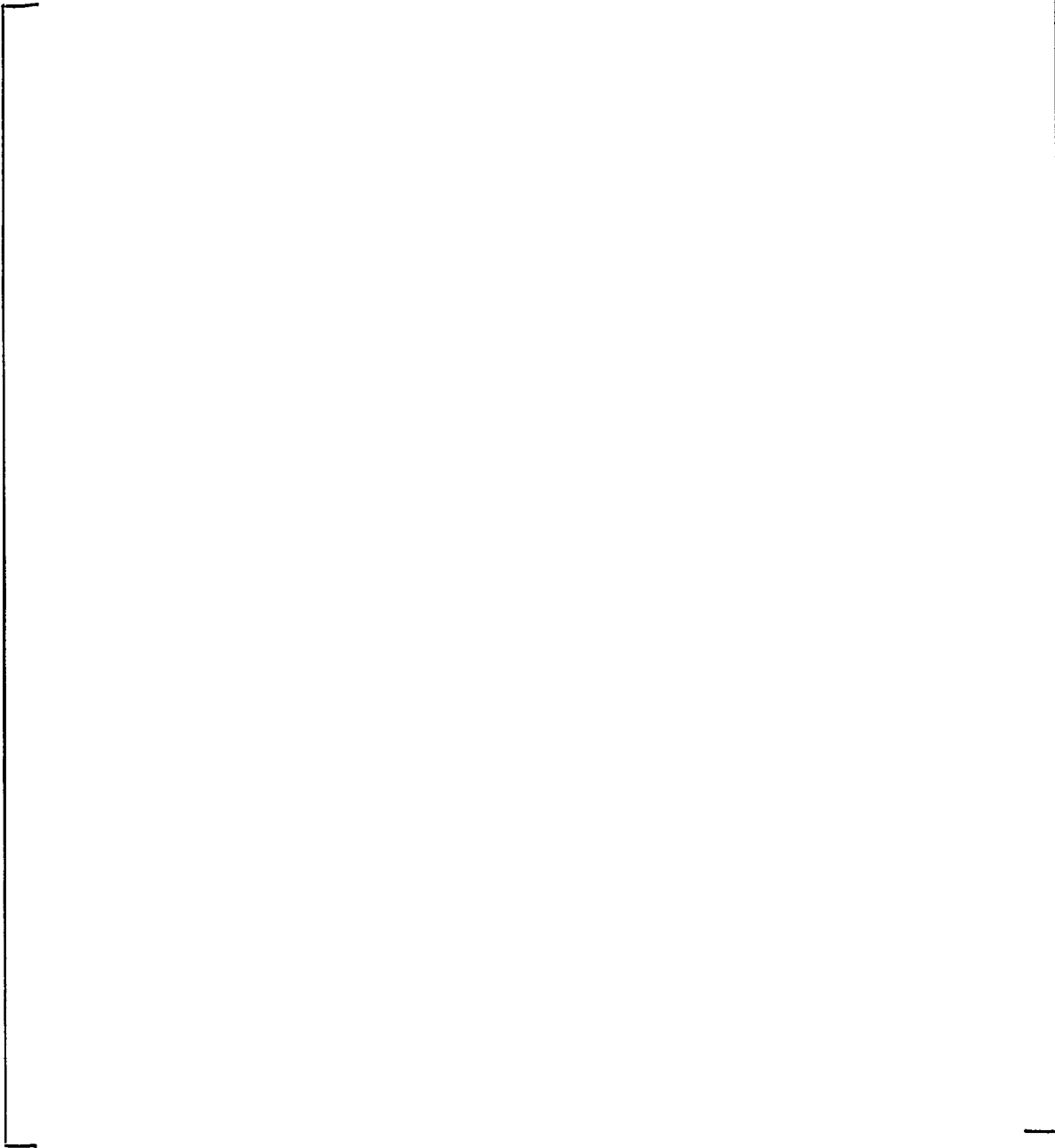


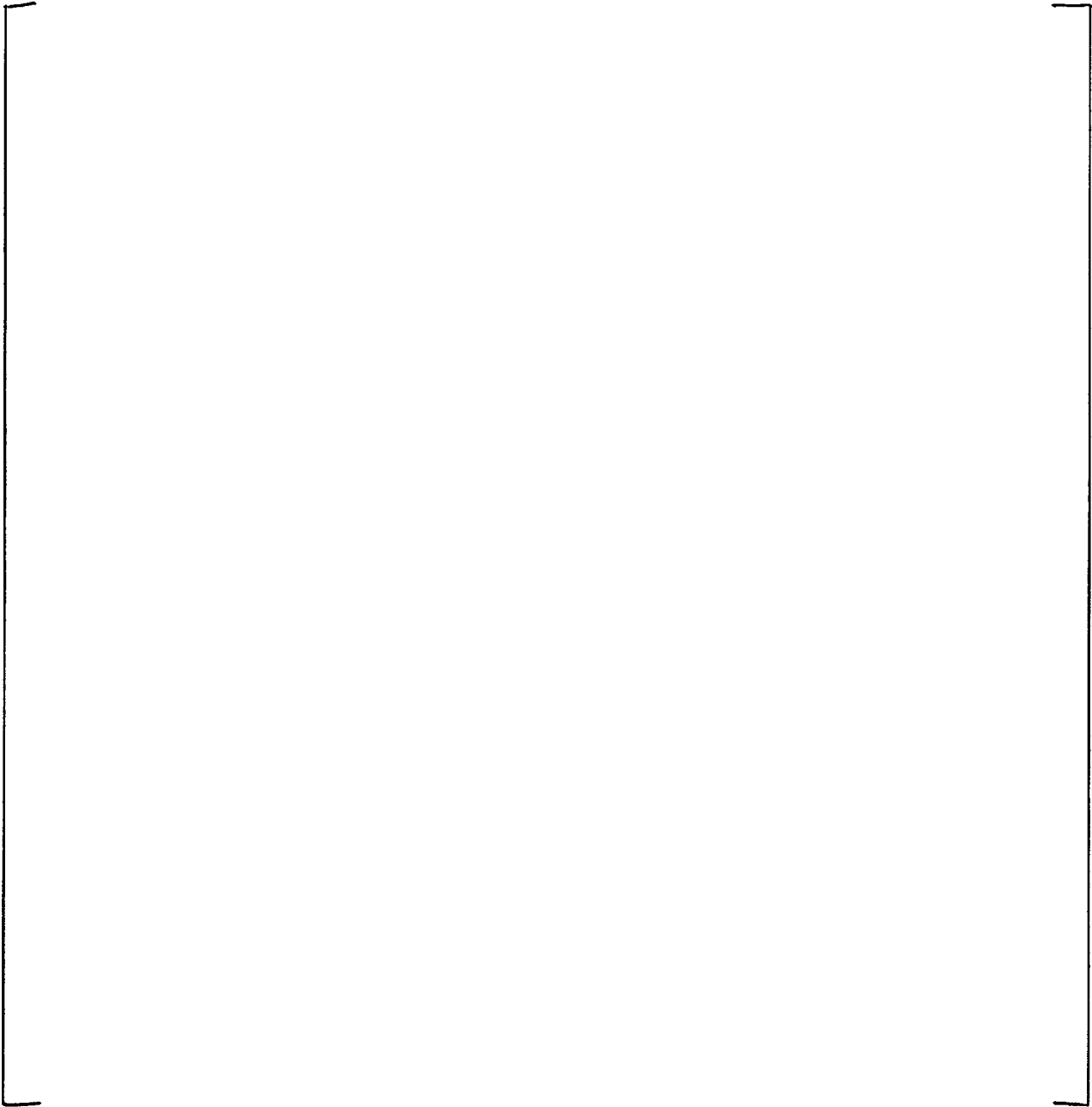


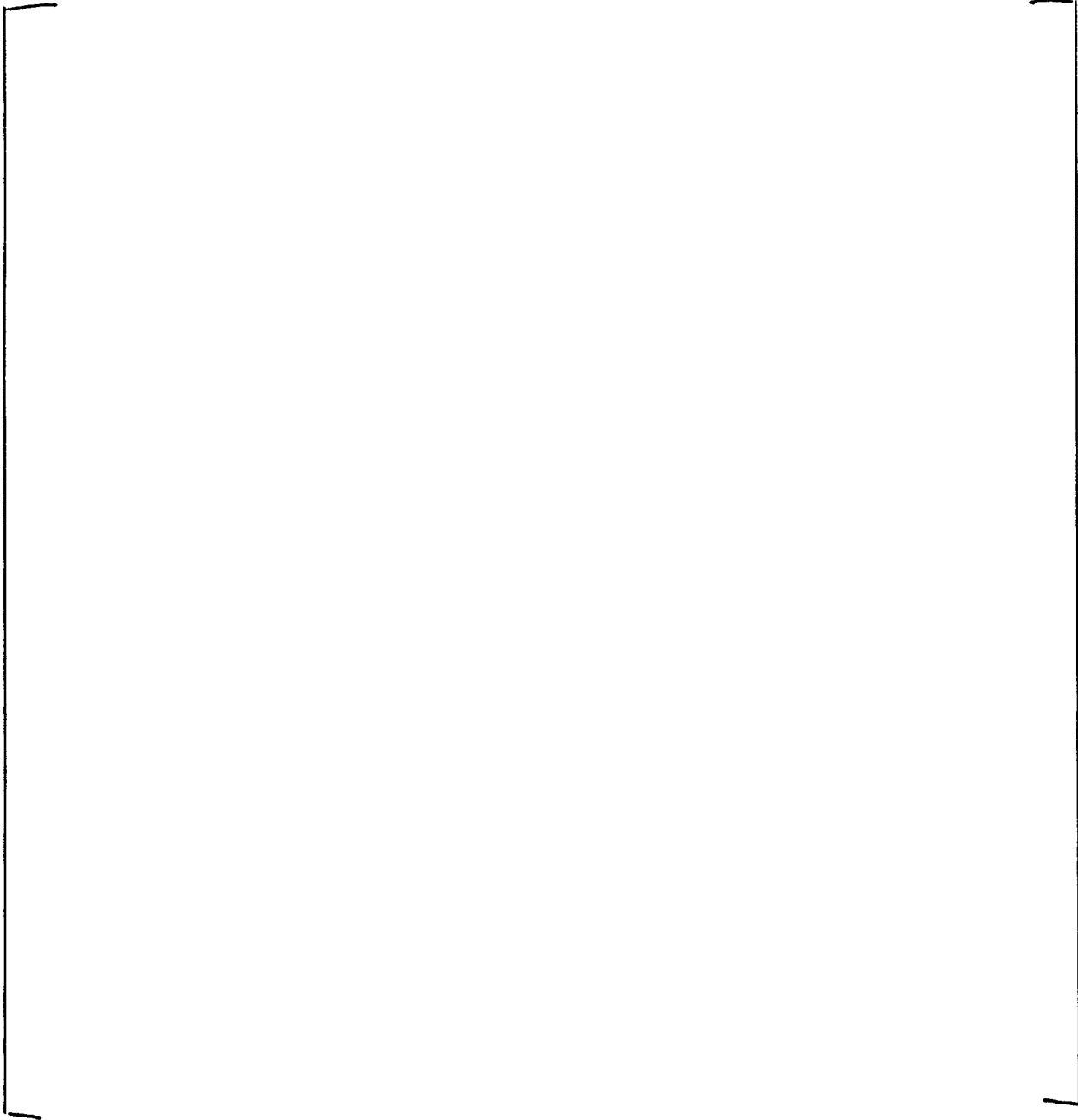




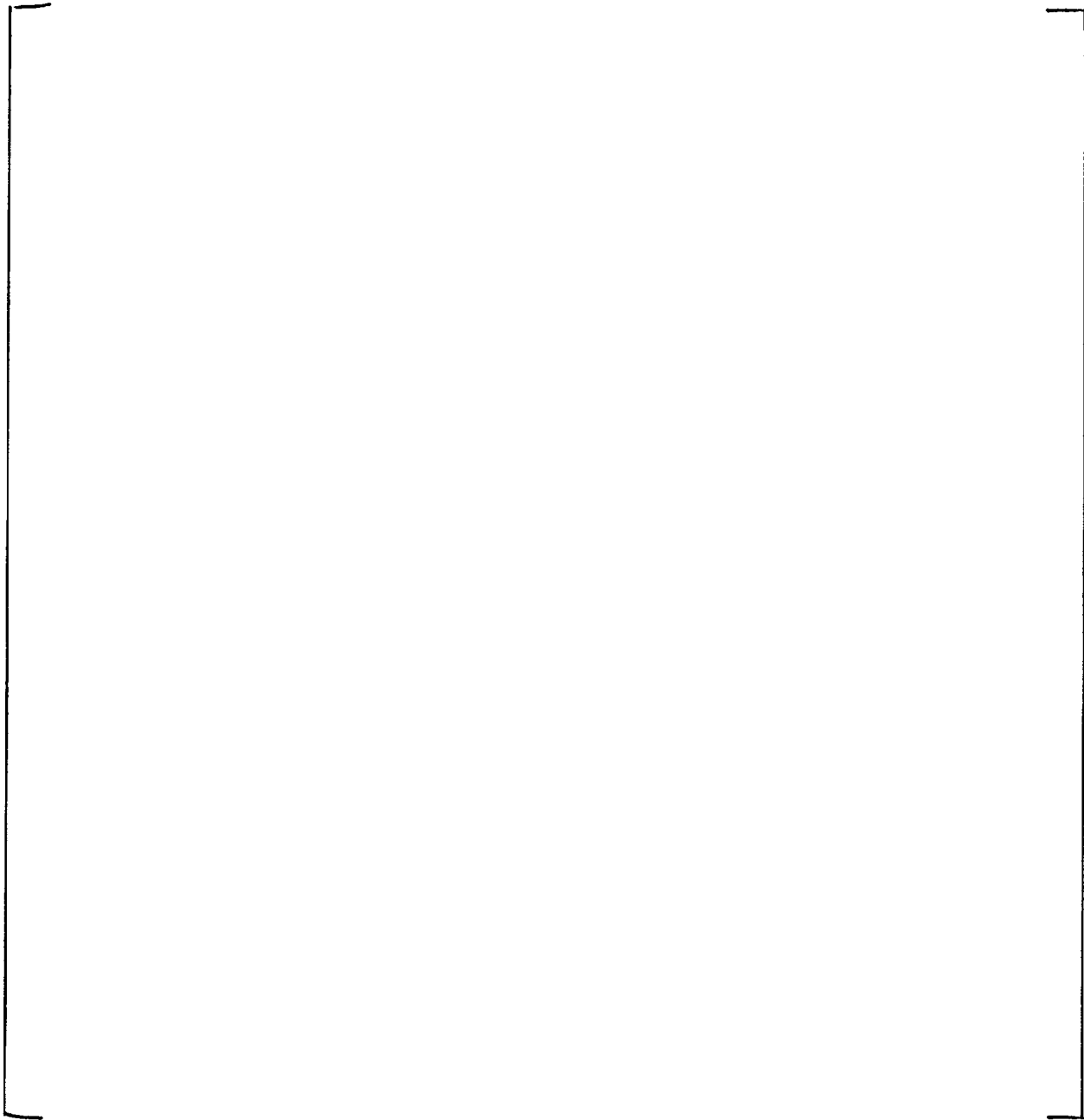


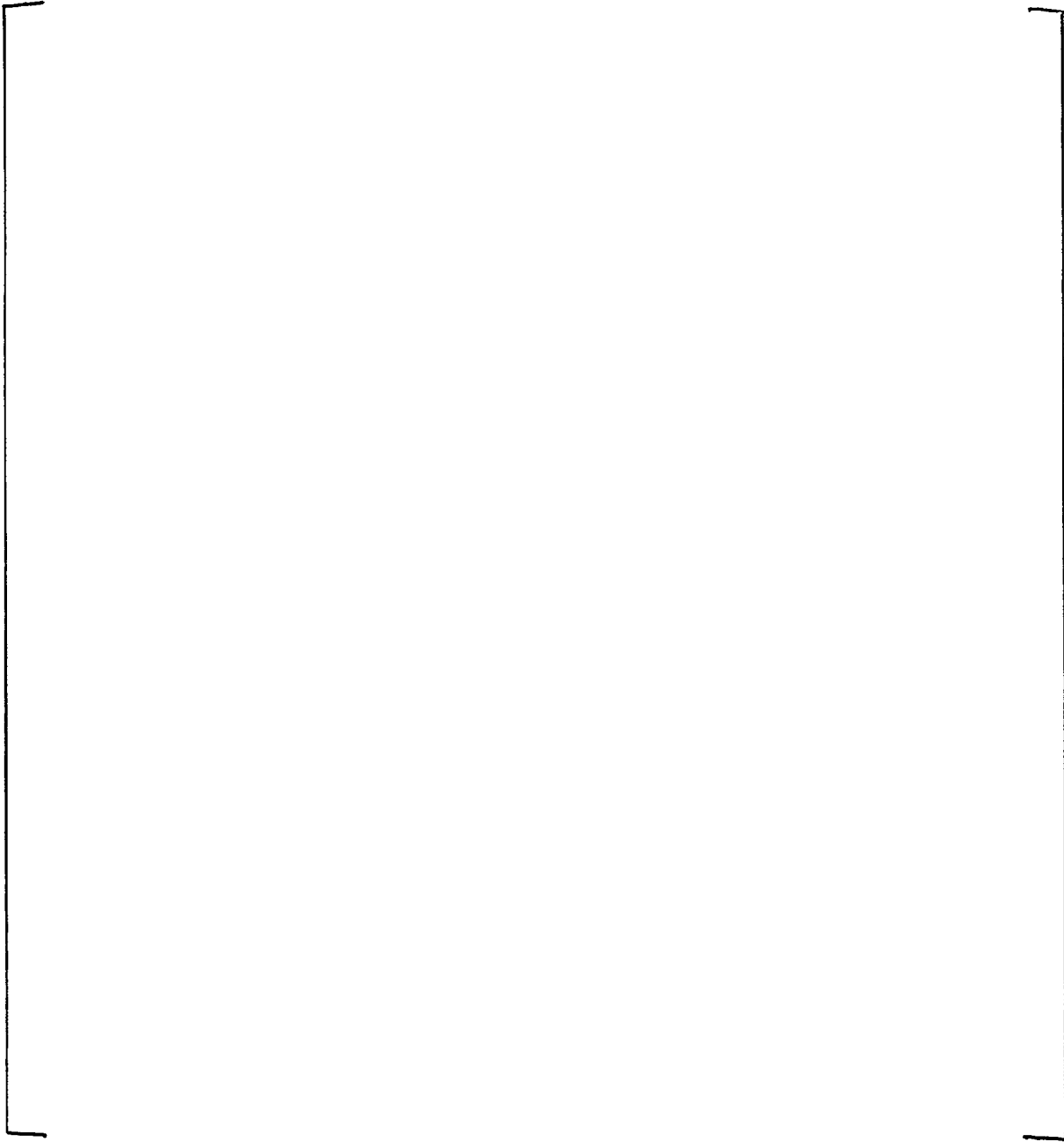


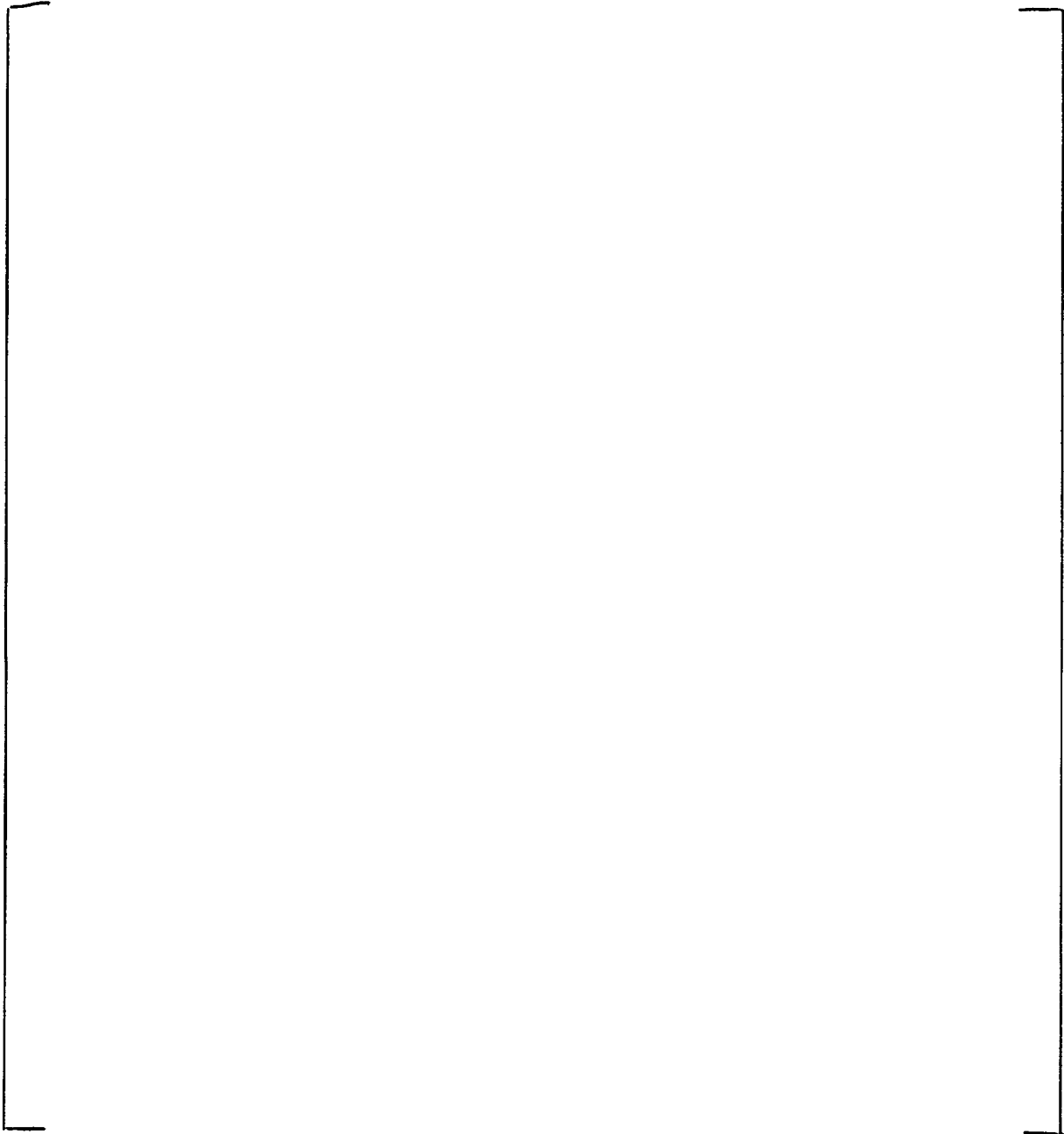


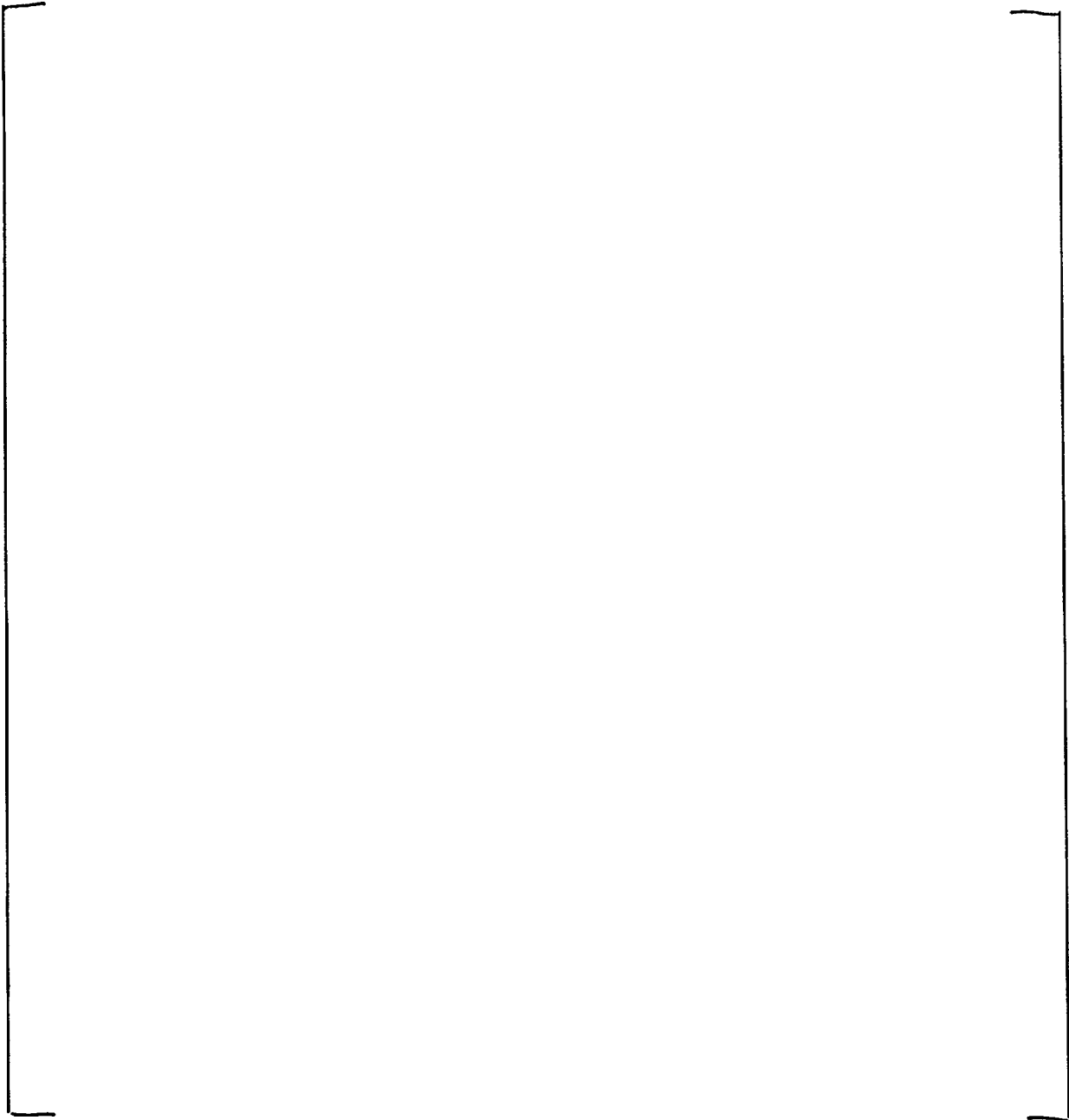


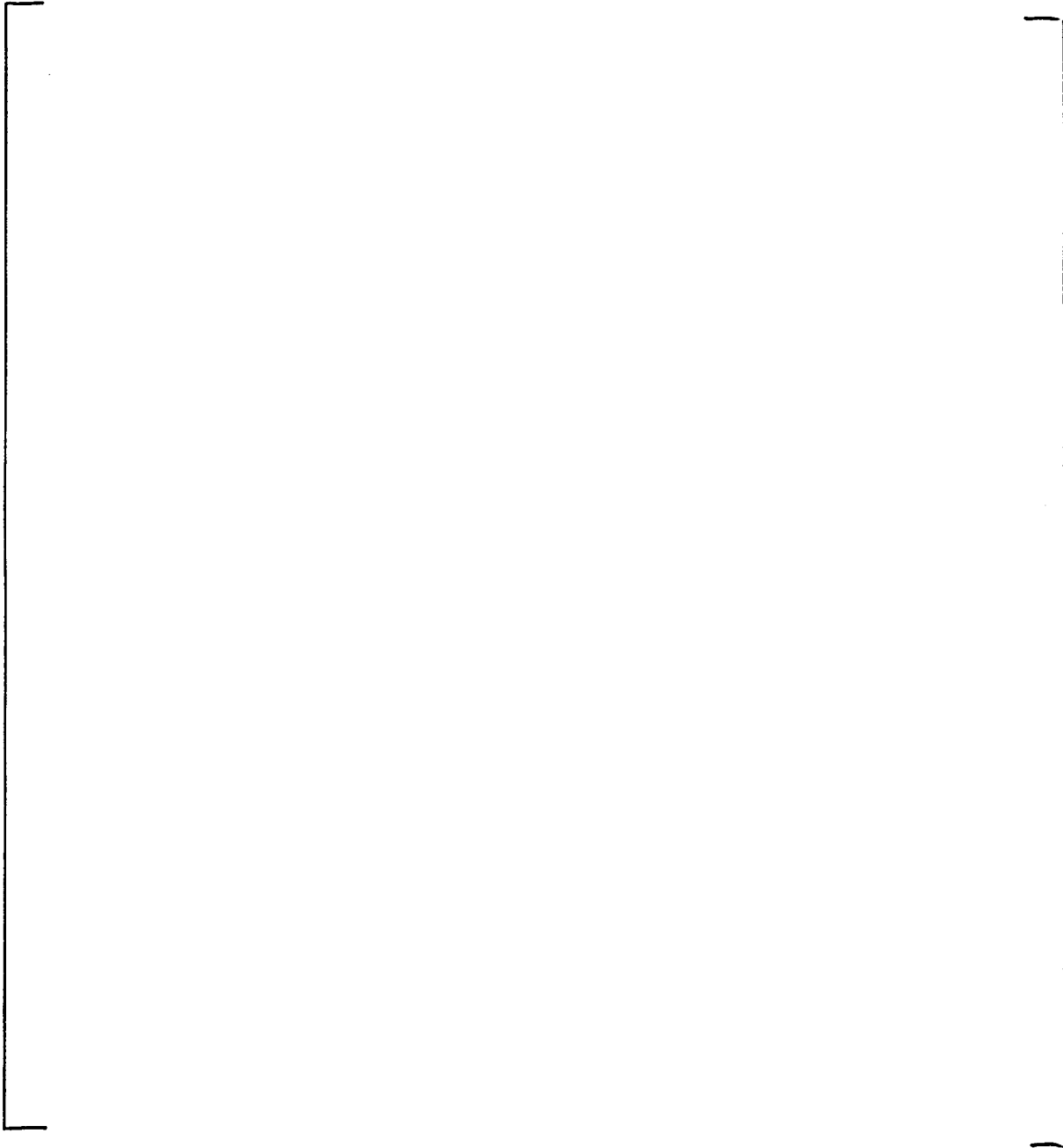


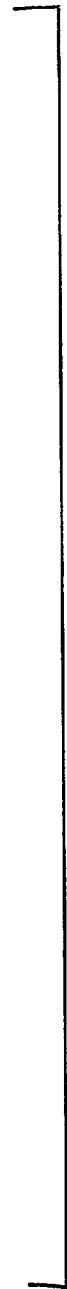


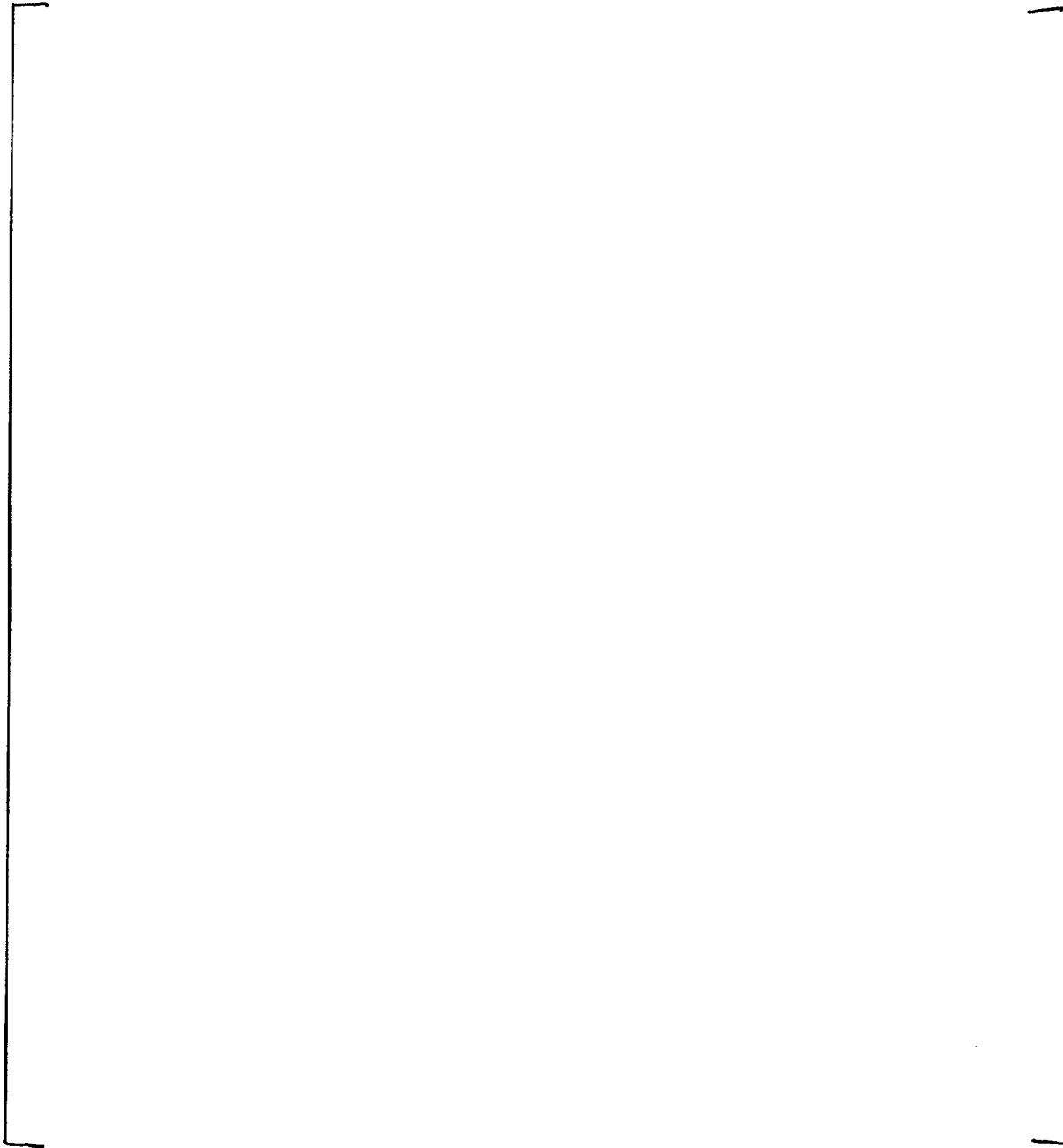


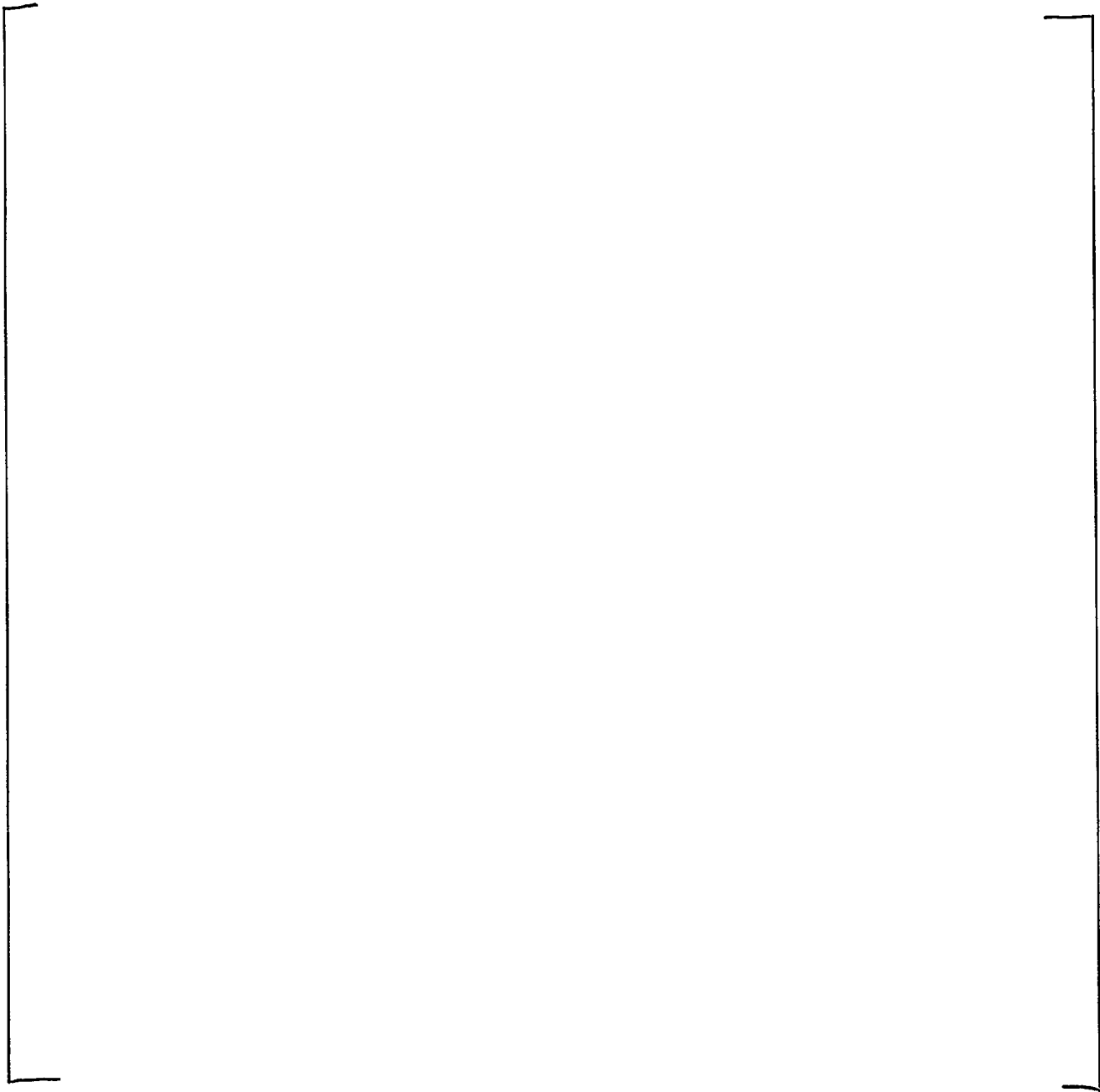




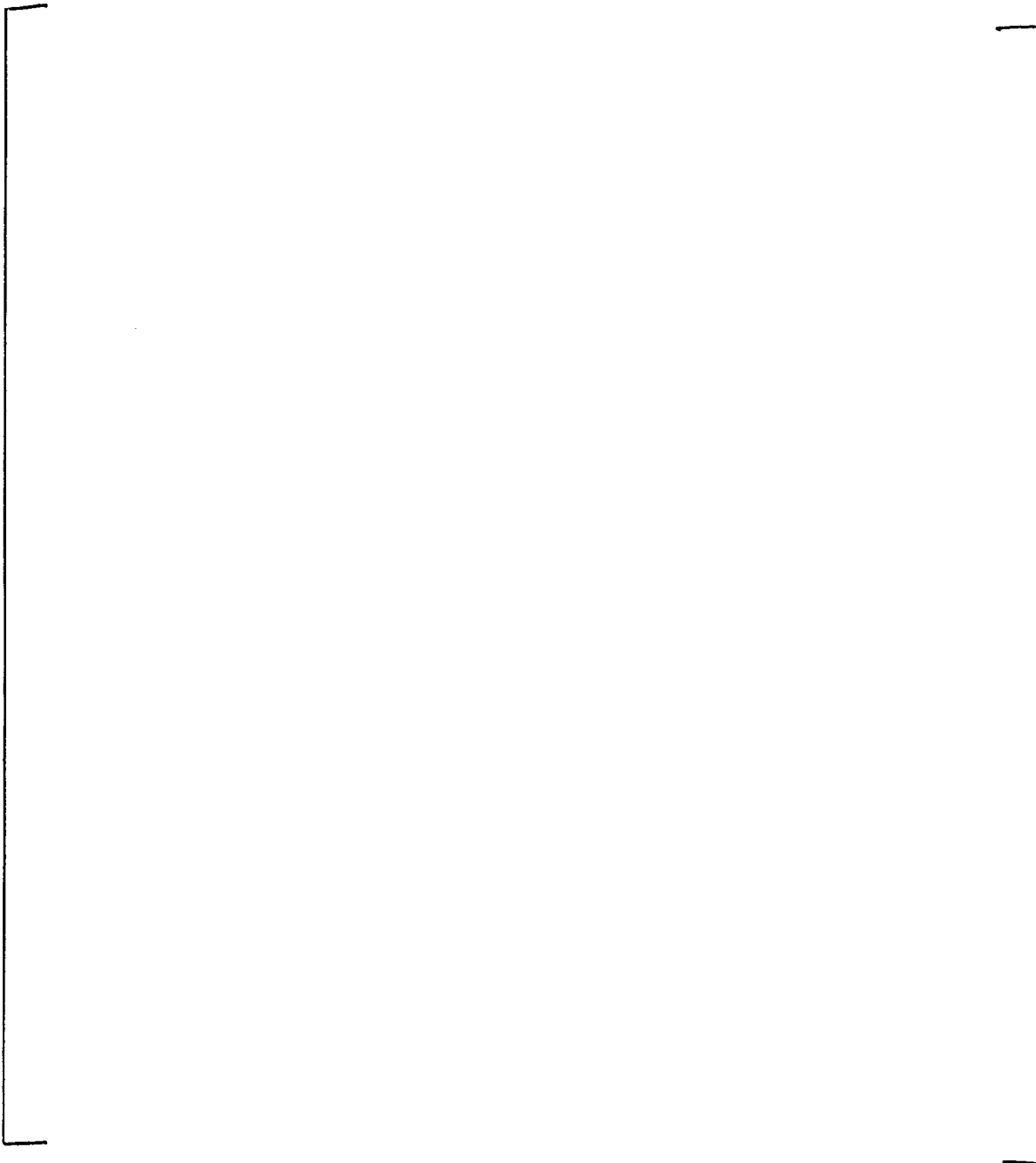




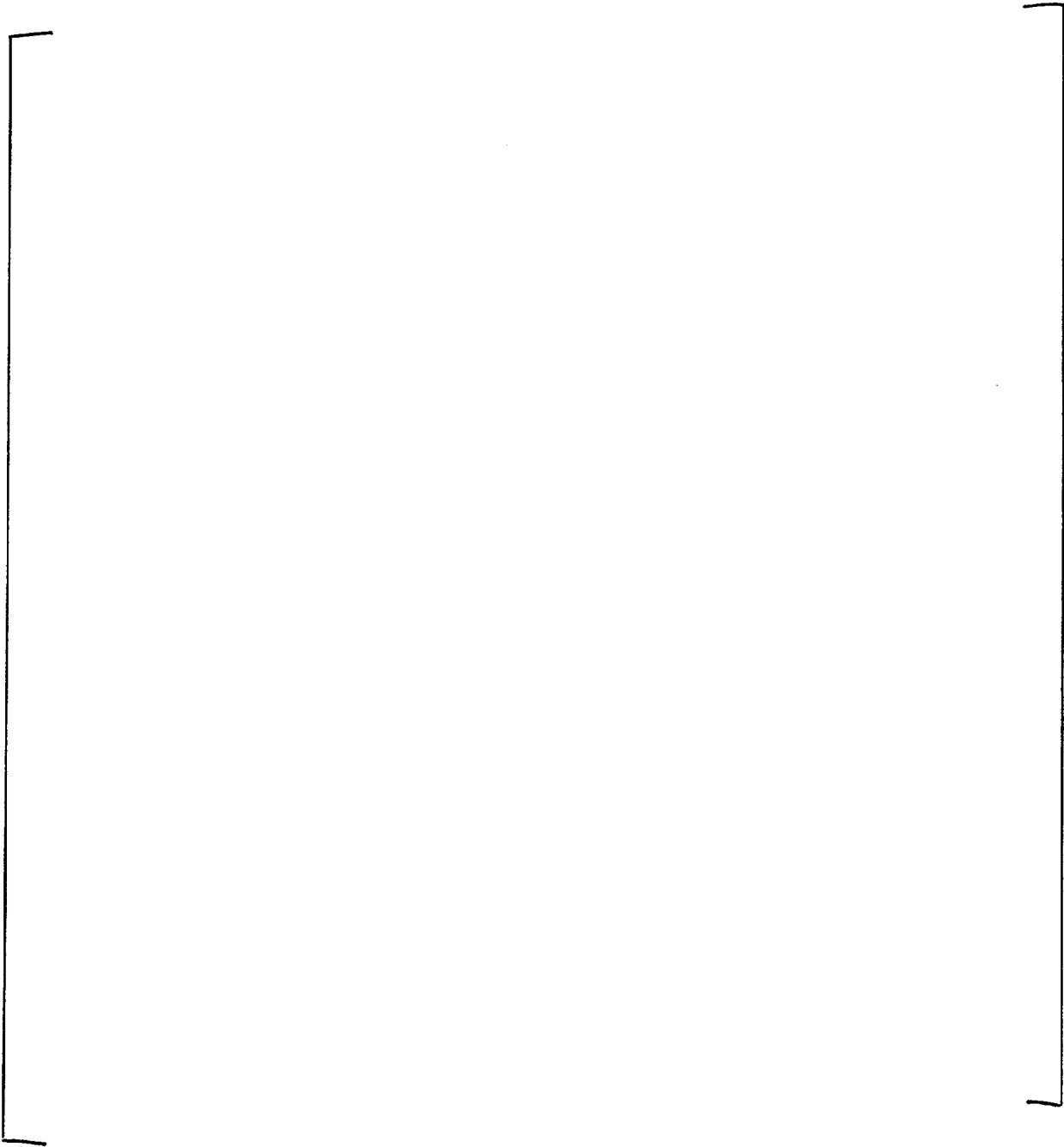


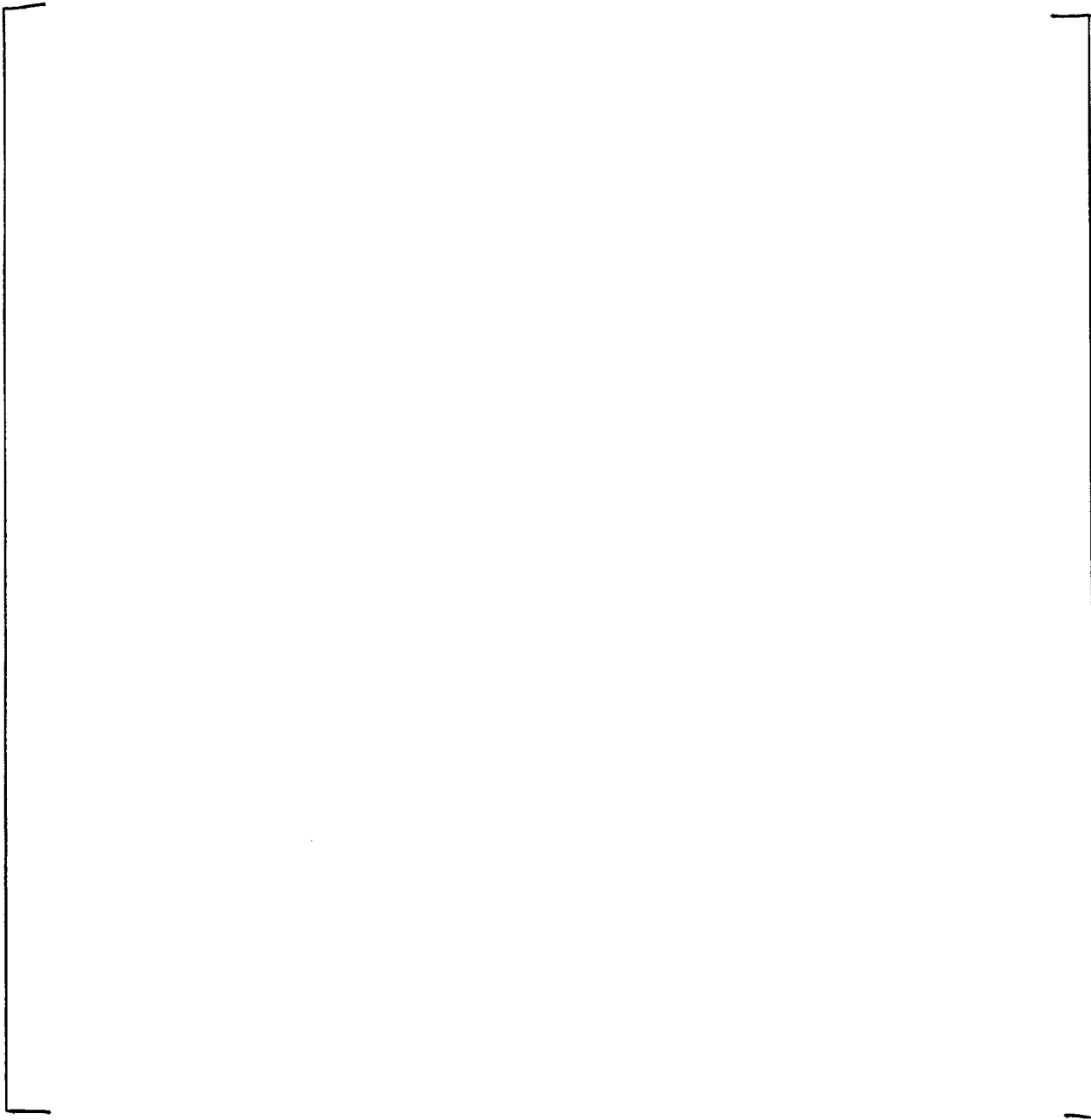


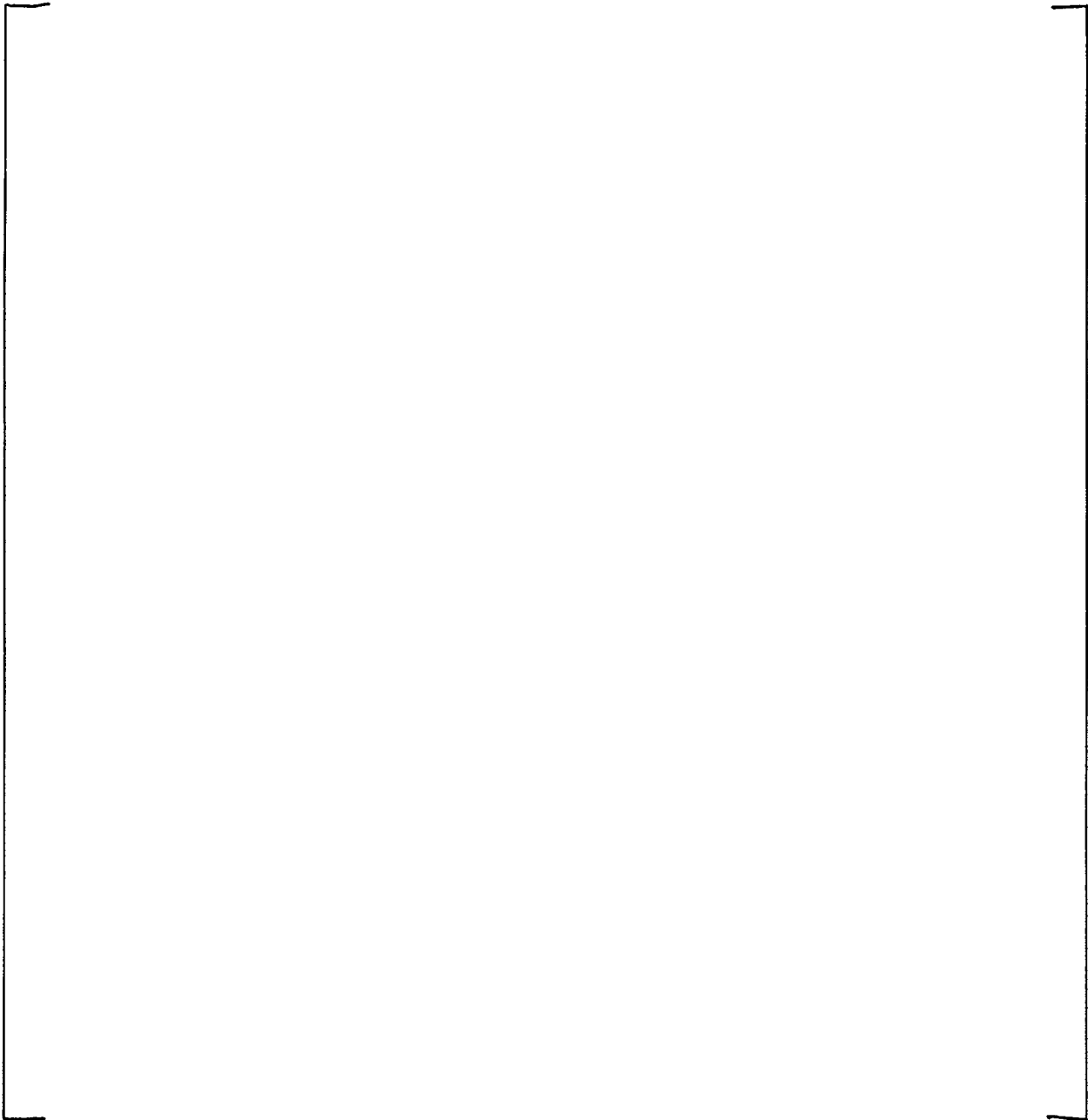


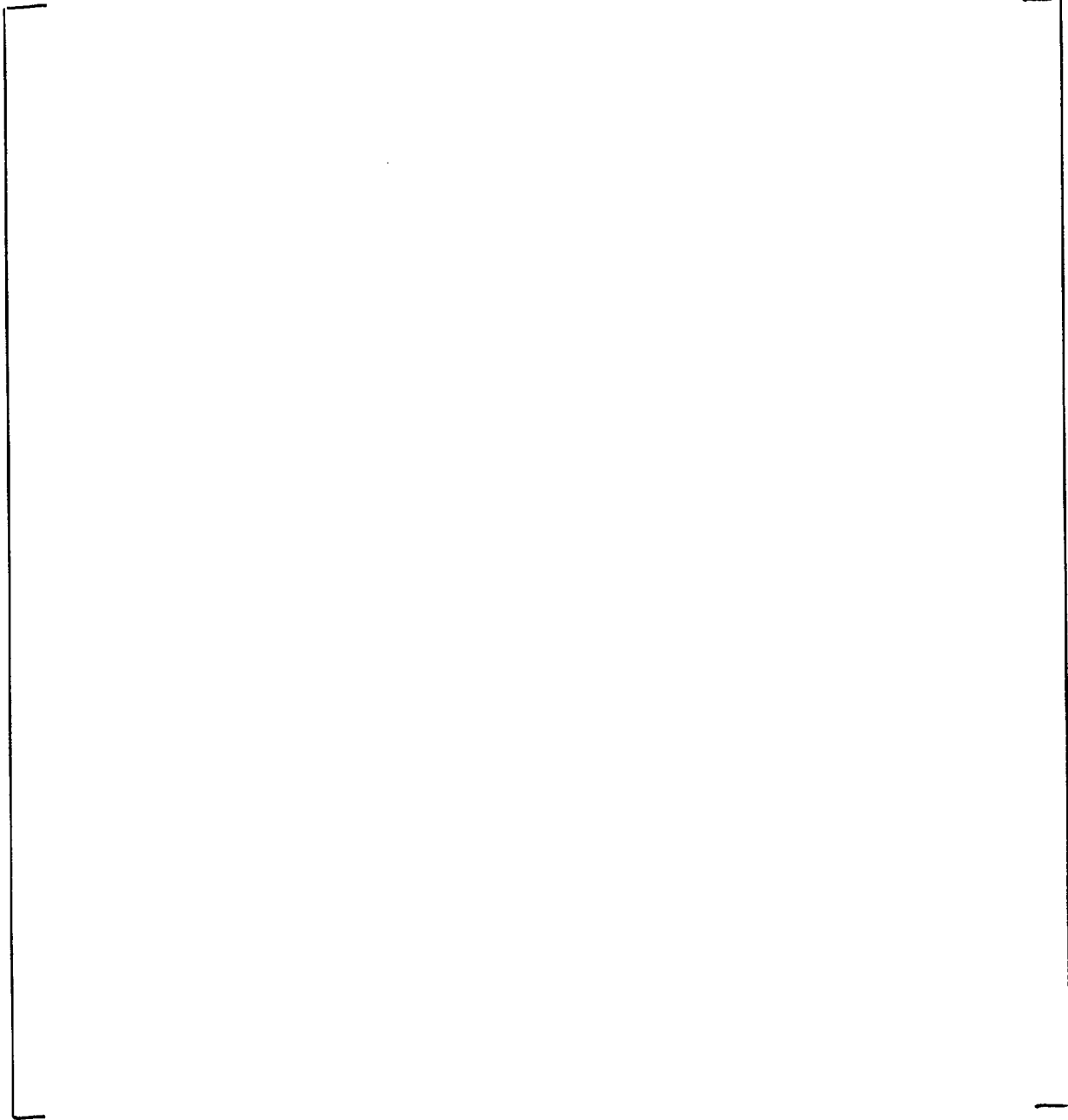


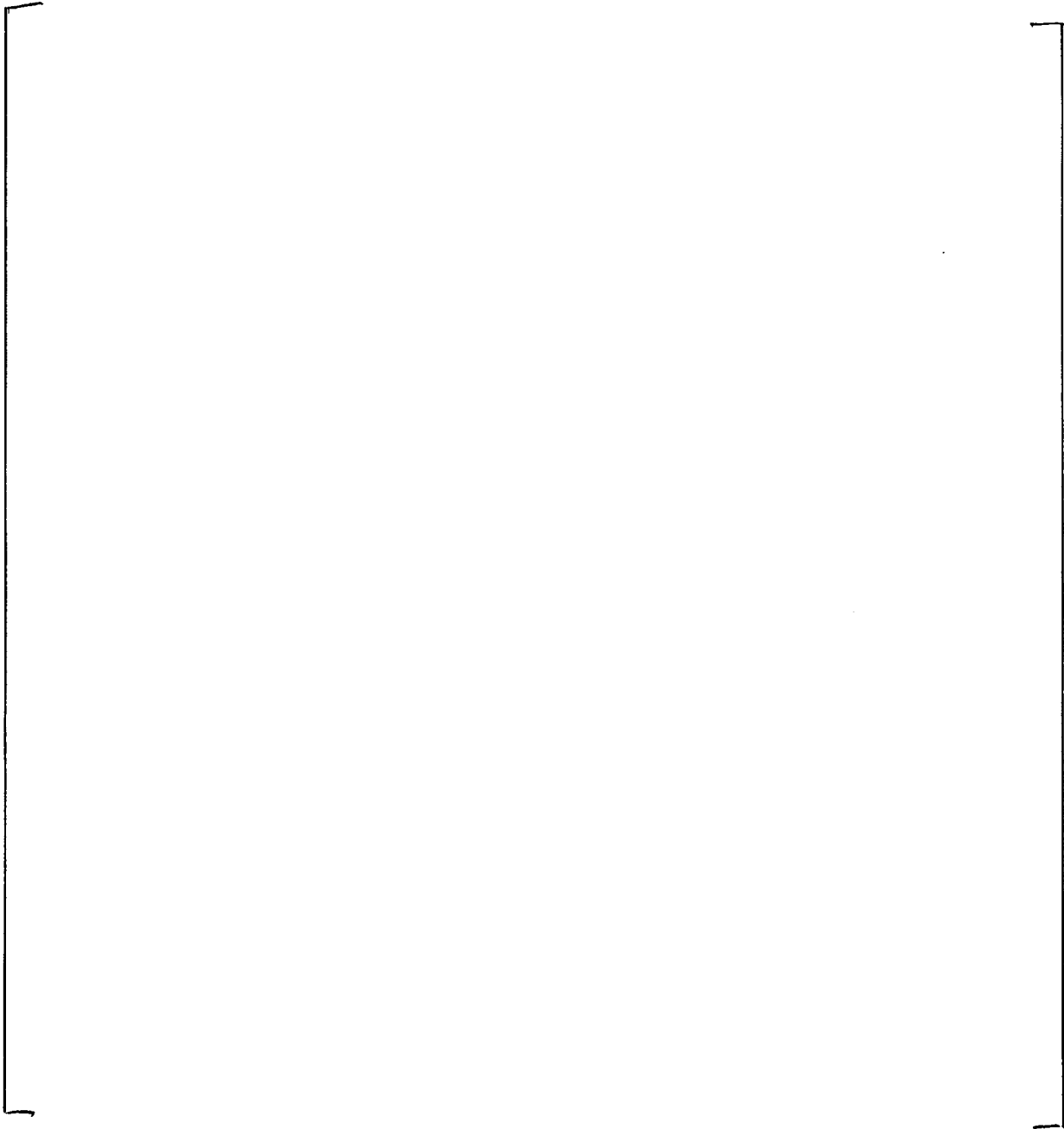


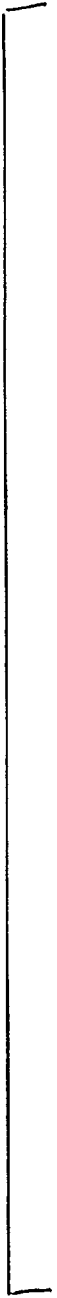




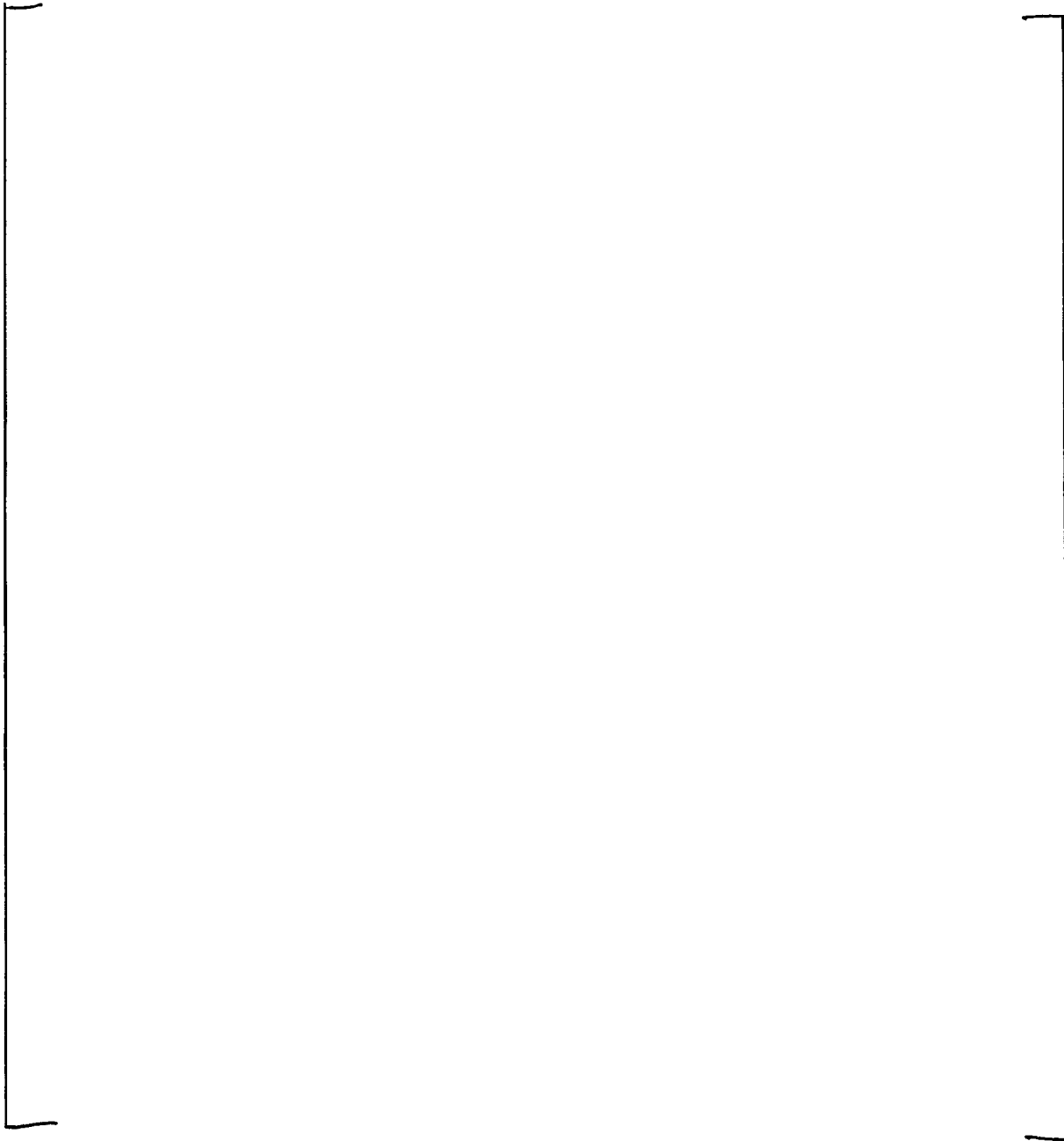




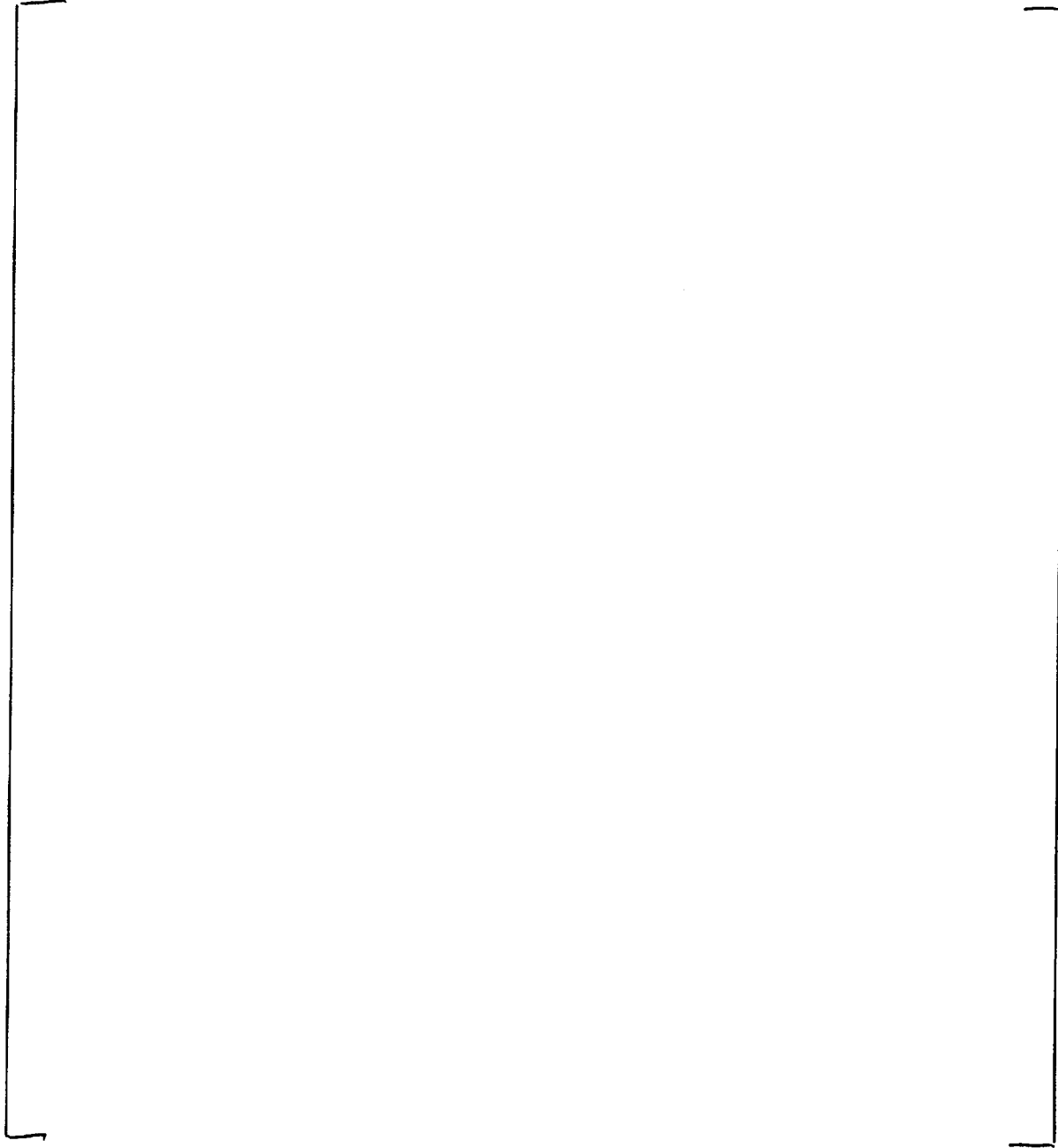


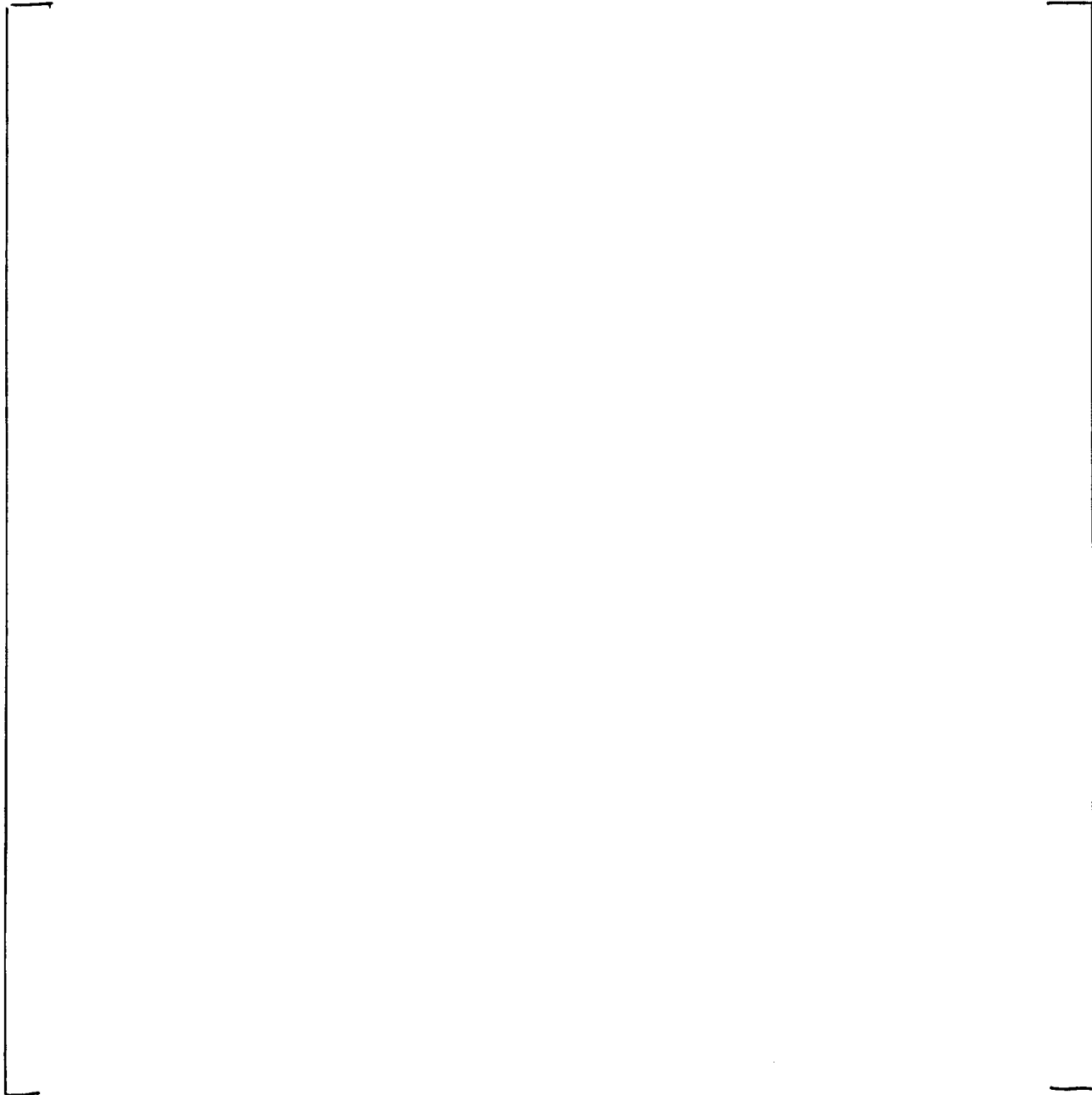


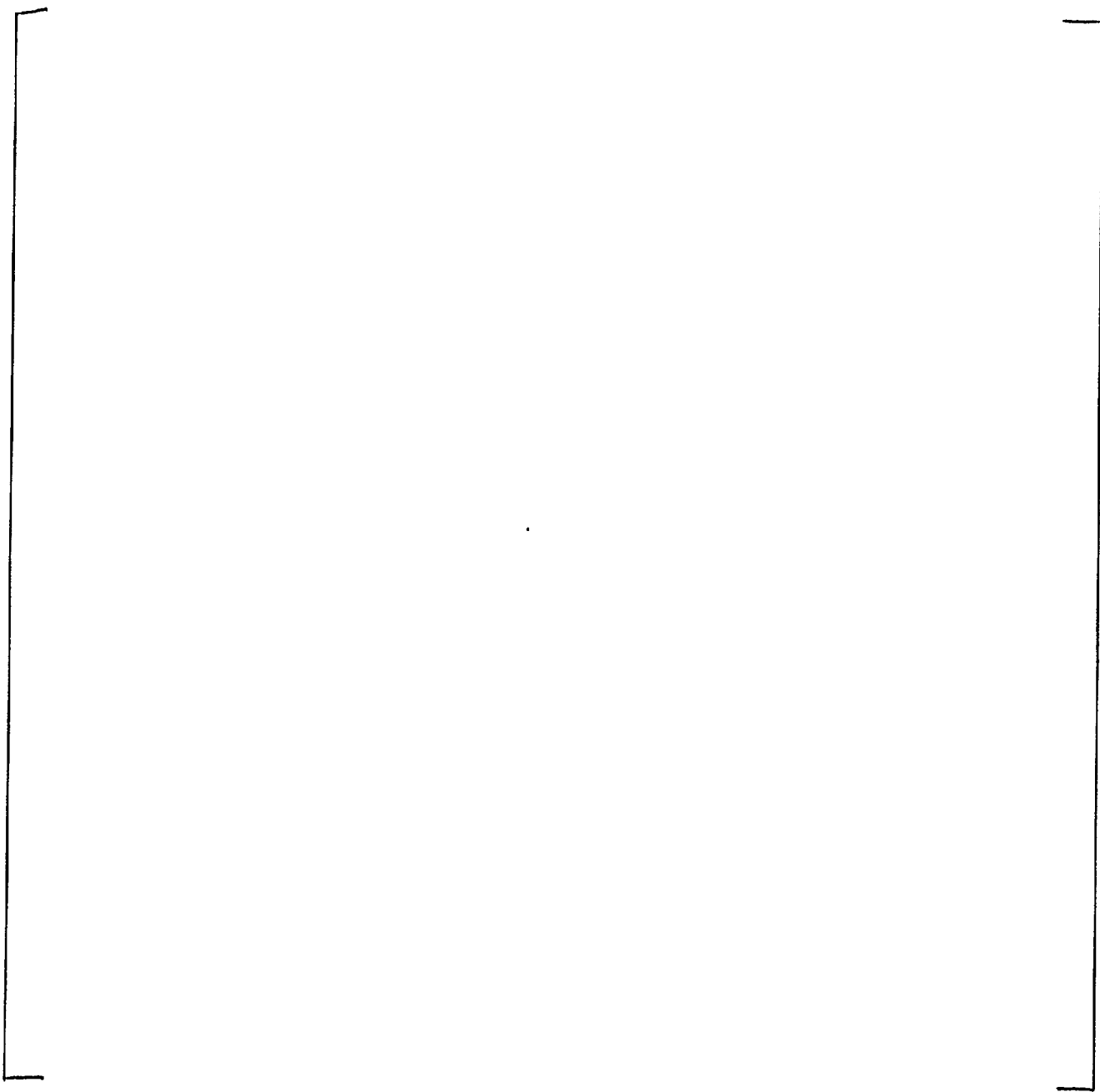


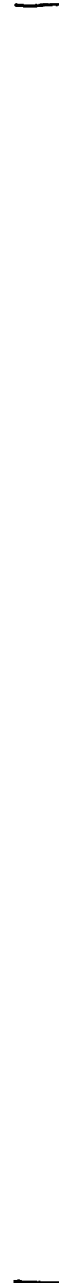


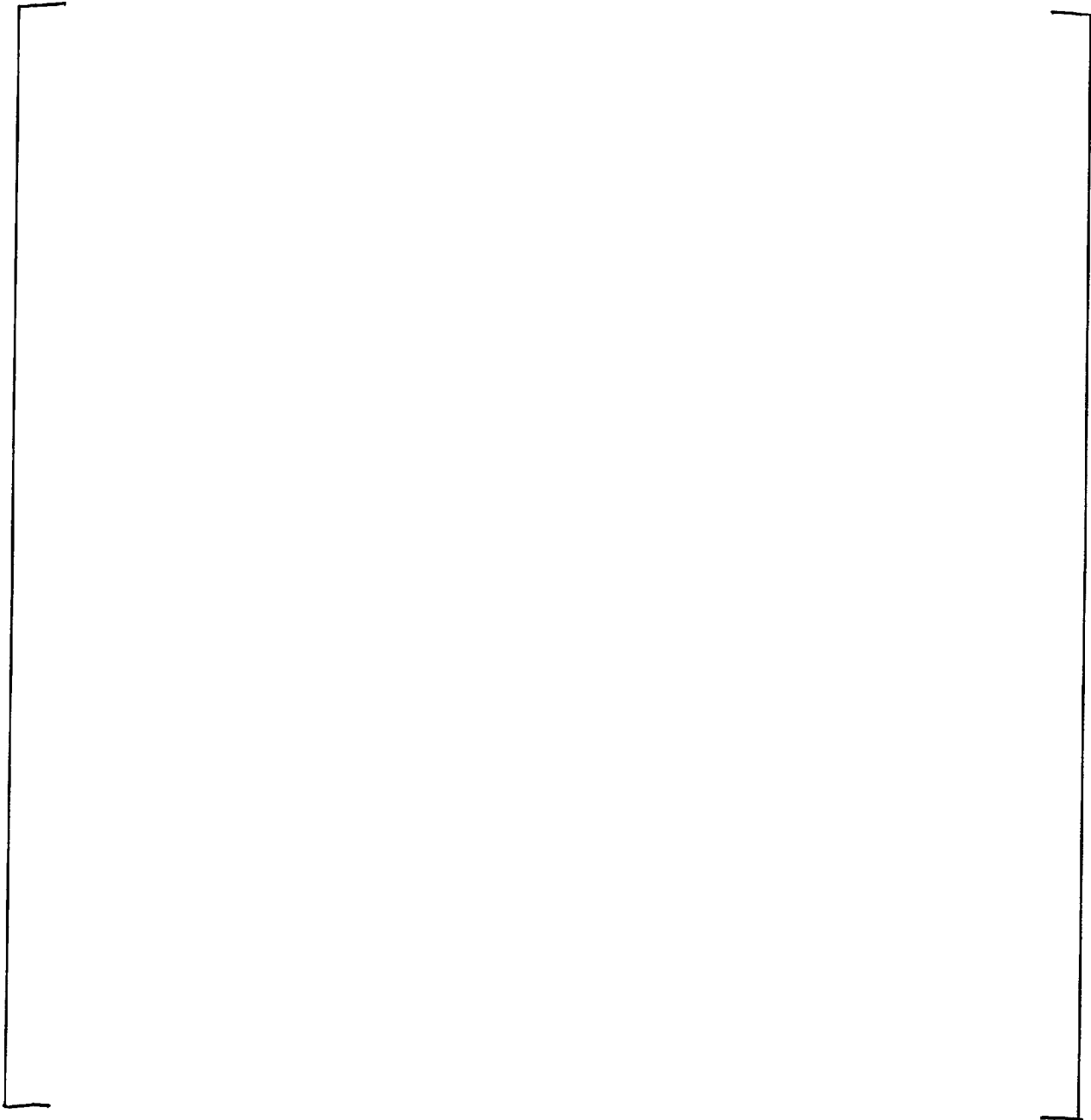


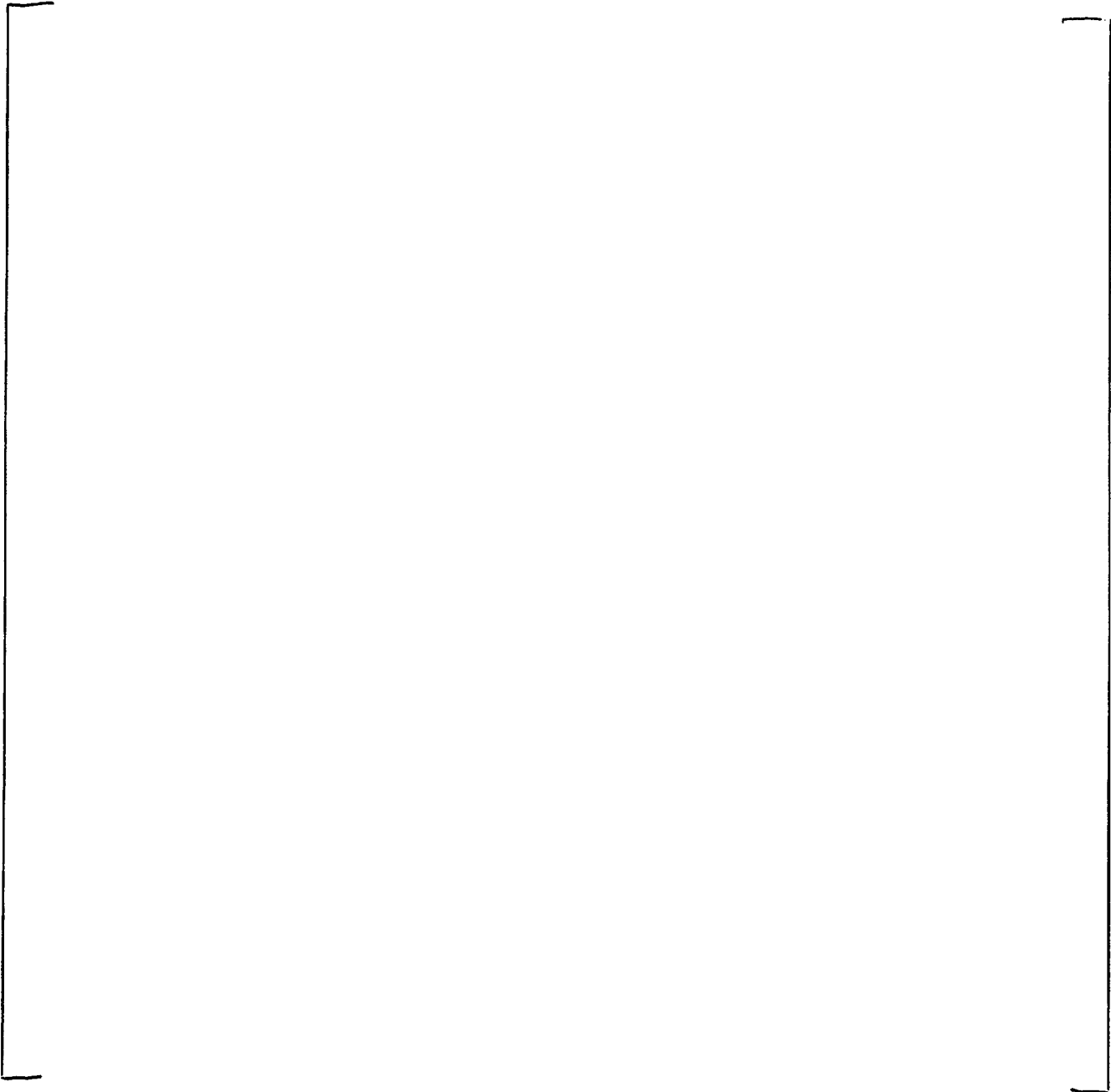














## APPENDIX D

### Response to the NRC Request For Additional Information

The NRC request for additional information is in the form of nine questions, Reference D-3. In these responses, each NRC question is repeated followed by the CENP response. For the transmission of this document, Proprietary information contained within brackets was removed.

#### **D1. NRC Question Number 1**

*On page 27 of the submittal, the last sentence of the first paragraph states that not all the data points were obtained at precisely the target condition. Please clarify.*

#### **Response**

The intent of showing the experimental data trends in Figures 3.11 through 3.24 is to demonstrate that the SVEA-96 critical power database is physically realistic and consistent with similar measurements for other assembly designs. For example, Figure 3.11 demonstrates that for a given axial power shape and an approximately constant radial power distribution, inlet subcooling, and system pressure, the critical power [ ] The statement that “not all the data points were obtained at precisely the target condition” reflects the fact that the radial power distribution, inlet subcooling, and system pressure were not exactly equal to the target values in each experimental data point. This situation introduces a minor spread in the experimental data points. The ABBD1.0 predictions were calculated at the target conditions.

To illustrate the statement “since not all the data points were obtained at precisely the target condition,” consider Figure 3.11 as an example. In this figure, the target conditions for the test cases are: [

] However, the actual test cases were [ as shown in the following table. ]


These small deviations in the experimental conditions introduce some spread in the measured points. It should be noted that the correlation development and validation are performed for the [ ]

**D2. NRC Question Number 2**

*Please explain why full bundle data is not considered necessary to confirm (validate) sub-bundle mismatch factor accuracies and full bundle correlation predictions.*

**Response**

The method for treating sub-bundle power mismatch in ABBD1.0 has been successfully applied to ABB watercross designs in the past. The method used for ABBD1.0 was also utilized for the XL-S96 CPR correlation described in Reference D-1 as well as the ABBD2.0 CPR correlation described in Reference D-2. The method was justified on physical grounds in Reference D-1. [

.] In Reference D-2, this method was qualified by comparison with test data. Specifically, the predictions of the ABBD2.0 CPR correlation were compared with CPR test data obtained with a 96-rod SVEA-96+ test assembly.

For ABBD1.0, full bundle data are not considered necessary to confirm (validate) the sub-bundle mismatch factor method for establishing full bundle correlation predictions for the following reasons:

1. The methodology used to establish the mismatch factor for ABBD1.0 is the same as that used for XL-S96 in Reference D-1 and ABBD2.0 in Reference D-2. The actual mismatch factor established by this methodology is specific to the ABBD1.0 correlation and reflects the actual SVEA-96 characteristics.
2. The radial configuration of the sub-bundles and integral water cross channel are [
- .]
3. Experience with the mismatch factor methodology indicates [

.]

**D3. NRC Question Number 3**

*Please provide additional information regarding the equation (on page 72) for calculating the sub-bundle power, FSUBS, (i.e., where does the value of the total bundle power come from)?*

**Response**

In a reload design application, the nuclear design lattice code is used to calculate the rod power distributions for each bundle. The relative sub-bundle power,  $FSUB_s$ , is then calculated as:

$$FSUB_s = \frac{4 \times \text{power for subbundle "s"}}{\text{total bundle power}}$$

Power for sub-bundle "s" is given by the sum of the 24 rod powers in sub-bundle "s," where "s" refers to sub-bundle 1, 2, 3 or 4. The total bundle power equals the sum of the 96 rod powers in the full bundle.

A typical example of the relative rod power distribution for the full bundle is shown below:


The sub-bundle powers and the values of  $FSUB_s$  are then calculated as follows:


**D4. NRC Question Number 4**

*Is Figure 5.2 representative of all the data, i.e., evaluation and validation data?*

**Response**

Yes, Figure 5.2 includes all of the SVEA-96 data points, including both evaluation and validation data.

**D5. NRC Question Number 5**

*Please explain the scattering of data in Figure 5.4 through 5.8.*

**Response**

The points in Figures 5.4 through 5.8 for which the magnitude of the prediction error is relatively large have been investigated to establish any correlation with process parameter (e.g. pressure, flow, etc.),

axial power distribution, or test rod location. Figures D5-1 through D5-10 are plots of the data for which the magnitude of the prediction errors are greater than [ ]. Figures D5-1 through D5-6 show the data for which the magnitude of the prediction errors are greater than [

.] Figures D5-7 through D5-

10 show the prediction errors as a function of the [

.] The following conclusions are based on the

data in Figures D5-1 through D5-10:

1. Figures D5-1 through D5-6 do not show any [

.]

2. Figures D5-7 through D5-10 indicate that [

.] However, these heater rods do not appear to consistently give anomalous results.

Therefore, it is concluded that any [

.]

3. Experience with dryout testing has indicated that thermocouples [

.]

## D6. NRC Question Number 6

*In Chapter 6, Section 6.1, page 114; please provide clarification (additional information) for the 3<sup>rd</sup> and 4<sup>th</sup> paragraphs.*

### Response

CPR correlations such as ABBD1.0, ABBD2.0 (Reference D-2), and XL-S96 (Reference D-1) typically used for monitoring the dryout behavior of fuel in commercial power reactors are correlated to describe well-established steady-state thermal-hydraulic conditions. As discussed in Section 6.1, an application of these correlations is the calculation of the change in CPR during a postulated transient. The correlation can be used for steady-state equilibrium CPR predictions in any code which reliably predicts those conditions. Therefore, the application of the correlation is straight forward for transients whose time dependence is sufficiently slow to justify their description as a series of steady-state conditions. The Rod Withdrawal Error and Loss of Feedwater Heating Anticipated Operational Occurrences are examples of "Slow Transients."

"Fast" transients, however, occur sufficiently rapidly that the hydraulic conditions during the event are not in thermal-hydraulic equilibrium. The pressurization transients caused by closure of the main steam line are generally the limiting fast transients in U.S. reactors and can be initiated, for example, by a turbine trip or a generator load rejection. Since CPR correlations typically used in the industry, such as ABBD1.0, predict dryout for equilibrium thermal-hydraulic conditions, it is not *a priori* clear that the correlation will necessarily accurately predict the change in assembly CPR during a fast transient.

[

]

The important factors determining the capability of a fast transient analysis code package to conservatively predict transient CPR performance using a given CPR correlation are the form of the CPR correlation and the methodology with which the CPR correlation is evaluated. Therefore, the system dynamic code used to calculate delta-CPR during a transient, the CPR correlation, and the manner in which the correlation is to be evaluated in design calculations should be compared with transient experimental data as an integrated package. For a given transient code and application methodology, the details of the assembly design are not of primary importance for the conservative prediction of delta-CPR if the form of the correlation is not changed, and the CPR correlation used adequately describes the steady-state CPR performance of the assembly. The important consideration in the transient application is whether or not the change in CPR is conservatively predicted during the transient.

[

.]

The comparisons of the ABBD1.0 predictions with the five SVEA-96 data points described in Section 6.3 provide a second, independent confirmation of the conclusion that the ABBD1.0 CPR correlation in conjunction with the BISON-SLAVE hot channel code using the same strategy for evaluating the correlation will provide conservative delta-CPR values during a fast transient. As discussed in Section 6.4, the results of these comparisons for SVEA-96 are very consistent with results in Section 6 of Reference D-2 for SVEA-96+. This conclusion was intended to be the primary message in paragraph 4 of Section 6.1.

**D7. NRC Question Number 7**

*Please provide additional technical justification as to why 5 data points constitute an "adequate" data base for validating the ABBD1.0 correlation in a transient mode.*

**Response**

In light of Response D6 above demonstrating that the transient test comparisons in Reference D-2 for

[

.]

Furthermore, all of our comparisons between the predictions of critical quality-boiling length correlations for 10x10 SVEA fuel in conjunction with the BISON-SLAVE code using the same strategy for selecting correlation inputs with transient test data have confirmed the conservative nature of the predictions. [

. ] Therefore, transient validation based on one of the ABBD-versions of CPR correlation and its associated measurements has proven to be applicable to all the ABBD-versions of CPR correlation.

In summary, the comparison for ABBD1.0 based on the 5 data points in Section 6.3 represents confirmation of a method of calculating delta-CPR which has been demonstrated for a much broader data base.

#### **D8. NRC Question Number 8**

*In Table 6.3, what is the difference between the Initial and the Minimum columns?*

#### **Response**

Table 6.3 shows the transient CPR results for the five flow reduction events calculated by ABBD1.0 in the BISON-SLAVE code simulations of the events. The "Initial" column provides the CPR predicted by the code at the initiation of the transient (time = 0.0 sec). The "Minimum" column provides the minimum CPR predicted in the BISON-SLAVE simulation of the event at any time during the transient.

#### **D9. NRC Question Number 9**

*Regarding mis-rotation of sub-bundles, please comment on the possibility of misloading/orienting a sub-bundle while preparing a full bundle during a fuel reload situation.*

#### **Response**

[

.]

Positive controls during the sub-bundle channeling operation preclude the possibility of loading the fresh sub-bundles incorrectly if they are delivered to the site in the correct orientation. [

] Accordingly, the manufacturing facility processes and site inspection procedures have been further strengthened to include:

1. [

.]

2. [

.]

3. The procedure for the QC inspection of the BWR assemblies at the manufacturing facility has been modified to require an independent verification [

.]

4. The fuel receipt inspection at the utility site requires the specific verification of proper location of all sub-bundles.

With these strengthened manufacturing and inspection procedures, it is judged that the probability of mis-orientation of the sub-bundles in the channel is less likely than other postulated BWR accident scenarios.

**REFERENCES**

- D-1. "SVEA-96 Critical Power Experiments on a Full Scale 24-Rod Sub-bundle," ABB Report UR-210-P-A (proprietary), UR-210-NP-A (non-proprietary), October 1993.
- D-2. "10x10 SVEA Fuel Critical Power Experiments and CPR Correlation: SVEA-96+," CENPD-389-P-A, September 1999.
- D-3. Letter, NRC to I. C. Rickard (ABB-CE), "Request for Additional Information (RAI) Regarding CENPD-392-P, 10x10 SVEA Fuel Critical Power Experiments and CPR Correlation: SVEA-96," January 13, 2000.
- D-4. Letter, I. C. Rickard (ABB-CE) to J. S. Cushing (NRC), "Transmittal of Meeting Slides concerning ABB Fuel Performance Update and Licensing Plans for Year 2000 (Proprietary Information)," February 11, 2000.
- D-5. CENPD-390-P. "The Advanced PHOENIX and POLCA Codes for Nuclear Design of Boiling Water Reactors," April, 1999.





*Figure D5-1 Prediction Error Vs. Mass Flux  
(for cases with error > 5%)*



*Figure D5-2 Prediction Error Vs. Outlet Pressure  
(for cases with error > 5%)*



*Figure D5-3 Prediction Error Vs. Inlet Subcooling  
(for cases with error > 5%)*



*Figure D5-4 Prediction Error Vs. R-factor  
(for cases with error > 5%)*



*Figure D5-5 Prediction Error Vs. Boiling Length  
(for cases with error > 5%)*



*Figure D5-6 Prediction Error Vs. Annular Boiling Length  
(for cases with error > 5%)*

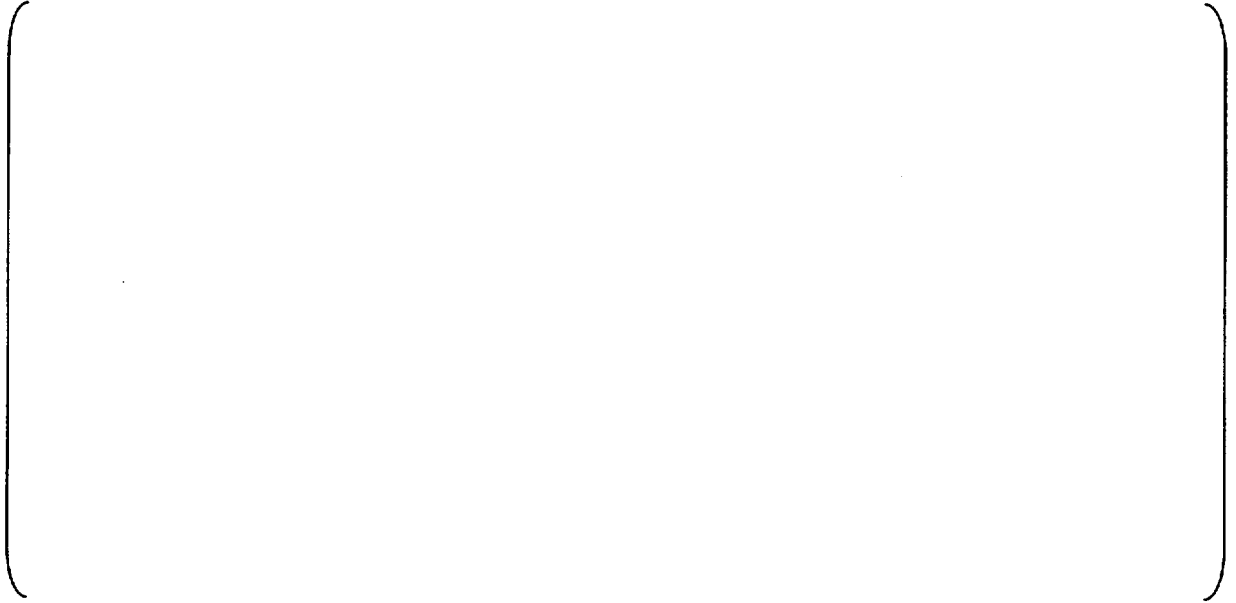


*Figure D5-7 Prediction Error Vs. Dry Rod Number  
(for cases with error > 5%)*



*Figure D5-8 Prediction Error Vs. Dry Rod Number  
(for cases with cosine axial power shape)*



*Figure D5-9 Prediction Error Vs. Dry Rod Number  
(for cases with bottom-peaked axial power shape)*

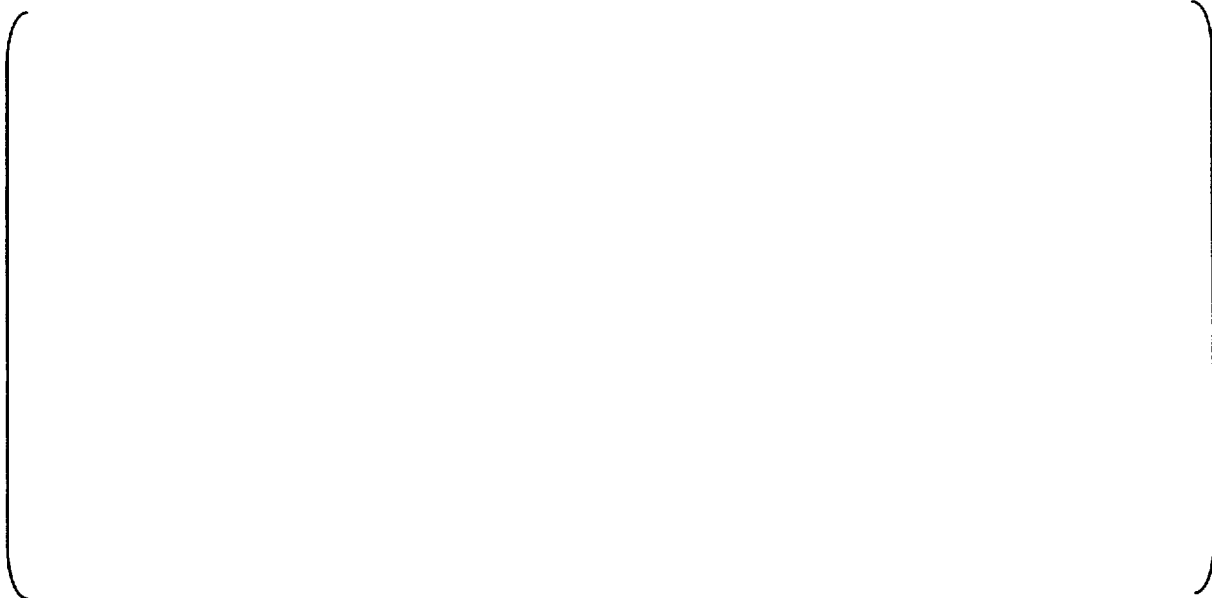


*Figure D5-10 Prediction Error Vs. Dry Rod Number  
(for cases with top-peaked axial power shape)*

**CE Nuclear Power LLC**

---

CE Nuclear Power LLC  
2000 Day Hill Road  
Post Office Box 500  
Windsor, Connecticut 06095-0500